T2R2 東京工業大学リサーチリポジトリ
Tokyo Tech Research Repository

# 論文 / 著書情報
# Article / Book Information

| | |
|---|---|
| 題目(和文) | エレクトロニクスへの応用のためのアモルファスシリコンおよびシリコーンポリマー |
| Title(English) | Amorphous silicon and silicone polymers for electronics applications |
| 著者(和文) | 中村隆司 |
| Author(English) | |
| 出典(和文) | 学位:博士(工学),<br>学位授与機関:東京工業大学,<br>報告番号:乙第3549号,<br>授与年月日:2001年7月31日,<br>学位の種別:論文博士,<br>審査員: |
| Citation(English) | Degree:Doctor (Engineering),<br>Conferring organization: Tokyo Institute of Technology,<br>Report number:乙第3549号,<br>Conferred date:2001/7/31,<br>Degree Type:Thesis doctor,<br>Examiner: |
| 学位種別(和文) | 博士論文 |
| Type(English) | Doctoral Thesis |

Powered by T2R2 (Tokyo Institute Research Repository)

# AMORPHOUS SILICON AND SILICONE POLYMERS FOR ELECTRONICS APPLICATIONS

A Thesis
Presented to
TOKYO INSTITUTE OF TECHNOLOGY

2001

TAKASHI NAKAMURA

# PREFACE

The present thesis is a collection of studies that have been carried out under the direction of Prof. Dr. Hideomi KOINUMA at The University of Tokyo during 1986 – 1987 and at Dow Corning Toray Silicone Co. Ltd. during 1987 – 2000. The studies are concerned with the development of novel amorphous silicon and silicone polymer based thin films and materials, and the mechanism understanding of their functions. Feasibility of their films and materials for electronics applications was also studied. Due to the attractive feature of the chemistry/physics involving silicon, interesting behaviors and advanced functions were observed on the films and materials. The results indicate that those amorphous silicon and silicone polymer based materials are potentially applicable for current and future electronics equipment or devices. These observations were analyzed chemically and physically in detail.

The author expresses his sincere gratitude to Prof. Dr. Hideomi KOINUMA of Tokyo Institute of Technology for his valuable advices and continuous encouragements through his work.

Grateful acknowledgement is made to Prof. Dr. Masashi Kawasaki (Tohoku University and Tokyo Institute of Technology), Assoc. Prof. Dr. Takahiro Seki, Assoc. Prof. Dr. Mamoru Yoshimoto, Assoc. Prof. Dr. Hiroshi Funakubo (Tokyo Institute of Technology), Mr. Masamitsu Tanimura, Mr. Hiroyuki Asai, Mr. Katsutoshi Mine, Mr. Ryuzo Mikami, Mr. Tsuneo Hanada, Mr. Akira Tazawa, Mr. Shin-ichi Sumimura, Mr. Osamu Tanaka (Dow Corning Toray Silicone Co., Ltd.), Mr. Toshio Saruyama (Dow Corning Asia, Ltd.), Prof. Dr. Koichi Kitazawa (The University of Tokyo), Prof. Dr. Yoshiharu Matsuda, Assoc. Prof. Dr. Hiromori Tsutsumi (Yamaguchi University), Assoc Prof. Dr. Kyoko Yatsuzuka (Yamagata University), Prof. Dr. Manshi Ohyanagi (Ryukoku University) and Assoc. Prof. Dr. Kota Sato (Chiba University) for their constructive comments and encouragements.

He is much indebted to active collaborators, Mr. Motoshi Sasaki, Mr. Kiyotaka Sawa, Mr. Akihiko Kobayashi, Mr. Manabu Sutoh (Dow Corning Toray Silicone Co., Ltd.), Mr. James A. Helwick, Mr. Philip D. Dembowski, Mr. Jeffrey N. Bremmer (Dow Corning Corporation) and Dr. Takuya Hashimoto (Nihon University) for their assistance and discussions in the studies.

All members in Koinuma Laboratory, Material Development Department, AETS & Development No.2 Department in Dow Corning Toray Silicone Co., Ltd. and SFM MM Group in Dow Corning Group offered kind assistances, for which he would like to thank deeply.

Finally the author expresses his deep gratitude to his family Chiho, Risa and Ruriko, parents Masatomi, Kimi and sister Miki.

July 31, 2001

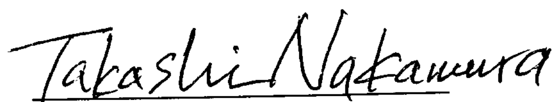

Takashi NAKAMURA

No. 1 Group,
AETS & Development No.2 Department,
S&T Division,
Dow Corning Toray Silicone, Co., Ltd.

# CONTENTS


Page

**Chapter 1 General introduction** 5

1.1 General background of studies on silicon containing materials 6

1.2 Background of typical types of silicon containing materials and potential for electronics application 7

1.3 Purpose of this study 13

**Chapter 2 Amorphous organosilicon films prepared by plasma CVD** 15

2.1 Introduction 16

2.2 Experimental part and calculations 18

2.2.1 Synthesis of amorphous films from phenylsilanes by plasma chemical vapor deposition 18

2.2.2 Glow discharge decomposition of phenylsilane in the presence of oxygen 20

2.3 Results 21

2.3.1 Synthesis of amorphous films from phenylsilanes by plasma chemical vapor deposition 21

2.3.2 Glow discharge decomposition of phenylsilane in the presence of oxygen 27

2.4 Discussion 33

2.3.1 Synthesis of amorphous films from phenylsilanes by plasma chemical vapor deposition 33

2.3.2 Glow discharge decomposition of phenylsilane in the presence of oxygen 35

2.5 Conclusion 38

**Chapter 3 Silicon based thin films for passivation of superconductors** 40

3.1 Introduction 41

3.2 Experimental part 42

3.3 Results 49

3.4 Discussion 60

3.5 Conclusion 62

**Chapter 4 Siloxane/PEO based polymer electrolytes for lithium battery** 64
4.1 Introduction 65
4.2 Experimental part 67
4.3 Results 72
4.4 Discussion 78
4.5 Conclusion 79

**Chapter 5 Siloxane ionomers for electrorheological fluids** 81
5.1 Introduction 82
5.2 Experimental part and results 84
5.3 Discussion 96
5.4 Conclusion 97

**Chapter 6 Polyhydrogensilsesquioxane thin films for inter layer dielectric applications** 99
6.1 Introduction 100
6.2 Dynamic viscoelastic behaviors of HSQ resin at high temperatures 106
6.2.1 Experimental part 106
6.2.2 Results 109
6.2.3 Discussion 110
Appendix (Fig. 2 - 17) 112
6.3 Oxidative curing of hydrogen silsesquioxane resin films enhanced by electron beam at ambient temperature and characterization of the cured films 120
6.3.1 Experimental part 120
6.3.2 Results 122
6.3.3 Discussion 130
6.4 Formation of HSQ based low-k films 133
6.4.1 Experimental part, results and discussion 133
6.5 Conclusion 134

**Chapter 7 Conclusion** 137

List of publications 141

# Chapter 1

# General introduction

1.1 General background of studies on silicon containing materials 6

1.2 Background of typical types of silicon containing materials and potential for electronics application 7

1.3 Purpose of this study 14

## 1.1 General background of studies on silicon containing materials

Silicon is currently the most valuable and practical element for industries especially of electronics. Silicon exists as various forms such as metal, amorphous, ceramic, inorganic and organic, since it has four covalent bonds and d orbitals. That is silicon can exist in any bond order from zero (Si) through four (eg, $SiO_2$).

There are two typical categories in study field for silicon containing materials. One category is solid-state physics that focuses on the nature of silicon as the semiconductor. Crystalline or amorphous silicon is the core material and its related alloys are also included in this category, which have been greatly influencing on the progress of electronics such as LSI and solar cell. The other category is chemistry that covers siloxanes, silanes or polysilanes. Some of those materials are already widely used as industry basis. Silicone (organo siloxane) is a typical example. Also, various studies have been active on this field. Those two types of study have been carried out independently since it has been believed that there is little relationship between the two groups.

However, the author believes that there should be a common part in physics and chemistry for all the silicon containing materials seeing the fundamental natures of "silicon". Preparation methods (typically CVD or wet chemical synthesis) being applied for each study field should be able to be applied to the different filed also. So that, seeing the whole picture of the two different study categories, ie, the "whole silicon", may give novel materials, functions and/or methods for preparation.

Synthetic routes for silicon based materials are mostly two ways. One is CVD (chemical vapor deposition) that is useful for thin film formation and the structure of the films could be continuously designed and controlled. Starting materials are silanes or small molecular compounds mostly. The other one is chemical reaction in solution. Much variety in chemical structure or synthetic route could be designed. Si-O bond is a core structure. Siloxanes ($RR'SiO_{1/2}$) and resins ($RSiO_{3/2}$) are generally known compounds. Carbon or hydrogen can be attached to silicon, so that various types of chemical modifications are possible on siloxanes or resins. Based on the excellent properties of Si-O bond based materials such as thermal resistance and mechanical strength, special functions could be added due to the modified parts.

It is well understood that future electronics equipment and devices require materials having high and novel performances. Silicon will probably continue to take the basic role on the electronics applications, since it exists rich in the earth, exist in

any bonding stage and can be modified in chemically in variety.

The purpose of this study is to look at the whole silicon containing materials combining methodologies in the two study categories and to develop or consider novel materials having advanced performances for electronics application. This is a first approach. Hence, the author will discuss amorphous silicon and silicone polymers for electronics application in this thesis.

In this thesis the author pays attention to bond order of silicon. Table 1 summarizes a classification of silicon containing materials by extending bond order around silicon and SiO bond order. The concept of them is similar to "dimension". Extending bond order around silicon is defined as the number of chain-extendable bond that the silicon atom has. SiO bond order is defined as the number of SiO bond that the silicon atom has. This is well used in the silicone filed. Scheme 1 illustrates the structural units of silicon containing materials classified by SiO bond order. The author believes that the whole picture of silicon containing materials be well understood and novel materials and methods for preparation be effectively found. The numbers of extending bond order around silicon or SiO bond order are not always in integral numbers. That is, the order of silicon changes continuously.

## 1.2 Background of typical types of silicon containing materials and potential for electronics application

In this section the background of typical types of silicon containing materials and their basic technologies are introduced.

### Amorphous or crystalline silicon

Amorphous or crystalline silicon is a core material for micro electronics applications such as LSI and solar cell. Basically it has no organic functionalities and is a semiconductor. Crystalline silicon can be valence state controlled giving p-n junctions.

Since Spear et al reported that an amorphous hydrogenated silicon (a-Si:H) film prepared from silane ($SiH_4$) by CVD could be valence state controlled, amorphous silicon has been recognized as a material for solar cell applications. Also, after that CVD technologies became expanded to prepare various silicon containing films.

Amorphous silicon carbide (a-SiC), one of silicon containing alloys, is an

Table 1. Extending bond order around silicon, SiO bond order, material, function and application.

| Extending bond order around Si | SiO bond order | Material (example) | Function | Application |
|---|---|---|---|---|
| 4 | 0 | Si | Valence state control, p-n junction | Solar cell, IC fabrication |
| 4 or (4-$\delta$) | | a-Si (a-Si:H) | | |
| | | a-SiC (a-SiC:H) | Wide band gap<br>Insulation/hard coating | Window material for solar cell<br>Hard mask for IC |
| 0 | 0 | $SiR_4$<br>(R = H, Alkyl, Aromatic) | | CVD precursor<br>Silane coupling agent |
| 2 | 0 | $(SiR_2)_n$<br>(R = H, Alkyl, Aromatic) | Photo active<br>Dopable | Photo resist |
| 2+$\delta$ | 0 | Polysilane alloy | Polysilane-like film | |
| 2 | 2 | $(SiMe_2O)_n$ | Thermal resistance, Insulating, Low Tg, etc. | Many industrial applications |
| | | $(SiRMeO)_n$ (R=functional group or segment) | Additional functions to dimethyl silicones | Many industrial applications |
| | | R = PEO w/ $Li^+$ | $Li^+$ conducting | Li battery |
| 2+$\delta$ | 2+$\delta$ | Cured (siloxane-PEO) w/ $Li^+$ | Solid polymer electrolyte | Li battery |
| | | Ionomers | Electrorheology | ER fluid |
| 3 | 3 | HSQ ($(HSiO_{3/2})_n$) | Soluble, Melting, Cured into $SiO_2$. | Interlayer dielectrics for LSI |
| 3+$\delta$ | 3+$\delta$ | Cured HSQ | Lowe k than $SiO_2$ | Interlayer dielectrics for LSI |
| 4 | 4 | $SiO_2$ | Insulating | Interlayer dielectrics for LSI |
| Hybrid | Hybrid | Plasma polymerized Si containing materials | Passivation | Passivation for ceramic superconductors |

Scheme 1. The structural units of silicon containing materials classified by SiO bond order[2,3].

| Structural formula | Composition | Functionality | Symbol |
|---|---|---|---|
| $R_3Si{-}O{-}$ | $R_3SiO_{1/2}$ | monofunctional | M |
| $-O-Si(R)(R)-O-$ | $R_2SiO_{2/2}$ | difunctional | D |
| $-O-Si(R)(O-)-O-$ | $RSiO_{3/2}$ | trifunctional | T |
| $-O-Si(O-)(O-)-O-$ | $SiO_{4/2}$ | tetrafunctional | Q[a] |

[a] The symbol "Q" is derived from "quadrifunctional" rather than "tetrafunctional" to distinguish it from T for "trifunctional".

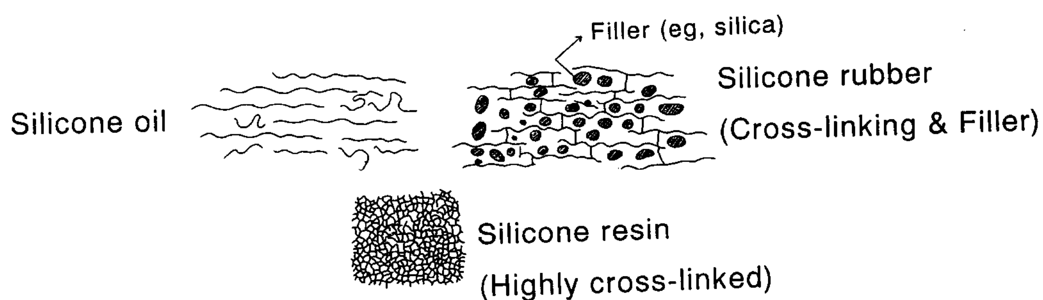

than amorphous hydrogenated silicon[4]. It is usable for window materials of solar cells. Koinuma et al found that methyl substituted silanes gave excellent a-SiC films by CVD and analyzed the CVD mechanism[5]. It seems that there are large opportunities remaining to study in a-SiC, however, not much studies are found yet. Additionally, CVD techniques is believed to introduce functional groups or structure in a-Si or a-SiC films resulting in obtaining films with novel functions.

Silane

Silane is expressed as $SiR_4$, ie, has the functionality of four. Silanes are rarely used as finishing products except as "silane coupling agents" that are typically used to modify or treat the surface of materials. They are mostly used as raw materials or precursors for polymers or network films by either CVD or wet chemical reaction. Various materials having various R groups are selected for the purpose of the study or application.

Polysilane

Polysilane is expressed as $(SiR_2)_n$, ie, has the functionality of two. It is mostly synthesized by the Wultz coupling reaction from chlrosilanes. However, its SiO bond order is zero, so that its properties are different from polysiloxane. The major applications of polysilane are raw material for SiC ceramics and photo resist. Polysilane has historically been believed to be just an insulator.

In 1981 West et al reported that the electric conductivity of a polysilane changed by diffusion of arsenic pentafuluoride[6]. Trefonas et al calculated the electronic state on a polysilane and found that $\sigma$ electrons are delocalized along with the main chain having a semiconductor like band structure[7]. Wolford et al reported a new structure of amorphous hydrogenated silicon containing polysilane structures, called "polysilane alloys"[8]. Mastumoto et al carried out systematic studies on polysilane, polysilane alloys and related materials and calculated and analyzed their electronic and optical states[9].

As above, polysilanes and polysilane like structures are believed to have potential performances for electronics application.

Siloxane

Siloxane has a SiOSi main chain and organic groups in the side chain. Its SiO bond order is two. Polyorganosiloxane is called silicone. Since Rochow found the "direct method" to synthesize alkylchlorosilanes[10] as the raw materials of siloxanes, silicone has been established as an industrially successful material. The most popular type of silicone is polydimethylsiloxane, $(Me_2SiO)_n$. It has both inorganic properties coming from the SiO bond and organic properties coming from the methyl groups. It has excellent properties such as stable properties in a very wide temperature range, a very low surface tension, resistances against chemicals and atmospheres, good electrically insulating properties, being inert to materials, etc. These excellent properties are due to the strong bond energy for the SiO bond, free rotation energies for the SiO and SiMe bonds and an effective coverage of the surface of molecule by methyl groups. Silicone exists as oil, gum, rubber (elastomer), film or powder depending on the molecular weight, cross-linking density and the structure. Many kinds of chemical groups and oligomeric segments can be introduced in the siloxane structures. Thus, various kinds of properties and functions could be given to silicone. That is, silicone is an excellent material for industry and has potential abilities for future.

Silicones have been historically synthesized in solution phase. Recently several efforts have been done to prepare polysiloxane based thin films by CVD starting from low molecular weight siloxane species[11,12]. This is called "plasma polymerization". Using this technologies several chemical groups such as trifuluoromethyl[13] and amino[14] groups were reported to be introduced in polysiloxane based thin films. Plasma polymerization of siloxanes are believed to have potential abilities to give thin films having advanced functions.

Silsesquioxane

The general sturucture of silsesquioxane is described as $RSiO_{3/2}$, where R is hydrogen or organic group, and its SiO bond order is three. Generally, silsesquioxane is more resin-like (ie, more inorganic) than siloxane. However, there are not much studies yet on silsesquioxane compared to siloxane. Several types of silsesquioxane such as phenyl[15], methyl[16] and hydrogen[17] were known and several of them are industrially used. Mostly they are synthesized from chlorosilanes or alkoxysilanes.

Typical structures of silisesquioxanes are cage and ladder. Structure is much dependent on synthesis method. Sometimes they have different properties even though they have a same formula.

Generally silsesquioxanes have high thermal stabilities and tough strengths. They can sometimes give thin films, and are believed to have potential abilities for future applications.

$SiO_2$

The SiO bond order for silicon dioxide is four. It is the completely inorganic material and well known as a stable, electrically insulating and hard material. It has several structures, however, the above properties are seen in any structure basically.

One of major application of silicon dioxide is inter layer dielectric in LSI. No other very excellent materials were found yet on this application. However, the dielectric constant of silicon dioxide, around 4, will not meet requirements for future LSI devices. “Low k” is indeed required. So that, technologies breakthroughs are needed.

### 1.3 Purpose of this study

To respond to requirements for highly advanced electronics applications, it is needed to design materials by correctively selecting a dimension of silicon and functions. Table 1 summarizes present and possible functions of silicon containing materials with regard to electronics application.

In this thesis novel advanced amorphous silicon and silicone polymers that could be applicable for electronics will be introduced. Novel areas on dimension or function for silicon were studied. Mechanism understanding for synthesis of the materials and their properties will be discussed. Also, application performances will be shown and discussed.

This thesis consists of seven chapters. Chapter 1 is an introduction of this thesis. Chapter 2 describes amorphous organosilicon films prepared by plasma CVD. Chapter 3 describes also CVD films that are applicable for passivation of ceramic superconductors. In Chapter 4 novel siloxane/PEO based polymer electrolytes are introduced. Those will be applicable for lithium batteries. Chapter 5 describes polysiloxane ionomers for ER (electrorheological fluid) applications. In Chapter 6 polyhydrogensilsesquioxane is introduced and its thin films for inter layer dielectrics applications are discussed. Finally Chapter 7 presents the conclusion of this thesis.

## References


1) W. E. Spear and P. G. LeComber, *Solid State Commun.*, **17**, 1193(1975)
2) W. Noll, *"Chemistry and Technology of Silicones", Academic Press*, 1968, p. 3
3) *"Silicone Materials Handbook", Dow Corning Toray Silicone Co., Ltd.*, Aug. 1993, p. 281
4) Y. Tawada, H. Okamoto and Y. Hamakawa, *Appl., Phys., Lett.*, **39**, 237(1980)
5) H. Koinuma, M. Funabashi, K. Kishio, M. Kawasaki, T. Hirano and K. Fueki, *Jpn. J. Appl. Phys.*, **25**, 1811(1986)
6) R. West, L. D. Daved, P. I. Djurovich, K. L. Stearly, K. S. V. Srinivasen and H. YU, *J. Am. Chem. Soc.*, **103**, 1352(1981)
7) P. Trefonas Ⅲ, P. I. Djurovich, H. Y. Zhang, R. West, R. D. Miller and D. C. Hofer, *J. Plym. Sci., Plym. Lett.*, Ed., **21**, 819(1983)
8) D. J. Wolford, J. A. Reimer and B. A. Scott, *Appl. Phys. Lett.*, **42**, 369(1983)
9) N. Matsumoto, H. Suzuki and H. Miyazaki, *"Silicon-Containing Polymers" (R.G. Jones et al (eds.), Kluwer Academic Publishers, 2000*), pp. 531
10) E. G. Rochow, *US Patent*, 2,380,995(1941)
11) Y. Osada, *Sen-i Gakkaishi*, **37**(7), 243(1981)
12) Y. Osada, *J. Polym. Sci. Polym. Lett. Ed.*, **19**, 369(1981)
13) A. F. Diaz and R. Hernandez, *J. Polym. Sci. Polym. Lett. Ed.*, **22**, 1123(1984)
14) N. Inagaki and K. Oh-ishi, *J. Polym. Sci. Polym. Lett. Ed.*, **23**, 1445(1985)
15) J. F. Brown, L. H. Vogt, A. Katchman, *J. Am. Chem. Soc.*, **82**, 6194(1960)
16) Y. Abe, *J. Polym. Sci. Part A: Polym. Chem.*, **33**, 751(1995)
17) C. L. Frye and W. T. Collins, *J. Am. Chem. Soc.*, **92**, 5586(1970)

## Chapter 2

## Amorphous organosilicon films prepared by plasma CVD

2.1 Introduction 16

2.2 Experimental part and calculations 18

2.2.1 Synthesis of amorphous films from phenylsilanes by plasma chemical vapor deposition 18

2.2.2 Glow discharge decomposition of phenylsilane in the presence of oxygen 20

2.3 Results 21

2.3.1 Synthesis of amorphous films from phenylsilanes by plasma chemical vapor deposition 21

2.3.2 Glow discharge decomposition of phenylsilane in the presence of oxygen 27

2.4 Discussion 33

2.3.1 Synthesis of amorphous films from phenylsilanes by plasma chemical vapor deposition 33

2.3.2 Glow discharge decomposition of phenylsilane in the presence of oxygen 35

2.5 Conclusion 38

## 2.1 Introduction

Since Spear et al. reported that amorphous silicon films prepared by plasma CVD (chemical vapor deposition) could be usable for solar cell applications[1], it has been focused as a key material for both academic and industrial studies. CVD technologies has been focused on not only amorphous silicon films but also other silicon based thin films such as $SiO_2$, SiC and SiN that are currently used and studied very widely at microelectronics applications such as for IC devices.

In this chapter studies on plasma CVD using organosilanes having phenyl and/or methyl groups as source gasses are described. Not many prior studies on this theme had been found. Silanes with aromatic substituents are expected to show specific reactivities in plasma reactions due to the possible contribution of $\sigma$ - $\pi$ conjugation, to deposit films having specific electronic properties.

Firstly basic understanding of the plasma reactions was investigated. Secondly film characterization was done and possible applications of the films were considered.

Haller et al. reported that phenyl substituted silanes were polymerized without splitting off the phenyl rings in an inductively-coupled plasma to give crosslinked polysilane chains with pendant phenyl groups[2-5].

Koinuma et al. prepared amorphous silicon carbide films by glow discharge decomposition of methylsilanes and observed a qualitative correlation between the bond energies in the methylsilanes and the structure of the deposited films. The calculated strong Si-C bonds in methylsilanes were hardly decomposed in plasma reactions using conventional radio frequency (*rf*)-power conditions; the Si-C bonds were incorporated into amorphous films with homogeneous distributions[6].

Systematic studies on plasma CVD of phenyl-substituted silanes are essentially meaningful, since they may give special electronic states in deposited films based on the aromatic rings and novel functions different from the films from methyl-substituted silanes were expected.

Amorphous films were prepared by glow discharge decomposition of phenylsilane ($SiH_3C_6H_5$)(PS) and methylphenylsilane ($SiH_2CH_3C_6H_5$)(MPS) in order to further investigate the reactivity of the source materials in a plasma process. The electronic states of the starting materials were estimated by a quantum chemical calculation based on the MNDO (Modified Neglect of Diatomic Overlap) method. Furthermore, the structure and properties of the films were examined as a function of

*rf*-power applied to the plasma decomposition system.

Then, the glow discharge decomposition of phenylsilane using a high vacuum chamber in the presence of specified amounts of oxygen is described to elucidate the role of oxygen.

In the synthesis of thin films via dehydrogenating chemical vapor deposition such as in the diamond-like film synthesis from mechane, oxygen was reported to play a specific role[7)]. On the other hand, it has been frequently observed by means of XPS (X-ray photoelectron spectroscopy) that the plasma polymerization of organosilicon compounds produces crosslinked organosilicon films containing significant amounts of oxygen even under conditions supposedly free of oxygen[8)]. Therefore, it is significant to strictly control the oxygen amount in the reaction system, in order to investigate the influence of oxygen.

## 2.2 Experimental part and calculations

### 2.2.1 Synthesis of amorphous films from phenylsilanes by plasma chemical vapor deposition

The molecular orbital (MO) calculation was conducted by the semi-empirical MNDO method using a Hitachi M-680H computer system at The University of Tokyo.

PS was prepared by hydrogenation of trichlorophenylsilane and purified by distillation; b.p. 119 ℃. MPS was a commercial product (from Chisso Co.); b.p. 139 – 140 ℃.

The films were deposited in a capacitively-coupled plasma CVD apparatus (13.56 MHz, electrode diameter: 10 cm, distance between the electrodes: 3 cm). Figure 1 illustrates the plasma deposition system used for this study. As PS and MPS are liquid at room temperature, the vapors of PS and MPS were saturated in a carrier gas (helium) at a constant temperature. Then, the gas mixture containing PS or MPS was introduced into the reactor at a flow rate of 10 $cm^3 \cdot min^{-1}$ (partial flow rate of PS or MPS = 0.8 $cm^3 \cdot min^{-1}$) to be decomposed by the glow discharge under the following conditions; total pressure $P_T$ = 40 – 93 Pa, *rf*-power = 0.5 – 80 W, substrate temperature : $T_S$ = 100 – 300 ℃. Both Corning #7059 glass and single-crystal silicon wafers were used as substrates. Table 1 summarizes the conditions for plasma CVD.

Thickness of the films was measured by a Taylor Hobson TALYSTEP. Infrared spectra were recorded on a Shimadzu FTIR-4000 spectrometer. Raman scattering measurements were performed in the back scattering configuration using a JASCO NR-1100 spectrometer. (An argon ion laser of 5145 Å was used for the pumping light.) The optical band gaps of the films were determined from the intercepts of the linear parts of $(\alpha \cdot h \cdot \nu)^{1/2}$ vs. $h \cdot \nu$ plots where the absorption coefficient $\alpha$ was derived from the UV-VIS spectra measured by a HITACHI-340 spectrometer. Electric conductivity was measured by the gap-cell method.

A substitutional doping was carried out by decomposing a mixture of PS/He or MPS/He (10 $cm^3 \cdot min^{-1}$) and $B_2H_6/H_2$ (4 $cm^3 \cdot min^{-1}$) (1 vol.%) in the plasma reactor under the conditions described above. The actual mole ratio of $B_2H_6$/(PS or MPS) was 1/20. A chemical doping was carried out by exposing a film with gold plated electrodes to $I_2$-vapor (saturated in vacuum at room temperature) for 24 hours, and evacuating the adsorbed iodine for 3 hours.

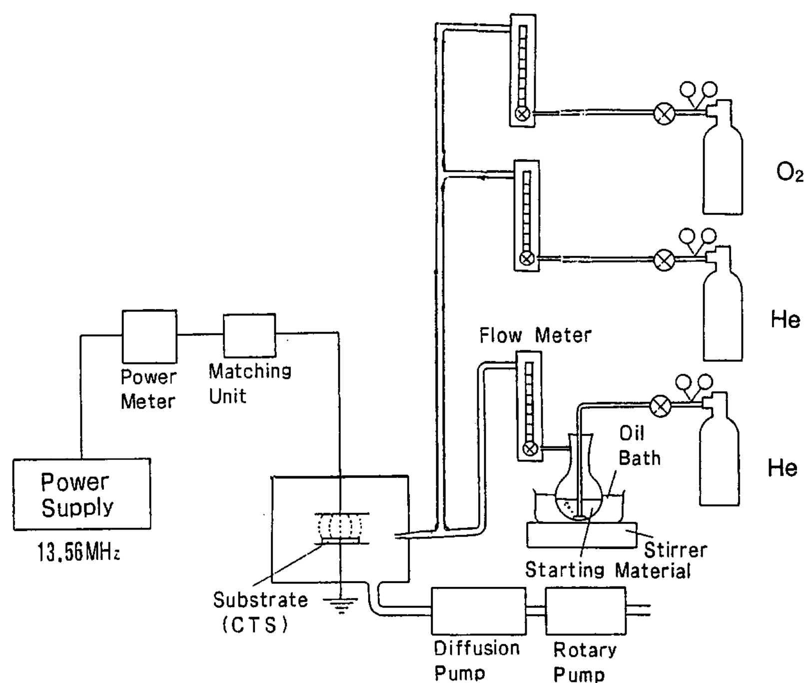


Fig.1. Plasma deposition system for phenylsilane and methylphenylsilane.

Table 1. Conditions for plasma CVD for phenylsilane and methylphenylsilane.

| Item | Condition |
|---|---|
| Plasma type | Capacitively-coupled |
| Frequency of power | 13.56 MHz |
| Electrode | Parallel plate, 10cm $\phi$ 3cm d |
| Carrier gas | Helium |
| Flow rate of mixed gas | 10 $cm^3 \cdot min^{-1}$ |
| Partial flow rate of PS/MPS | 0.8 $cm^3 \cdot min^{-1}$ |
| Total pressure | 40 - 93 Pa |
| *Rf* power | 0.5 - 80 W |
| Substrate temperature | 100 - 300 ℃ |
| Substrate | Corning #7059, Silicon wafer |

### 2.2.2 Glow discharge decomposition of phenylsilane in the presence of oxygen

Experiments were carried out in the same manner as in the Section 2.2.1 except the followings.

Molecular oxygen was mixed with phenylsilane (mole ratio $O_2/C_6H_5SiH_3$ = 0.5 at highest) and the mixed gas was decomposed by an *rf* plasma as shown in Section 2.2.1. Prior to introducing the mixed gas, the base pressure in the reaction chamber was below $6.7 \times 10^{-5}$ Pa. Helium as carrier gas was introduced into a bubbler filled with phenylsilane at 50 ℃, where the vapor pressure of phenylsilane was $8.0 \times 10^3$ Pa. Oxygen (99.99 %) was diluted to 1 vol.% with helium. The mixed gasses of 8 vol.% $C_6H_5SiH_3$/He and 1 vol.% $O_2$/He were introduced into the reactor through different mass flow controllers at flow rates of 10 sccm (standard cubic centimeter per minute) and 0 – 40 sccm, respectively. Thus, the $O_2/C_6H_5SiH_3$ mole ratio was varied from 0 to 0.5. The mixed gas was decomposed by the glow discharge under the following conditions; total pressure 40 Pa, *rf* power 0.5 – 80 W, substrate temperature 100 ℃.

XPS spectra were recorded on a JEOL JPS-80 spectrometer under the following conditions; X-ray target: aluminum, X-ray power: 12 kV / 15 mA. The sample surfaces were etched by argon plasma to the depth of about 100 nm before the measurement. Atomic compositions of the films were analyzed on the basis of the peak areas for $Si_{2p}$, $C_{1s}$ and $O_{1s}$ in the XPS spectra.

Table 2. Conditions for plasma CVD for phenylsilane in the presence of oxygen.

| Item | Condition |
|---|---|
| Plasma type | Capacitively-coupled |
| Frequency of power | 13.56 MHz |
| Electrode | Parallel plate, 10cm φ 3cm d |
| Carrier gas | Helium |
| Flow rate of 8 vol. % PS/He | 10 $cm^3 \cdot min^{-1}$ |
| Flow rate of 1 vol.% $O_2$/He | 0 - 40 $cm^3 \cdot min^{-1}$ |
| Total pressure | 40 Pa |
| *Rf* power | 0.5 - 80 W |
| Substrate temperature | 100 ℃ |
| Substrate | Corning #7059, Silicon wafer |

## 2.3 Results

### 2.3.1 Synthesis of amorphous films from phenylsilanes by plasma chemical vapor deposition

Table 3 shows the results of the MNDO MO calculation on PS and MPS, together with that on methylsilane ($SiH_3CH_3$)(MS), listed for comparison. The two center bond energies for the Si-H and the Si-C bonds in PS and MPS are almost the same as the corresponding energies in MS. The differences between the HOMO (Highest Occupied Molecular Orbital) and the LUMO (Lowest Unoccupied Molecular Orbital) energies, $\Delta E$, for PS and MPS are smaller than $\Delta E$ for MS.

Figure 2 shows the dependence of the film deposition rate in the glow discharge decomposition of PS and MPS on the *rf*-power. The deposition rate decreases as the *rf*-power increases. The films deposited at relatively high *rf*-powers from both PS and MPS were hard and had dark brown colors, whereas those deposited at lower *rf*-powers were apparently softer and almost colorless.

A part of the IR spectra of the deposited films is shown in Fig.3. The films prepared from PS and MPS at the same *rf*-powers gave almost the same spectral patterns. In addition to the absorption due to the C-H stretchings at 2800 – 3100 $cm^{-1}$, shown in Fig.3, $Si\text{-}H_n$ (n = 1,2) stretching and C-C skeletal vibration absorption bands are clearly seen at 2100 – 2200 $cm^{-1}$ and about 1430 $cm^{-1}$, respectively, in the films prepared at lower *rf*-powers ($\leq$ 2 W). The absorption at 3050 $cm^{-1}$, which can be assigned to the C-H bond in the phenyl group, is stronger in the spectra of the films prepared at lower *rf*-powers, whereas it is scarcely observed in the spectra of the films prepared at higher *rf*-powers ($\geq$ 10 W). In the spectrum of the film prepared at an *rf*-power of 0.5 W, the aromatic C-H absorption is larger than the aliphatic C-H absorption at 2900 $cm^{-1}$.

Figure 4 shows the Raman spectra of the films deposited from PS at *rf*-powers of 0.5 and 80 W. In the spectrum of the film prepared at 0.5 W, no Raman bands were observed except the sharp band at 521 $cm^{-1}$, which is assignable to the Si-Si band of the crystalline silicon substrate. Other bands are hidden by the strong background luminescence. The spectrum of the film prepared at 80 W has two weak and broad bands at about 1360 and 1590 $cm^{-1}$.

Figure 5 shows the dependences of the optical band gaps ($E_{opt}$) of the films on the *rf*-power used for the film deposition; the $E_{opt}$ decreases with increasing rf-power.

Table 3. Two-center bond energies and frontier orbital energies for methylsilane, phenylsilane and methylphenylsilane, calculated by the MNDO[a] method.

| Molecule | Two center bond energy in eV | | | | | |
|---|---|---|---|---|---|---|
| | Si—H | Si—C(Me) | Si—C(Ph) | C—H(Me) | C—H(Ph) | C—C |
| $CH_3SiH_3$ | −12,39 | −14,67 | | −12,30 | | |
| $C_6H_5SiH_3$ | −12,68 | | −16,30 | | −12,90 | −20,01 |
| $C_6H_5Si(CH_3)H_2$ | −12,30 | −14,51 | −15,87 | −12,30 | −12,90 | −20,01 |

| Molecule | Orbital energy in eV | | |
|---|---|---|---|
| | HOMO[b] | LUMO[c] | $\Delta E$[d] |
| $CH_3SiH_3$ | −11,53 | 2,54 | 14,07 |
| $C_6H_5SiH_3$ | −9,38 | 0,17 | 9,55 |
| $C_6H_5Si(CH_3)H_2$ | −9,38 | 0,18 | 9,56 |

[a] Modified Neglect of Diatomic Overlap.
[b] Highest Occupied Molecular Orbital.
[c] Lowest Unoccupied Molecular Orbital.
[d] Engery difference between HOMO and LUMO.

Fig.2. Dependence of the deposition rate of films from phenylsilane (○) and methylphenylsilane (●) plasmas on the *rf*-power. $P_T$ (total pressure) = 40 Pa; $T_S$ (substrate temperature) = 100 °C

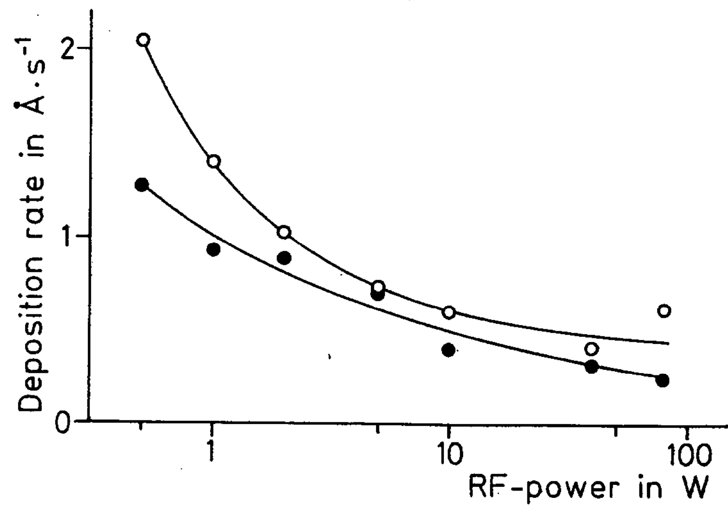


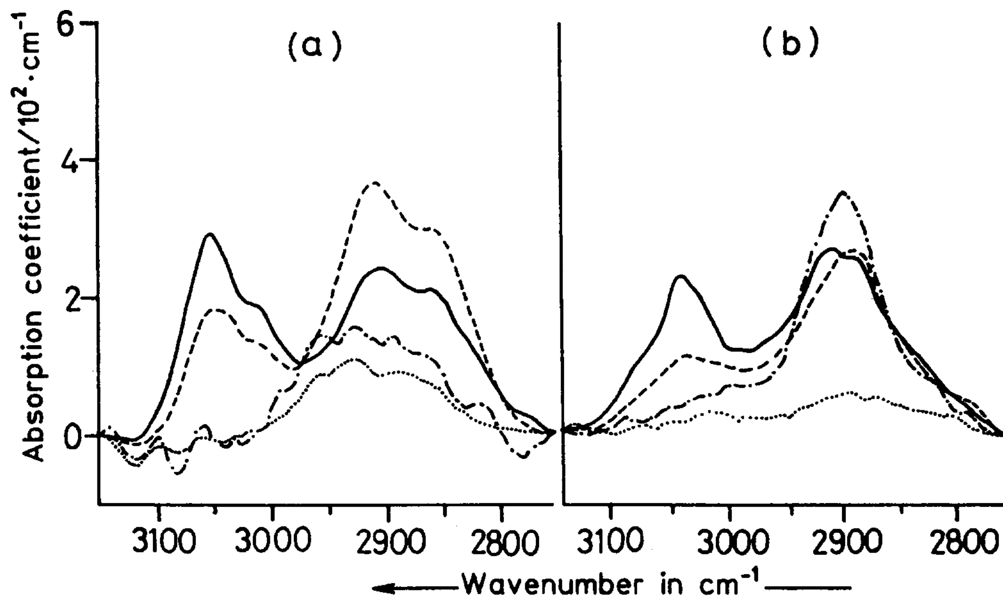


Fig.3. Infrared spectra of films prepared from phenylsilane (a) and methylphenylsilane (b) at different *rf*-powers. (———): 0,5 W, (– – –): 1 W, (– · –): 10 W, (· · ·): 80 W. $P_T$ = 40 Pa, $T_S$ = 100 °C

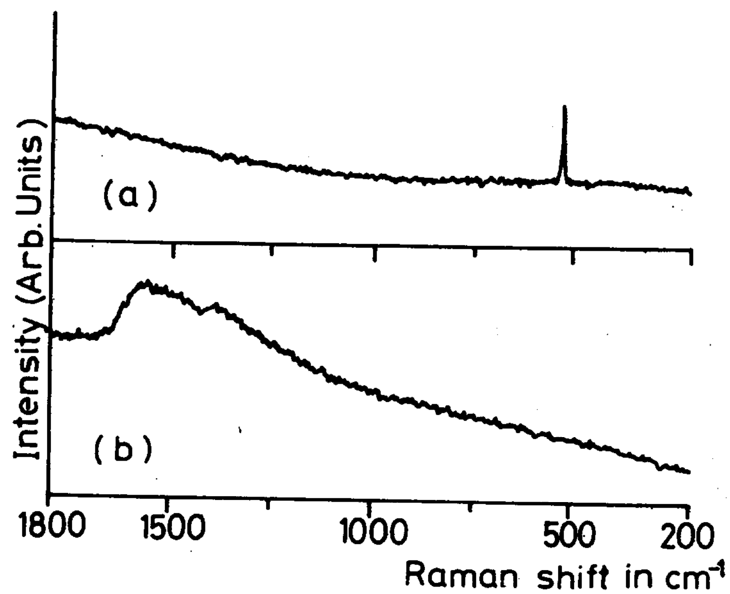


Fig.4. Raman spectra of films prepared from phenylsilane at different *rf*-powers of 0,5 W (a) and 80 W (b). $P_T$ = 40 Pa, $T_S$ = 300 °C

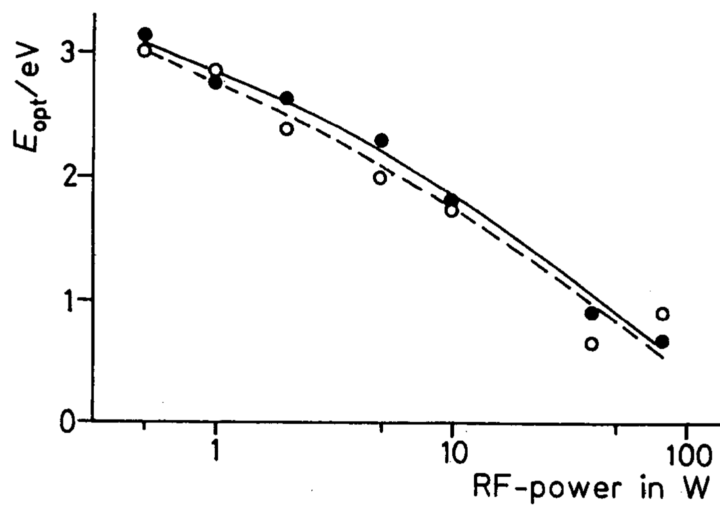


Fig.5. Optical band gaps of films prepared from phenylsilane (○) and methylphenylsilane (●) as a function of *rf*-power. $P_T$ = 40Pa, $T_S$ = 100 °C

The dark conductivities of the as-deposited films were in the range $10^{-10} - 10^{-12}$ $S \cdot cm^{-1}$ and $10^{-9} - 10^{-11}$ $S \cdot cm^{-1}$ for the films prepared from PS and MPS, respectively. None of the films showed photoconductivities when the films were irradiated from a Xe-lamp. Table 4 shows the conductivities of the films doped substitutionally with $B_2H_6$ or chemically with $I_2$. Almost all the samples tested showed conductivity enhancements as much as four orders of magnitude by the boron doping and six orders by the iodine doping. The conductivities of the iodine doped films dropped almost instantaneously (< 1 min) by one to two orders of magnitude when the films where irradiated with a Xe-lamp, probably due to the partial evaporation of iodine absorbed in the films. Similar but slower decreases in the conductivities were detected when the films were kept standing in air. The conductivities were recovered by exposing the film again to $I_2$ vapor. The conductivities of the boron doped films were unchanged by such a treatment as the light irradiation.

The UV-VIS spectra of films changed by iodine doping in the films, deposited at an *rf*-power of 0.5 W, as shown in Fig.6. The spectra scarcely changed in the films deposited at higher *rf*-powers. A new absorption band appeared at 370 nm.

In all these experiments, the presence of methyl group in MPS has little influence on the doping property of deposited films, as compared with the films prepared from PS.

Table 4. Dark conductivities ($\sigma_{dark}$) of as-deposited, substantially (boron) doped[a] and chemically (iodine) doped[b] films prepared from phenylsilane (PS) and methylphenylsilane (MPS)

| Source material | *rf*-power[c] in W | $\sigma_{dark}/(S \cdot cm^{-1})$ | | |
|---|---|---|---|---|
| | | as-deposited | boron doped | iodine doped |
| $C_6H_5SiH_3$ | 0,5 | $4,7 \cdot 10^{-12}$ | $5,4 \cdot 10^{-9}$ | $2,5 \cdot 10^{-8}$ |
| | 2 | $5,1 \cdot 10^{-12}$ | $1,8 \cdot 10^{-10}$ | $4,2 \cdot 10^{-6}$ |
| | 5 | $1,2 \cdot 10^{-11}$ | $3,5 \cdot 10^{-9}$ | $1,2 \cdot 10^{-9}$ |
| | 40 | $1,2 \cdot 10^{-10}$ | $1,9 \cdot 10^{-8}$ | $1,9 \cdot 10^{-8}$ |
| $C_6H_5Si(CH_3)H_2$ | 0,5 | $1,8 \cdot 10^{-9}$ | $1,5 \cdot 10^{-8}$ | $2,2 \cdot 10^{-6}$ |
| | 2 | $1,1 \cdot 10^{-11}$ | $1,7 \cdot 10^{-9}$ | $5,6 \cdot 10^{-9}$ |
| | 5 | $1,1 \cdot 10^{-9}$ | $6,2 \cdot 10^{-10}$ | $1,7 \cdot 10^{-8}$ |
| | 40 | $4,5 \cdot 10^{-11}$ | $5,0 \cdot 10^{-7}$ | $4,8 \cdot 10^{-7}$ |

[a] Decomposing a mixture of $B_2H_6$/(PS or MPS) (mole ratio 1/20) in the plasma reactor.
[b] Exposing a film to $I_2$ vapor (saturated i. vac. at room temp.) for 24 h.
[c] Applied to the film deposition.

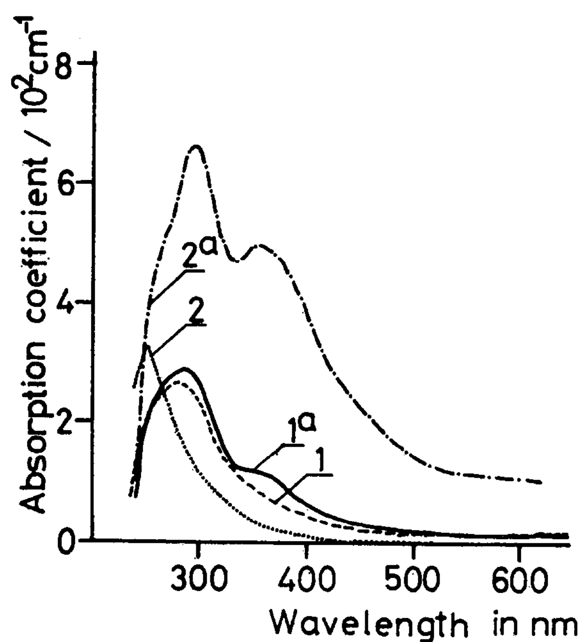


Fig.6. Ultraviolet and visible spectra of as-deposited and iodine doped films prepared from phenylsilane (PS) and methylphenylsilane (MPS) at an *rf*-power of 0,5 W. (1): as-deposited from PS, (1a): after exposing (1) to $I_2$ vapor for 24 h; (2): as-deposited from MPS, (2a): after exposing (2) to $I_2$ vapor for 24 h

### 2.3.2 Glow discharge decomposition of phenylsilane in the presence of oxygen

*Deposition rate*

Figures 7 and 8 show the dependences of the film deposition rate on the *rf* energy and the oxygen content in the source gas, respectively. The deposition rates in both the pure $C_6H_5SiH_3$ and the $O_2/C_6H_5SiH_3$ (mole ratio 0.025) mixture systems decreased as the rf energy increased. The deposition rate was higher for the $O_2/C_6H_5SiH_3$ (0.025) mixture system than for the pure $C_6H_5SiH_3$ system at low rf energies ($\leq$ 10 W). However, the rate decreased as the $O_2/C_6H_5SiH_3$ mole ratio increased further and was lower in the $O_2/C_6H_5SiH_3$ (0.5) system than that in the pure $C_6H_5SiH_3$ system.

*Structure of deposited film*

Figure 9 shows the infrared spectra of films deposited at different *rf* energies. The spectra of the films prepared from $O_2/C_6H_5SiH_3$ (0.025 and 0.1) mixtures are analogous to those of films prepared from pure $C_6H_5SiH_3$. It is noteworthy that absorptions at 1000 – 1100 $cm^{-1}$ assignable to the Si-O-Si structure were not detected even for the films prepared from $O_2/C_6H_5SiH_3$ mixtures with a mole ratio as high as 0.5. For *rf* energies lower than 10 W, both of the $O_2/C_6H_5SiH_3$ and the pure $C_6H_5SiH_3$ systems led to deposited films having characteristic absorptions at 2800 – 3100 $cm^{-1}$, 2100 – 2200 $cm^{-1}$ and 1430 $cm^{-1}$, which could be assigned to C-H stretching, Si-$H_n$ stretching and Si-$C_6H_5$ stretching modes, respectively. These films also have weak absorptions around 1600 $cm^{-1}$ and 1500 $cm^{-1}$ assignable to C=C skeletal in-plane vibration in the phenyl ring. These absorptions except the one around 2900 $cm^{-1}$ decreased for films prepared at higher *rf* energies. The films deposited at *rf* powers higher than 40 W exhibited little organic moiety, clearly indicating that phenylsilane was highly fragmented in such an *rf* energy range[9)]. The absorption around 3050 $cm^{-1}$ assignable to the aromatic C-H bond was detected in the films prepared at the *rf* power range lower than 10 W, besides the absorption around 2900 $cm^{-1}$ assignable to an aliphatic C-H bond. The absorption around 2900 $cm^{-1}$ increased as the *rf* energy increased and decreased again in the higher (> 10 W) *rf* energy range.

Figure 9 shows that the absorptions due to Si-$H_n$ and Si-$C_6H_5$ structures are significant in the films prepared from $O_2/C_6H_5SiH_3$ (0.025).

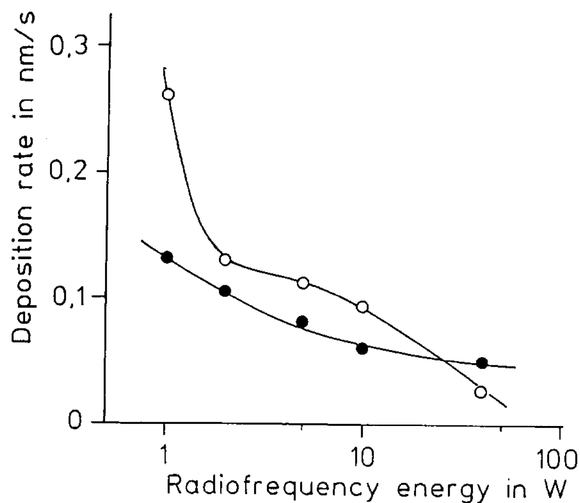


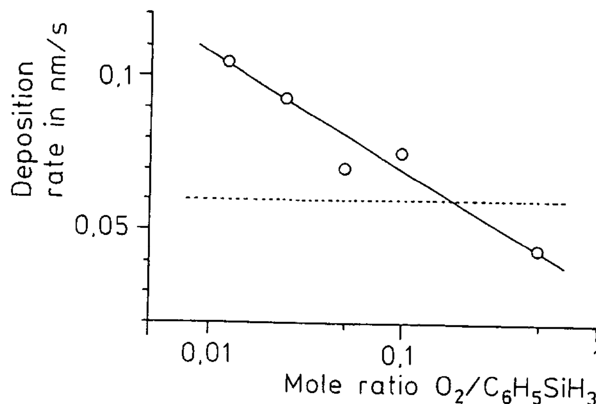


Fig.7. Dependence of the deposition rate of films from pure phenylsilane (●) and a mixture of phenylsilane and oxygen (mole ratio $O_2/C_6H_5SiH_3$ = 0,025) (○) on the rf energy. (The reliability of each datum affected by experimental errors lies within ±15%)

Fig.8. Dependence of the deposition rate of films on the mole ratio $O_2/C_6H_5SiH_3$ in the source gas; rf energy: 10 W. Dashed line indicates the value of the deposition rate of film prepared from pure phenylsilane. (The reliability of each datum affected by experimental errors lies within ±15%)

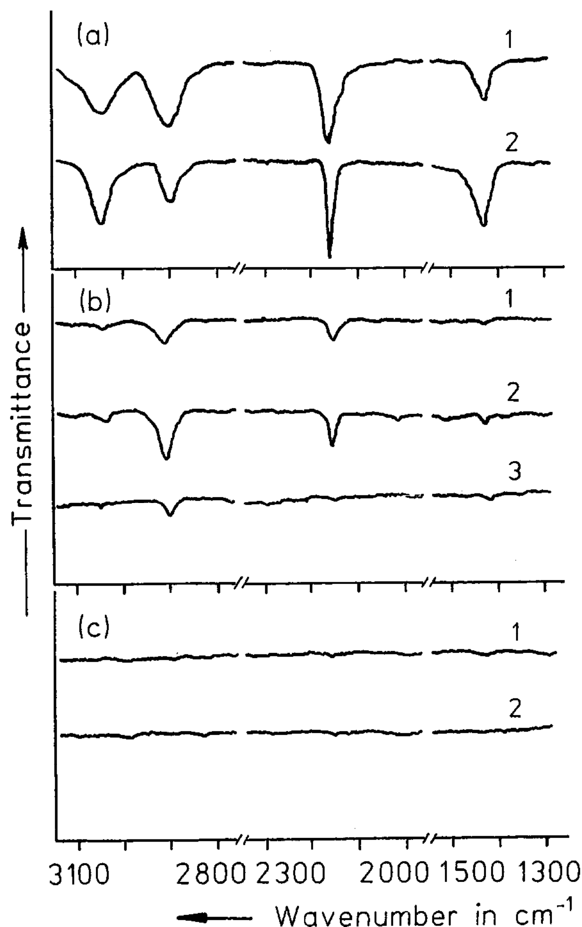


Fig.9. Infrared spectra of films prepared from pure phenylsilane and a mixture of phenylsilane and oxygen at rf energies of 1 W (a), 10 W (b) and 40 W (c), 1: pure $C_6H_5SiH_3$; 2: mole ratio $O_2/C_6H_5SiH_3$ = 0,025; 3: mole ratio $O_2/C_6H_5SiH_3$ = 0,1

Table 5 shows the atomic compositions of the deposited films analyzed from the XPS data. In all of the films, considerable amounts of oxygen were detected even in the film prepared from the pure $C_6H_5SiH_3$ system. The mole ratios C/Si in all the films were slightly higher than the stoichiometric value (6.0) in the starting material.

*Properties of deposited films*

Figures 10 and 11 show the optical band gap values $E_{opt}$ of films prepared at different *rf* energies and oxygen contents in the source gas. The films deposited from both the $O_2/C_6H_5SiH_3$ (mole ratio 0.025) mixture and the pure $C_6H_5SiH_3$ systems at low *rf* energies exhibit $E_{opt}$ values of about 3.0 eV which is considerably larger than 1.7 eV that is observed in ordinary hydrogenated amorphous silicon films. The $E_{opt}$ values decreased as the *rf* energy increased, and they were higher for the films prepared from $O_2/C_6H_5SiH_3$ systems with mole ratios lower than 0.05 than in the films prepared from pure $C_6H_5SiH_3$ at *rf* energies higher than 1 W.

Table 6 shows the electric conductivity ($\sigma_{dark}$) of the films measured before (as-deposited) and after the exposure of the films to iodine vapor at 25 ℃. The as-deposited films from systems with added $O_2$ had values of $10^{-11}$ to $10^{-7}$ $S \cdot cm^{-1}$, which are comparable to the value observed for the film prepared from the pure $C_6H_5SiH_3$ system. The electric conductivity of almost all specimens was enhanced by iodine doping as much as four orders of magnitude.

*Plasma diagnostics*

In QMS (quadrupole mass spectrometry) analysis of the pure $C_6H_5SiH_3$ plasma ($O_2$-free) without using an ionizing filament, five main ionic species with mass numbers *m/z* = 15, 26, 28, 78 and 107 were detected. These species can be assigned to $CH_3^+$, $C_2H_2^+$, $Si^+$, $C_6H_6^+$ and $SiH_2C_6H_5^+$, respectively. The number of ionic species was increased by the addition of oxygen. Besides these five species, a species with *m/z* = 18 was clearly detected which can be assigned to $H_2O^+$. Furthermore, unspecified ionic species with *m/z* = 27, 29, 38, 41, 42, 70 and 72 were detected in the systems with added $O_2$.

Table 5. Atomic composition in films prepared from phenylsilane and a mixture of phenylsilane with oxygen as analyzed with X-ray photoelectron spectra[a].

| Mole ratio of $O_2/C_6H_5SiH_3$ | rf Energy power[b] in W | Atomic composition in % | | | Mole ratio C/Si |
|---|---|---|---|---|---|
| | | Si | C | O | |
| Pure $C_6H_5SiH_3$ | 10 | 9,2 | 62,8 | 28,0 | 6,80 |
| 0,025 | 1 | 11,3 | 71,2 | 17,5 | 6,30 |
| 0,025 | 10 | 11,6 | 78,4 | 10,0 | 6,76 |
| 0,025 | 40 | 10,6 | 72,6 | 16,8 | 6,85 |
| 0,05 | 10 | 9,6 | 73,5 | 16,9 | 7,66 |
| 0,5 | 10 | 9,2 | 72,6 | 18,3 | 7,89 |

a) The atomic compositions were analyzed using $Si_{2p}$, $C_{1s}$ and $O_{1s}$ peak areas. Measurement conditions; X-ray target: Al, X-ray power: 12 kV, 15 mA.

b) Applied to film deposition.

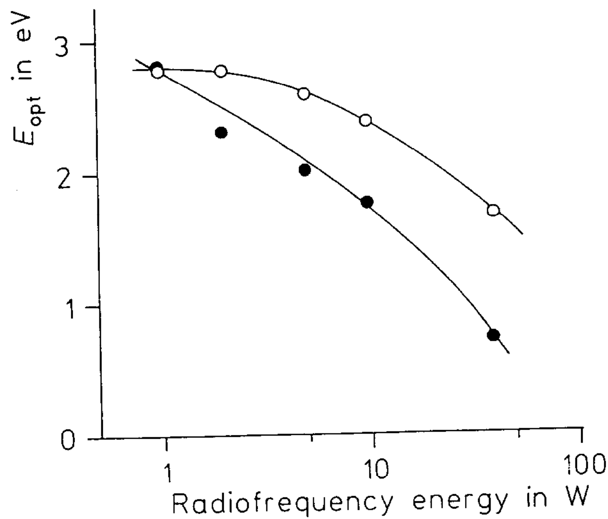


Fig.10.

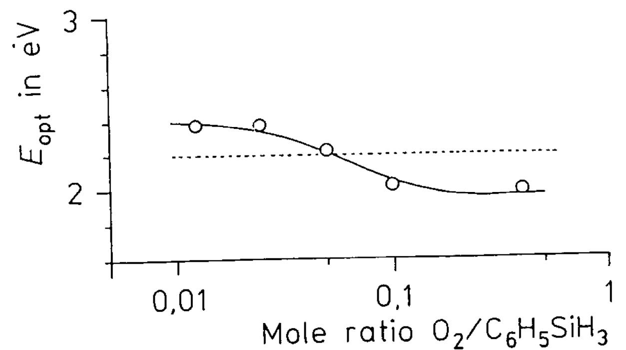


Fig.11

Fig.10. Optical band gaps $E_{opt}$ of films prepared from pure phenylsilane (●) and a mixture of phenylsilane and oxygen (mole ratio $O_2/C_6H_5SiH_3$ = 0,025) (○) as a function of rf energy applied to film deposition. (The reliability of each datum affected by experimental errors lies within ±5%)

Fig.11. Optical band gaps $E_{opt}$ of films prepared from a mixture of phenylsilane and oxygen as a function of mole ratio $O_2/C_6H_5SiH_3$ in the source gas; rf energy: 10 W. The dashed line indicates the value of $E_{opt}$ of a film prepared from pure phenylsilane. (The reliability of each datum affected by experimental errors lies within ±5%)

Table 6. Electric conductivities $\sigma_{dark}$[a)] of as-deposited and iodine-doped[b)] films prepared from phenylsilane and a mixture of phenylsilane and oxygen.

| Mole ratio $O_2/C_6H_5SiH_3$ | rf Energy in W[c)] | $\sigma_{dark}/(S \cdot cm^{-1})$ | |
|---|---|---|---|
| | | as-deposited | iodine-doped |
| Pure $C_6H_5SiH_3$ | 10 | $5,2 \cdot 10^{-11}$ | $1,2 \cdot 10^{-8}$ |
| 0,0125 | 10 | $3,2 \cdot 10^{-11}$ | $1,8 \cdot 10^{-8}$ |
| 0,025 | 1 | $4,5 \cdot 10^{-7}$ | $1,3 \cdot 10^{-6}$ |
| 0,025 | 2 | $4,5 \cdot 10^{-7}$ | $1,1 \cdot 10^{-6}$ |
| 0,025 | 5 | $1,0 \cdot 10^{-8}$ | $6,3 \cdot 10^{-7}$ |
| 0,025 | 10 | $1,7 \cdot 10^{-11}$ | $2,9 \cdot 10^{-9}$ |
| 0,025 | 40 | $3,8 \cdot 10^{-7}$ | $3,4 \cdot 10^{-7}$ |
| 0,05 | 10 | $2,0 \cdot 10^{-10}$ | $4,8 \cdot 10^{-6}$ |
| 0,1 | 10 | $1,0 \cdot 10^{-9}$ | $4,5 \cdot 10^{-6}$ |
| 0,5 | 10 | $8,0 \cdot 10^{-9}$ | $1,6 \cdot 10^{-8}$ |

a) Without light irradiation.

b) Exposing a film to pure $I_2$-vapour for 24 h with saturation vapour pressure at room temperature.

c) Applied to film deposition.

Figure 12 shows the partial pressure of ionic species with *m/z* values assignable to $CH^+$, $H_2O^+$, $C_2H_2^+$, $Si^+$, $C_6H_6^+$ and $SiH_2C_6H_5^+$ versus the *rf* energy. In the plasma system of pure $C_6H_5SiH_3$, the major ionic species were molecular ion $SiH_2C_6H_5^+$ in a low *rf* energy range, $Si^+$ and $C_6H_6^+$ in a middle *rf* energy range, and $CH_3^+$ and $C_2H_2^+$ in a high *rf* energy range. In the plasma system with added $O_2$ (mole ratios $O_2/C_6H_5SiH_3$ 0.025 and 0.05), the amounts of all ionic species were higher than those in the pure $C_6H_5SiH_3$ system resulting in increasing deposition rate.

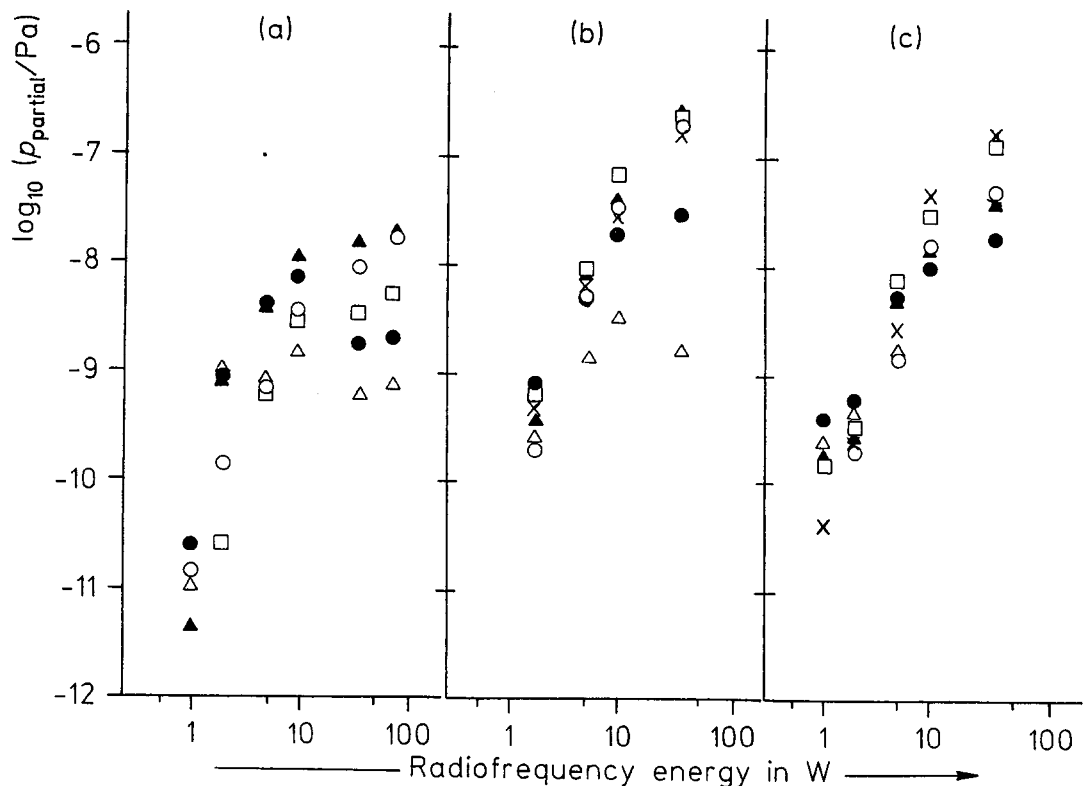


Fig.12. Dependence of partial pressure $p_{partial}$ of ionic species in pure phenylsilane (a), a mixture of phenylsilane and oxygen (mole ratio $O_2/C_6H_5SiH_3$ = 0,025 (b) and 0,05 (c) on the rf energy; mass numbers *m/z* (○): 15, (×): 18, (▲): 26, (□): 28, (●): 78, (△): 107 as measured with a quadrupole mass spectrometer without using an ionizing filament

## 2.4 Discussion

### 2.4.1 Synthesis of amorphous films from phenylsilanes by plasma chemical vapor deposition

The calculated bond strengths for PS and MPS appear to be consistent with the results of Haller et al., who reported the presence of Si-Ph bonds preserved in the film.

The decreased deposition rate at high *rf*-power conditions is considered to originate from the enhanced decomposition of PS and MPS in the gas phase. As it will be discussed later, the more Si-Ph bonds could be cleaved and the split phenyl groups be further fragmented with increasing *rf*-power. Then, relatively high concentration of carbon containing and lower concentration of silicon containing fragments are generated to be the film precursors in the chamber where the pressure is kept constant. The sticking probabilities of carbon containing species were reported to be lower than those of silicon containing species[10]. The deposition rate is presumed to be proportional to the sum of products of the concentrations and sticking probabilities of precursors.

Although the IR spectra of films prepared from PS and MPS are substantially the same, the ratio of the intensities, i.e., (aromatic C-H)/(aliphatic C-H) in the films deposited at low *rf*-powers is slightly larger in the films prepared from PS than the ratio in the films prepared from MPS.

The bands at 1360 and 1590 $cm^{-1}$ in the Raman spectrum for the film prepared at 80 W can be ascribed to the C-C bond in glassy carbon (partially graphatized carbon) structure[11].

According to the data of the IR spectra, the films prepared at low *rf*-powers (< 10 W) should have higher contents of phenyl and Si-H groups. In a diagnosis of the plasma system of PS or MPS by quadrupole mass spectroscopy, it was observed that the concentration of $C_6H_6^+$ and its fragmented ionic species such as $CH_3^+$ and $C_2H_2^+$ increase with increasing *rf*-power. The Si-Ph bond and the phenyl ring in PS and MPS are not decomposed to such a high extent at a low *rf*-power condition, and precursors containing Si-Ph structure could be incorporated in the film. Therefore, the results of Haller et al. agree with ours only when we prepared films at lower *rf*-power conditions.

The $E_{opt}$ values for $\alpha$-Si:H and $\alpha$-SiC:H films, which were prepared from silanes and mixtures of silanes and alkenes, respectively, are known to increase with increasing hydrogen content[12] or C/Si atomic ratio[13]. The one-dimensional polysilane

structure also gave wide $E_{opt}$ values[14]. The large $E_{opt}$ value around 3 eV (much larger than 1.7 eV in the conventional $\alpha$-Si:H) in the films prepared from PS and MPS at low *rf*-powers should be originated from the presence of phenyl groups and polymeric (or so called "pseudo one-dimensional" polysilane) structure. In contrast, the films prepared at high *rf*-powers ($\geq$ 10 W) have smaller contents of phenyl groups and total (C-H and Si-H) hydrogens. Judging from the dark-brown colors and the smaller $E_{opt}$ values (1.5 – 2.0 eV), the films are estimated to have mixed structures of graphite-like carbon clusters and amorphous silicon carbide.

The deposition parameters other than the *rf*-power, such as total pressure and substrate temperature, did not make significant changes in the deposition rates, the film structures and the optical band gaps.

Scheme 1 illustrates the structures of the deposited films from PS and MPS.

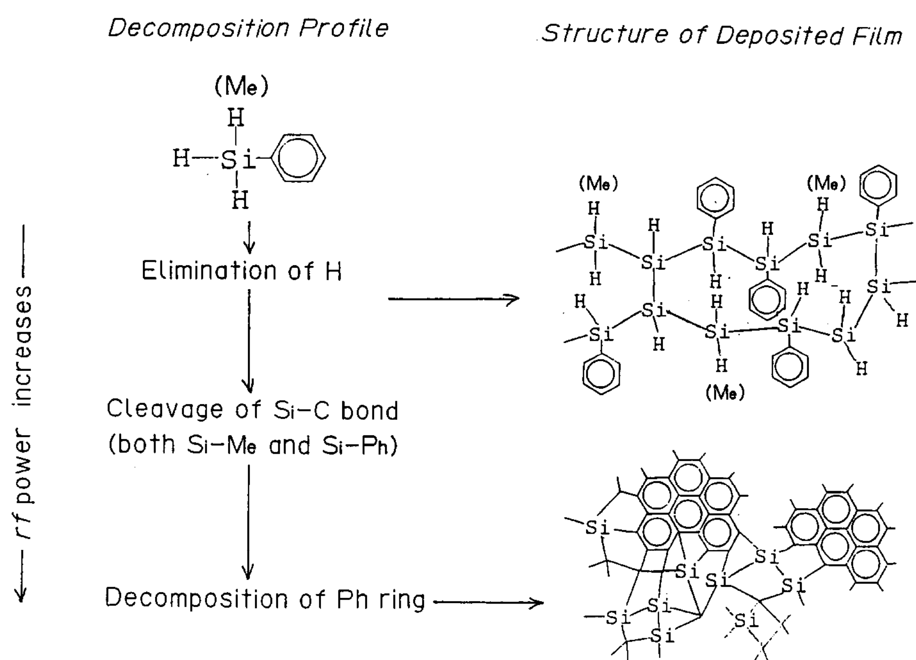


Scheme 1. Schematic drawing of structures of deposited films from phenylsilane and methylphenylsilane.

The new absorption band appeared at 370 nm in the ultra violet and visible spectrum for the iodine doped film is due presumably to a charge-transfer complex formation between the film and the dopant iodine (Eq.(1)).

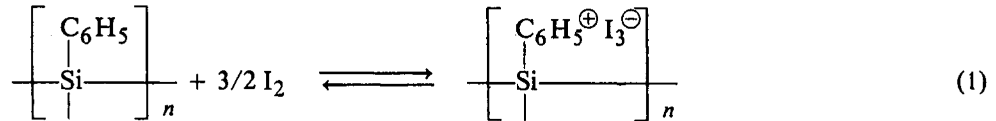

In conclusion, the reaction mode of the Si-C bonds in the glow discharge decomposition of PS and MPS in strongly dependent on the rf-power applied to the plasma decomposition system. The Si-Ph bond is preserved in the film only when the film is deposited at low rf-power conditions, to give $E_{opt}$ values around 3 eV. The films prepared at high rf-powers had lower hydrogen contents and had $E_{opt}$ values of 1.5 – 2.0 eV. The facile cleavage of the Si-Ph bond under high rf-power conditions is rather contradictory to the theoretical calculation which results in a strong Si-Ph bond. This contradiction may be solved by taking into account the electronic excitation of PS and MPS, since the HOMO-LUMO energy gaps, calculated for phenylsilanes, are apparently lower than the gaps for methylsilane

### 2.4.2 Glow discharge decomposition of phenylsilane in the presence of oxygen

*Structure of deposited film*

According to the infrared spectra, it can be concluded that oxygen is scarcely incorporated in the bulk of deposited films even when they were obtained from $O_2/C_6H_5SiH_3$ (mole ratio $\leq$ 0.5) mixtures. The film deposited at the lower *rf* energy range contains larger amounts of $Si\text{-}H_n$ and $Si\text{-}C_6H_5$ structures. The addition of moderate amounts of oxygen may give an effect for preserving monomeric structure in the film. The effect of oxygen described above may be compared with the oxygen effect in a diamond film formation by CVD. In the case of a thermal CVD of a diamond film from a mixture of either methane or ethanol and hydrogen, the addition of the appropriate amount of oxygen was reported to work for facilitating the formation of a

diamond structure at an elevated deposition rate without significant oxygen contamination[7,15].

Judging from the infrared spectra the oxygen containing species in the films are not in the form of siloxane and can be incorporated in the films after the films are exposed to air. Further analyses are needed to clarify the origin of oxygen incorporation in the films.

*Properties of deposited films*

The high band gap numbers for the films prepared at low rf energies should be attributed to such origin as the high contents of hydrogen and carbon[12], the presence of phenyl rings, and "pseudo one-dimensional" polysilane structures[14].

The films prepared from systems added with $O_2$ are expected to retain a higher content of polysilane portions with pendant phenyl groups. As described in Section 2.4.1, the structure of the films deposited from phenylsilane at high *rf* energies is carbon-rich amorphous silicon carbide containing partially graphatized clustered carbon as a result of the cleavage of the Si-$C_6H_5$ bond and the degradation of the phenyl ring.

*Plasma diagnostics*

The decomposition of phenylsilane is considered to occur in the following order as the rf energy increases: the cleavage of an Si-H bond, the cleavage of an Si-$C_6H_5$ bond and then the decomposition of a phenyl ring.

According to molecular orbital calculations for phenylsilane and methylsilane[9], the Si-H bond in phenylsilane may be cleaved via the lowest triplet-excited state slightly more easily than the Si-$C_6H_5$ bond in phenylsilane, and the Si-$C_6H_5$ bond in phenylsilane cleaves more easily than the Si-$CH_3$ bond in methylsilane. These results agreed qualitatively with the plasma reaction mode of phenylsilane which was experimentally obtained using QMS[16], i.e., the reaction proceeded in the following order as the *rf* energy increased: elimination of hydrogen, split of the phenyl ring and fragmentation of the phenyl ring.

The moderate amount of oxygen existing in a $C_6H_5SiH_3$ plasma seems to play a role of promoting a plasma polymerization of $C_6H_5SiH_3$.

Because of the weak O-O bond in oxygen, it is considered that oxygen radicals

are generated easily in a plasma and that the active oxygen radicals extract hydrogen atoms from phenylsilane as well as from the growing film surface. The oxygen radicals can also etch the film with evolution of $H_2O$, $CO$, $CO_2$ and $SiOx$ gases from the surface to decrease the film deposition rate. This etching effect is presumed to be the reason for the decreasing deposition rate observed when the mole ratio $O_2/C_6H_5SiH_3$ was higher than 0.1.

## 2.5 Conclusion

1) The mechanisms for glow discharge decomposition of phenylsilane and methylphenylsilane and the structures of the deposited films were quite similar and significantly dependent on *rf* power applied for the CVD's. Extending bond order around silicon was controllable continuously from 2+ $\delta$ to 4 with *rf* power. As the result, the structure and properties of the deposited films were found to be controlled by silicon bond dimension. Below summarizes the conclusion.

| | Low *rf* power | High *rf* power |
|---|---|---|
| Major degradation | Si-H, C-H | Si-C, Aromatic ring |
| Extending bond order around silicon for deposited film | 2 + $\delta$ | ~4 |
| Structure of film | Polysilane alloy (with Ph groups) | Graphite + a-SiC |
| Optical band gap | ~3 eV | < 1 eV |

2) The SiC bonds in phenylsilane and methylphenylsilane were degradated by plasma more easily than that in methylsilane, although their two center bond energies were similar. Energy difference between HOMO and LUMO can explain the experimental results.

3) The electric conductivities of all the deposited films increased by doping the films with iodine or boron with any *rf* power applied. Application for electrically conductive films is expected.

4) Film deposition rate for the plasma CVD of phenylsilane was promoted with oxygen added to the plasma system.

## References

1) W. E. Spear and P. G. LeComber, *Solid State Commun*., **17**, 1193(1975)

2) I. Haller, *Symp.Proc.-Int. Symp. Plasma Chem.* 5th, 1981, Vol. 1, p. 249; *Chem. Abstr.*, **97**, 145378s(1982)

3) I. Haller, *J. Electrochem. Soc.*, **129**, 180(1982)

4) P. Oelhafen, J. A. Cutro and I. Haller, *J. Electron Spectrosc. Relat. Phenom.*, **34**, 105(1984)

5) J. A. Cutro and I. Haller, *Mater. Res. Soc. Symp. Proc.*, 1985, Vol. 38, p. 343; *Chem. Abstr.*, **103**, 79650p(1985)

6) H. Koinuma, M. Funabashi, K. Kishio, M. Kawasaki, T. Hirano and K. Fueki, *Jpn. J. Appl. Phys.*, **25**, 1811(1986)

7) T. Kawato and K. Kondo, *Jpn. J. Appl. Phys.*, **26**, 1429(1987)

8) Y. Chaterine and A. Zamouche, *Plasma Chem. Plasma Process.*, 5, 353(1985)

9) T. Hirano, K. Sato, T. Nakahira, S. Iwabuchi, K. Kojima, T. Nakamura, V. A. Sinigersky, K. Fueki and H. Koinuma, *Extended Abstracts (The 48th Autumn Meeting, 1987), The Japan Society of Applied Physics*, No. 1, p. 291

10) K. Tachibana, H. Harima and Y. Urano, *Symp. Proc.-Int. Symp. Plasma Chem. 8th*, 1987, Vol. 1, p. 590

11) M. I. Nathan, J. E. Smith Jr. and K. N. Tu, *J. Appl. Phys.*, **45**, 2370(1974)

12) D. J. Wolford, B. A. Scott, J. A. Reimer, R. M. Plecenik and J. A. Bradley, *Bull. Am. Phys. Soc.*, **27**, 145(1982)

13) D. A. Anderson and W. E. Spear, *Philos. Mag.*, **35**, 1(1977)

14) S. Furukawa and N. Matsumoto, *Solid State Cummun.*, **48**, 539(1983)

15) Y. Hirose, *Extended Abstracts (The 48th Autumn Meeting, 1987), The Japan Society of Applied Physics*, No. 3, p. 897

16) T. Nakamura, V. A. Sinigersky, K. Fueki and H. Koinuma, *Extended Abstracts (The 48th Autumn Meeting, 1987), The Japan Society of Applied Physics*, No. 1, p. 290

## Chapter 3

# Silicon based thin films for passivation of superconductors

3.1 Introduction 41

3.2 Experimental part 42

3.3 Results 49

3.4 Discussion 60

3.5 Conclusion 62

### 3.1 Introduction

In this chapter passivation effect as a basic ability of silicon dioxide or silicon nitride is focused on. Extended performances on passivation were studied to respond to requirements on high temperature ceramic superconductors.

Since the Tc (superconducting transition temperature) reached over the boiling point of nitrogen (77 K) for the Y-Ba-Cu-O system in 1987, ceramic superconductors have been focused most intensively as the new industrial material as well as academic interest.

Later in 1987 the oxide system $Tm_{1-x}Ba_xCuO_y$ system was found to exhibit Tc above 90 K for the nominal compositions with $x = 0.6 - 0.8$. The single phase composition was obtained for the specimens around $x = 0.7$. The crystal structure was to be an oxygen deficient perovskite structure reported for the Y-Ba-Cu-O system[1)].

Efforts had started then to prepare ceramic superconducting films. Screen printing was proved to be a promising method for the preparation of superconducting films having Tc's higher than 77 K. The film properties were highly sensitive to the substrate material. A Yb-Ba-Cu-O film prepared on yttria stabilized zirconia substrate has Tc onset and zero resistivity temperatures of 99.1 K and 77.2 K, respectively[2)].

On the other side, these ceramic high temperature superconductors are known to be easily deteriorated in Tc or critical electric current if they contact some gasses or materials, especially water or water vapor. It was reported that conventional inorganic films were not available as passivation layers for the ceramic high temperature superconductors since some chemical reactions occurred during the film deposition[3)]. Among organic films as the passivation layer, a fluoro carbon based film prepared by plasma polymerization was reported to show an excellent passivation against water[3-6)]. Organosilicon compounds can give films having various functions due to their wide abilities of chemical modification.

In this chapter five model species of organosilicon compounds were selected and were plasma polymerized into films. Their ability to passivate ceramic high temperature superconductors was investigated. As well as resistance against water, ability to keep the characteristic of the superconductors at elevated temperatures that correlates to oxygen absorption/desorption at those temperatures will also be discussed.

### 3.2 Experimental part

*Preparation of superconductor samples*

Three types of ceramic high temperature superconductors were selected: Y-system ($YBa_2Cu_3O_x$), Bi-system ($Bi_{0.7}Pb_{0.3}SrCaCu_{1.8}O_x$) and Tl-system ($Tl_2Ba_2Ca_2Cu_3O_x$). Samples were prepared by manually mixing raw material powers in the bulk form into pellets having 1 cm diameter for testing.

Reagents as starting materials were of 99.99 % purity purchased from Furuuchi Chemical. Following is the sample preparation procedure in the case of Y-system. 0.6780 g of $Y_2O_3$, 2.3700 of $BaCO_3$ and 1.4327 g of CuO were mixed with a slight amount of ethanol and grinded thoroughly in an agate mortar, then ethanol was evaporated. The obtained mixed powder of gray color was put on a boat made of high purity alumina and pre-baked at 900 ℃ for 3 h in a muffle furnace (push in at 900 ℃). The atmosphere in the furnace was circulated with outer air involved slightly. The resulting material was black containing slight green that means a ceramitizing reaction took place. After it was cooled, it was grinded again and then baked at 900 ℃ for 3 h in the muffle furnace, followed by cooling down to room temperature in the furnace for 12 h. The obtained ceramic material was grinded into powder and molded into pellets having 1 cm diameter and 0.5 – 1 mm thickness by a pelletizer with about 150 kg/cm pressure applied. The pellets were further baked at 900 ℃ for 3 h in the muffle furnace. The baked pellets were black and had plain surfaces, but were fragile.

In the case of Bi-system, 1.4296 g of $Bi_2O_3$, 0.6009 g of $Pb_3O_4$ and 1.2940 g of $SrCO_3$ and 0.8773 g of $CaCO_3$ were mixed and baked in the same manner. The pre-bake and final bake was carried out 850 ℃ for 24 h and 850 ℃ for 96 h, respectively. The obtained pellets were very hard, but their surfaces were a little rough.

In the case of Tl-system, 2.0497 g of $Tl_2O_3$, 1.7713 g of $BaCO_3$, 0.8982 g of $CaCO_3$ and 1.0708 g of CuO were used. Since $Tl_2O_3$ is volatile, the pre-bake was carried out on the mixture of other ingredients than $Tl_2O_3$. The pre-bake was done in two steps: 850 ℃ for 96 h then 900 ℃ for 120 h. After the pre-bake, $Tl_2O_3$ was added and the mixture was baked at 875 ℃ for 3 h. To prevent the $Tl_2O_3$ material from escaping away from the system, the mixture was put in a crucible with a lid attached for baking. The obtained pellets were hard and had plain surfaces.

*Measurement of electric resistivity*

Electric resistivity was measured by the four-probe method as illustrated in Fig.1. The superconductor pellets were cut into suitable sizes for samples. Gold thin films (thickness about 100 nm) as electrodes were formed on the surface of the sample by vacuum vapor deposition. Copper leading wires of 0.1 mm$\phi$ were attached to the gold electrodes with an electro conducting glue bound. Resistivity was measured under constant currents of either 4 mA or 80 mA. The size of the measured part was ca. 2 mm (L) x 5 mm (W) x 0.7 mm (T). 4 mA as the current *i* corresponds to 0.1 A/cm$^2$ as the current density *J*. The testing unit was slowly taken down in the headspace of a pot in which liquid nitrogen existed to control the temperature of the piece, finally it was dipped in the liquid nitrogen. Resistivity was measured on time to plot between resistivity and temperature.

*Observation of property change with time*

The testing units as illustrated in Fig.1 were stored in various atmospheres. They were taken out from the atmospheres periodically for analysis of the resistivity-temperature relation. The conditions for storing in water vapor were either 25℃/RH100% or 85℃/RH85%. Absorption/desoprption behaviors were investigated as follows. After the testing units were stored in argon atmosphere of 1 atm at 400 ℃ for 10 min, resistivity was measured, then they were stored in air of 1 atm at 400 ℃ for 10 min. In order to minimize the loss time for storing, complete resistivity-temperature plots were not taken but only resistivities at either at room temperature ($R_n$) or at the liquid nitrogen temperature ($R_{liqN2}$) were measured.

*Formation of passivation films*

Passivation films were formed on the testing units as illustrated in Fig.1 by plasma CVD. The CVD apparatus is illustrated in Fig.2. Thickness of the passivation films was 3 $\mu$m as the standard. In a part of the study, the effect of thickness on passivation facility was investigated in the range of 0.1 to 5 $\mu$m by changing the CVD reaction time. Storing tests were carried out on the same test unit in series.

A Samco International PD-2s plasma CVD system was used. It has a glass bell jar with 25 cm diameter and parallel plate electrodes made of stainless steel. The lower

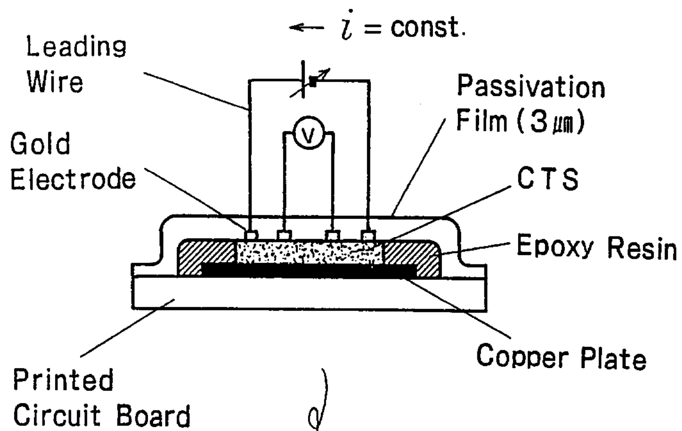


Volume Resistivity

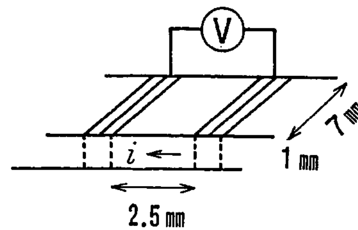


$$R = \frac{V}{i} \cdot \frac{0.7\times 0.1}{0.25}\ (\Omega\text{-cm})$$

**Fig. 1.** Schematic diagram for measurement of electric resistivity of test piece: CTS, ceramic high temperature superconductor.

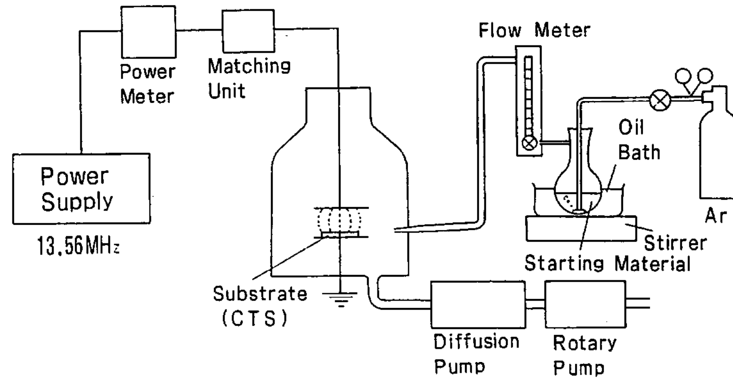


**Fig. 2.** Schematic diagram for plasma CVD system: CTS, Ceramic high temperature superconductor.

electrode has 100 mm diameter and was grounded. The supply electrode having 80 mm diameter was set 20 mm above the lower electrode. Gasses including monomers were introduced to between the electrodes with a flowing rate of 10 ml/mm, and films were deposited on the substrate by keeping the pressure in the range of 30 to 50 Pa and supplying 13.56 MHz *rf* power in the range of 0.064 to 0.20 W/cm$^2$ for glow discharge. Glass plates and silicon wafers were put on the substrate in the neighbor of the test unit for analyses of thickness measurement and FT-IR respectively. A porous polypropylene film, "Duragard 2400" of Polyplastics Co. (thickness: 25 $\mu$m, maximum pore size: 0.02 x 0.2 $\mu$m), was used for permeability testing for oxygen or water vapor. Passivation films were deposited on it. Table 1 summarizes the conditions for plasma CVD.

The monomer liquid was stirred in the flask and bubbled by argon gas, and the vapor of the monomer was introduced by the argon flow into the CVD chamber. The feed rate of the argon gas was changed depending on the vapor pressure of the monomer. In the case of a monomer having a very high vapor pressure, a nozzle was equipped between the flask and the chamber to avoid over reactions due to excess feed of the monomer. Temperature of the substrate was kept at 10 ℃ with chilled water circulated.

In this study five model monomers were selected. Table 2 shows names, formulae and symbols of the monomers. For SX, SZ and F-SZ commercial products or an intermediate of Dow Corning Toray Silicone Co., Ltd. were used. F-SX was obtained by a hydrolysis of F-SZ and purified with distillation for use. CF (gas) was selected as a reference material in this study since it has no silicon atoms. A commercial product having 99.99 % purity purchased from Takachiho Chemical Industry Co., Ltd. was used.

Table 1. Conditions of plasma CVD

| Item | Condition |
|---|---|
| Plasma type | Capacitively-coupled |
| Frequency of power | 13.56 MHz |
| Electrode | Parallel plate, 10cm/8cm ϕ 2cm d |
| Carrier gas | Argon |
| Flow rate of mixed gas | 10 $cm^3 \cdot min^{-1}$ |
| Partial flow rate of PS/MPS | Depending on monomer's vapor pressure at RT. |
| Total pressure | 30 - 50 Pa |
| *Rf* power | 0.064 to 0.20 $W/cm^2$ |
| Substrate temperature | 10 ℃ |
| Substrate | Super conductor testing piece, Glass plate, Silicon wafer, Duragard 2400 |

Table 2. Monomers for plasma polymerization

| Name | Formula | Symbol |
|---|---|---|
| Hexamethyldisiloxane | $(Me_3Si)_2O$ | SX |
| Hexamethyldisilazane | $(Me_3Si)_2NH$ | SZ |
| 1,3-Bis(γ-trifluoropropyl·dimethyl) disiloxane | $(CF_3CH_2CH_2SiMe_2)_2O$ | F-SX |
| 1,3-Bis(γ-trifluoropropyl·dimethyl) disilazane | $(CF_3CH_2CH_2SiMe_2)_2NH$ | F-SZ |
| Trifluoromethane | $CHF_3$ | CF |

*Observation of deposited films*

Films deposited on silicon wafers were observed by a microscope to see if any cracks or other types of physical defect are present. If any defects are found in a film, the film is no longer investigated for passivation since physical defects will negatively impact the passivation effect.

*Observation of passivation effects*

Passivation films originated from the five monomers were deposited on the test units for Y-, Bi- and Tl-systems. Passivation effects were observed to see the change of electric properties with time under the storing conditions shown in the former section.

*FT-IR*

Measurements were done under nitrogen flow with a Parkin Elmer 1600 FT-IR spectrometer. Spectra for the monomers except CF were also recorded using KBr disks.

*Water vapor permeability*

Testing was carried out based on JIS Z-0208 at 40 ℃ / RH90%. The polypropylene porous films with the plasma polymerized films coated were set on the cell. Thickness of the plasma polymerized films was 10 $\mu$m in this measurement.

*Oxygen permeability*

Measurement of oxygen permeability was on a Yanagimoto Works GTR-10 gas permeability analyzer. Thickness of the plasma polymerized films was 3 $\mu$m in this measurement. The oxygen transporting speed $Q$ was calculated with the following equation.

$$Q = q \cdot k / \Delta p \cdot a \cdot t \quad (\mathrm{cm^3(STP)/cm^2 \cdot s \cdot cmHg}) \qquad (1)$$

Where $q$: absolute transporting volume of oxygen ($cm^3$(STP)), $k$: equipment constant (1.70 in this study), $\Delta p$: pressure difference (cmHg) (22.3 in this study), $a$: area ($cm^2$) (15.2 in this study), $t$: time for transporting (s). Measurements were done after the transport reached to an equiblium state.

### 3.3 Results

*Change of properties of ceramic high temperature superconductors over time*

Firstly, Initial properties (resistivity-temperature curves) of the superconductors under a current density of 0.1 A/cm$^2$ are discussed. Figure 3 shows the result for Y-system. The resistivity at room temperature, $R_{rt}$, was 7.4 x 10$^{-3}$ Ω·cm that is in the semiconductor region. The resistivity increased as the temperature went down. The onset temperature, $T_{on}$, was 88.6 K and the resistivity at that temperature, $R_{on}$, was 1.3 x 10$^{-2}$ Ω·cm. $T_{zero}$ was 81.4 K. Bi-system showed a similar semiconductor like tendency, however, it was not as typical as Y-system. $T_{on}$ was 115 K, rather high. $T_{zero}$ was very broad at around 80 K which means a broad transition into the superconducting state. $R_{rt}$ and $R_{on}$ were 7.4 x 10$^{-2}$ Ω·cm and 9.0 x 10$^{-2}$Ω·cm, respectively. Tl-system showed a metallic tendency not like the other two systems. $T_{on}$ was 112 K and $T_{zero}$ was 111 K, those were high. Its transition was in a very sharp range. $R_{rt}$ and $R_{on}$ were 1.8 x 10$^{-2}$ Ω·cm and 2.0 x 10$^{-2}$Ω·cm, respectively.

Secondly, property change after stored in water vapor without passivation films are discussed. In the case of Y-system under the condition of 25 ℃/ RH100 %, the offset resistivity became not zero and the resistivity in the whole temperature range increased after 1 h of storage (see Fig. 3), and a big deterioration that the surface of the superconductor become white colored occurred after 17 h (see Fig.4). The speed of deterioration was higher under the condition of 85 ℃/ RH85 %. A big deterioration occurred after 1 h (see Fig.5).

In the case of Bi-system, the speed of deterioration was much slower than that in Y-system. $T_{on}$ decreased 12 K and the resistivity increased almost double after 300 days passed under 25 ℃/ RH100 %. Thus, Bi-system is suggested to be very resistant against water compared to Y-system. However, the degree of deterioration after 300 days is really a issue for practical use. Such an increase of resistivity occurred after about 3 months under the condition of 85 ℃/ RH85 %.

In the case of Tl-system, the speed of deterioration was close to that in Y-system. The resistivity-temperature curve became semiconductor like and $R_{on}$ became fifth times after 17 h at 25 ℃/ RH100 %. The speed of deterioration was higher at 85 ℃/ RH85 %. A big deterioration occurred after about 10 minutes.

Thirdly, change of properties after storage in a complete argon atmosphere is discussed. Experiments were carried out for only Y-system. The resistivity increased

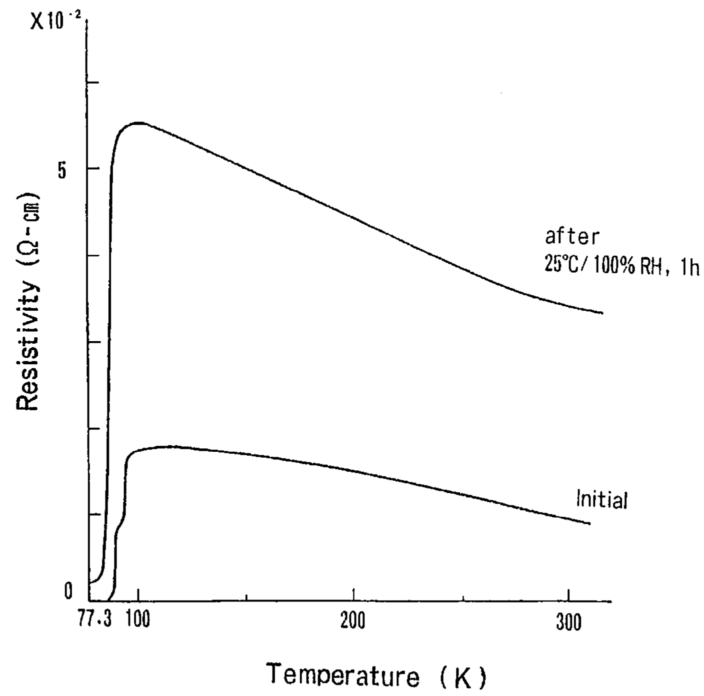


**Fig. 3.** Dependence of electric resistivity on temperature for Y-system ($YBa_2Cu_3O_{7-\delta}$) and that after exposure to 25℃/RH100% air for 1 h: Current density=0.1 A/cm$^2$.

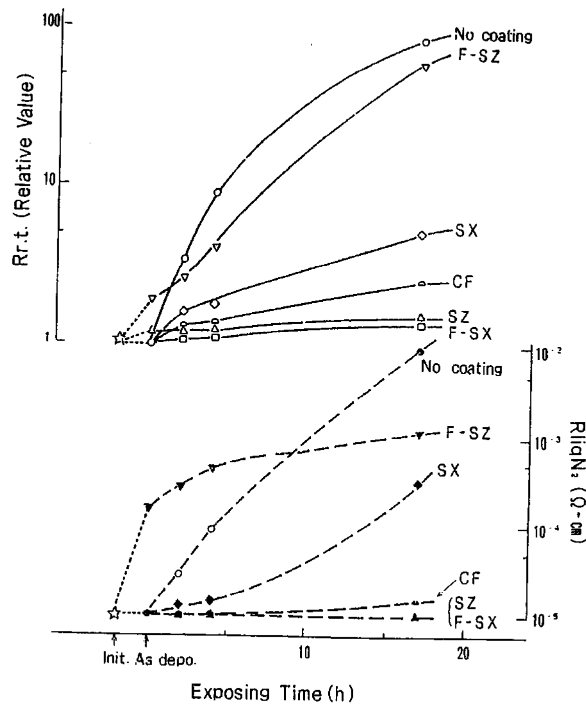


**Fig. 4.** Dependence of electric resistivities at 298.3 K ($R_{r.t.}$) and at 77.3 K ($R_{liqN_2}$) on exposing time to 25℃/RH100% air for Y-system ($YBa_2Cu_3O_{7-\delta}$) coated with plasma polymerized films: Film thickness $=3\,\mu m$, Current density$=0.1\ A/cm^2$. Note: "Init.", initial value (*i.e.*, no deposition or no exposure to water vapor); "As depo.", as deposited (*i.e.*, zero exposing time).

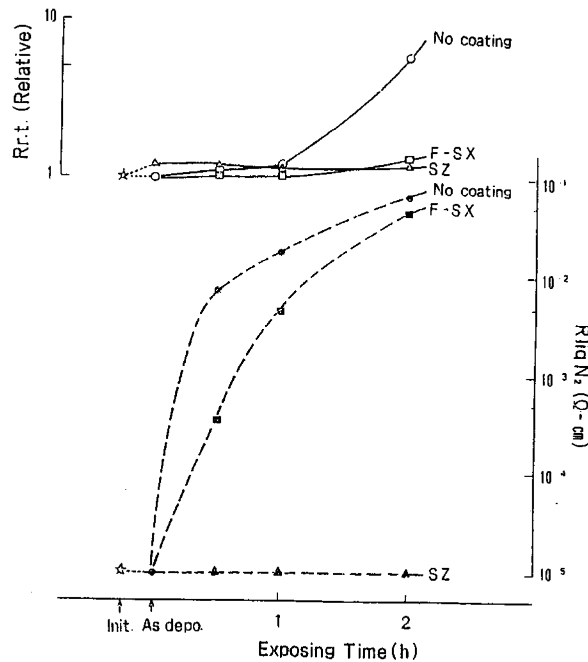


**Fig. 5.** Dependence of electric resistivities at 298.3 K ($R_{r.t.}$) and at 77.3 K ($R_{liqN_2}$) on exposing time to 85℃/RH85% air for Y-system ($YBa_2Cu_3O_{7-\delta}$) coated with plasma polymerized films: Film thickness $=3\,\mu m$, Current density$=0.1\ A/cm^2$. Note: "Init.", initial value (*i.e.*, no deposition or no exposure to water vapor); "As depo.", as deposited (*i.e.*, zero exposing time).

after 10 minutes of storage, then the test unit was transferred into air at room temperature and the resistivity increased after 10 minutes. This phenomenon is probably due to oxygen desorption/re-absorption which affects superconducting properties.

Effect of current density was also investigated. In any system, $T_{on}$ and $T_{zero}$ kept the original values even when the density was up to 2 A/cm$^2$, however, $R_{rt}$ and $R_{on}$ increased. The tendency of deterioration at 2 A/cm$^2$ was similar to that at 0.1 A/cm$^2$.

*Formation of passivation films*

In the case of SX, a power formation that was probably due to an over reaction was observed if the *rf* power density was over 0.07 W/cm$^2$. In the cases of the other monomers, stable plasma of purple colored was generated in any *rf* power range. The deposition rate for F-SZ was very slow. Several days were required to achieve 3 $\mu$m thickness. This was probably because of the low vapor pressure of F-SZ and/or special vapor phase reactions. In other monomers 3 $\mu$m thickness was obtained within several hours.

In any monomer films having good uniformity and good adhesion with substrates were obtained. That means good adhesive forces between the passivation films and the superconductors. No cracks or physical defects were found in those films.

*Passivation effects*

Passivation effects were investigated with fixing the current density as 0.1 A/cm$^2$ ($i$ = 4 mA).

Results are shown for only Y-system. Figures 4 and 5 show the results at 25 ℃/ RH100 % and 85 ℃/ RH85 %, respectively.

Increase of resistivity due to the formation of the passivation film was significantly observed in F-SZ. $R_{rt}$ became double after the passivation film was formed. A slight incease of resistivity after the plasma deposition was observed in SZ.

SZ and F-SX showed excellent passivation effects at 25 ℃/ RH100 % (see Fig.4). Those kept the initial resistivity values even after 17 h. Those were superior to the effect by films from CF. SX gave a slightly insufficient effect. The effect by the films from F-SZ was small. Resistivity change over time was observed for only SZ and F-SX (see Fig.5). SZ showed a perfect passivation effect for 2 hours without

change of appearance. However, F-SX kept its passivation effect for little time.

The test units were taken out after 2 hour storage at 85 ℃/ RH85 % for analysis of the surface and cross section by SEM. The films from SZ showed no change in film morphology and adhesion with the superconductor, while the films from fluorine containing monomers, ie F-SX, F-SZ and CF, showed cracks.

Effect of thickness on passivation was investigated in SZ. Thickness was varied in the range of 0.1 to 5 $\mu$m on Y-system. Rrt was observed after 2 hours at 85 ℃/ RH85 %. Passivation effect was higher when the thickness was larger. It was significantly low if the thickness was smaller than 0.2 $\mu$m (see Fig.6).

In the case of Bi-system, no passivation film caused increase of resistivity due to the deposition. For passivation effect, the result was similar to that in Y-system 85 ℃/ RH85 %. At 25 ℃/ RH100 % results were not as different among monomers as those in Y-system. Initial resistivity values were kept after storage except in SX. At 85 ℃/ RH85 % SZ showed a good effect. In the case of Tl-system, under the condition of 25 ℃/ RH100 % for 17 h, SZ and F-SX showed good results. However, no remarkable results were obtained in any passivation film under 85 ℃/ RH85 %. Resistivity increase due to deposition was in a similar trend to that in Y-system.

Effect of deposition on resistivity is summarized in Table 3, and passivation effects against water vapor are summarized in Table 4.

Figure 7 shows the testing result under argon ambient for Y-system. F-SX and SZ showed very little change in resistivity. The films from F-SX or SZ are supposed to reduce the oxygen desorption from the superconductor. Passivation effects are summarized in Table 5. Totally concluding, with regard to avoidance of deterioration against water vapor and due to desorption of oxygen, the films polymerized from SZ (hexamethyldisilazane) showed very excellent passivation effects.

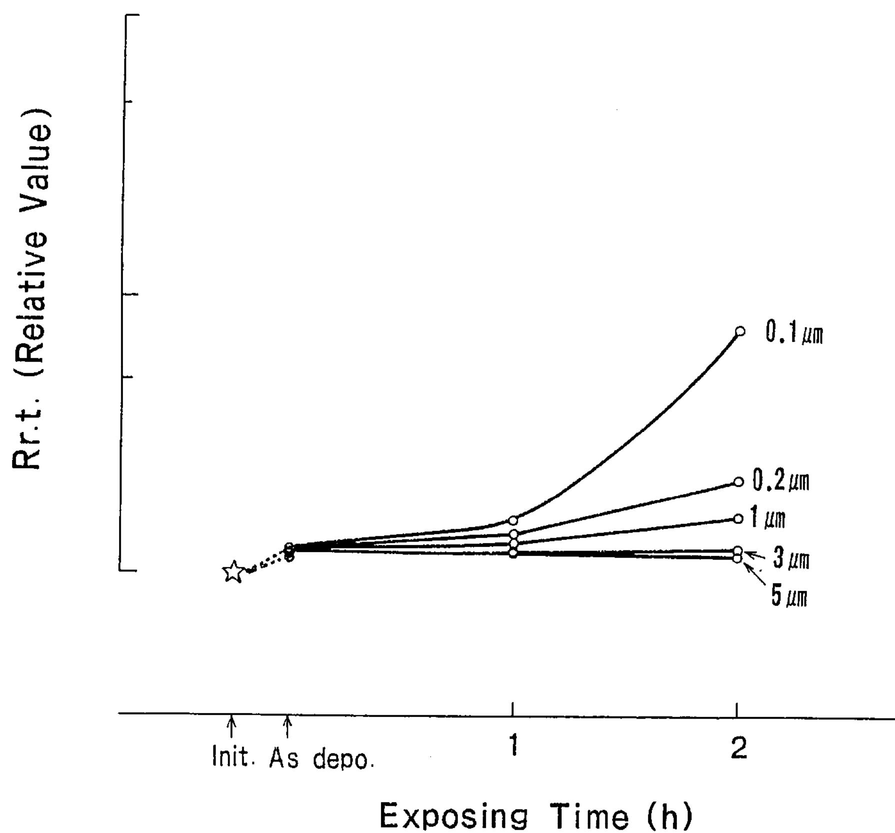


**Fig. 6.** Effect of thickness of plasma polymerized films from hexamethyldisilazane (SZ) on electric resistivity of Y-system ($YBa_2Cu_3O_{7-\delta}$) at 298.3 K after exposure to 85°C/RH85% air: Current density=0.1 A/cm$^2$. Note: "Init.", initial value (*i.e.*, no deposition or no exposure to water vapor); "As depo.", as deposited (*i.e.*, zero exposing time).

Table 3. Influence of deposition of plasma polymerized films on electric resistivity of ceramic high temperature superconductors at 298 K

(Film thickness = 3 $\mu$m; current density = 0.1 A/cm$^2$.)[a]

| Monomer | Y-System | Bi-System | Tl-System |
|---|---|---|---|
| SX | 1 | 1 | 1 |
| SZ | 1~2 | 1 | 1~2 |
| F-SX | 1 | 1 | 1 |
| F-SZ | 4~5 | 1 | 2 |
| CF | 1 | 1 | 1 |

[a] Evaluation rate is defined by the degree of increase in electric resistivity between before and after film deposition. 1, no change (best); 2, ~20%; 3, 20~50%; 4, 50~100%; 5, 100%~ (worst).

Table 4. Effect of plasma polymerized films on protection of ceramic high temperature superconductors against water vapor evaluated by the pattern of electric resistivity *vs.* temperature curve

(Film thickness = 3 $\mu$m. Conditions for measurement of electric resistivity: current density = 0.1 A/cm$^2$; temperature range, 77 K~298 K.)

| Monomer | Y-System | | Bi-System | | Tl-System | |
|---|---|---|---|---|---|---|
| | Cond-1[a]/17 h | Cond-2[b]/2 h | Cond-1/300 days | Cond-2/250 h | Cond-1/17 h | Cond-2/30 min |
| No coating | 5 | 5 | 2 | 3 | 5 | 5 |
| SX | 3 | 3 | 1 | 3 | 4 | 4 |
| SZ | 1 | 1 | 1 | 1 | 1 | 4 |
| F-SX | 1 | 3 | 1 | 2 | 1 | 4 |
| F-SZ | 4 | 4 | 1 | 2 | 4 | 4 |
| CF | 2 | 4 | 1 | 2 | 2 | 4 |

[a] Condition-1: Exposure to 25℃/RH100% air. [b] Condition-2: Exposure to 85℃/RH85% air.

Evaluation rate is defined by the degree of change in pattern of electric resistivity *vs.* temperature curve between before and after water vapor exposure.

1, no or very little change (best); 2, resistivity increased. However, its order was the same level over the whole temperature range; 3, the order resistivity increased in a specific temperature range; 4, the order of resistivity increased over a wide (but not the whole) temperature range; 5, the order of resistivity increased over the whole temperature range (worst).

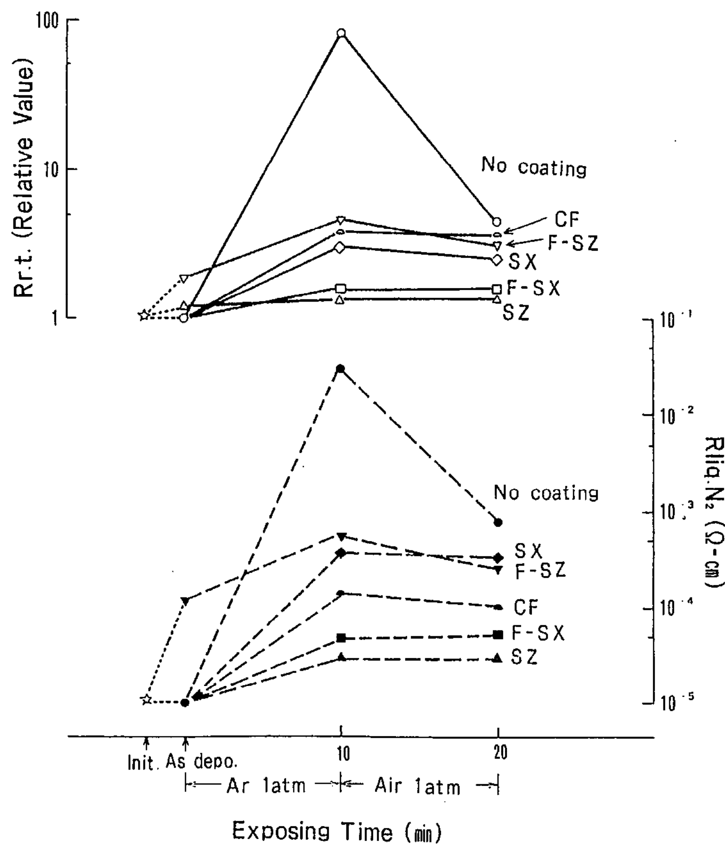


**Fig. 7.** Electric resistivities of Y-system ($YBa_2Cu_3O_{7-\delta}$) coated with plasma polymerized films at 298.3 K ($R_{r.t.}$) and at 77.3 K ($R_{liqN_2}$) after exposure to argon at 400℃ for 10 min and then to air at 400℃ for 10 min: Film thickness = 3 μm, Current density = 0.1 A/cm². Note: "Init.": initial value (*i.e.*, no deposition or no exposure to water vapor); "As depo.", as deposited (*i.e.*, zero exposing time).

Table 5. Effect of plasma polymerized films on protection of ceramic high temperature superconductors against argon gas at 400℃ for 10 minutes evaluated by electric resistivity at 298 K[a)]

(Film thickness = 3 $\mu$m. Conditions for measurement of electric tesistivity: current density = 0.1 A/ $cm^2$.)

| Monomer | Y-System | Bi-System[b)] | Tl-System[b)] |
|---|---|---|---|
| No coating | 5 | 1 | 1～2 |
| SX | 3 | | |
| SZ | 1 | | |
| F-SX | 1 | | |
| F-SZ | 3 | | |
| CF | 3 | | |

[a)] Evaluation rate is defined by the degree of change in electric resistivity between before and after the argon gas exposure.

1, no or very little change (best); 2, ～100% increased; 3, 100～500% increased; 4, 5～10 times increased; 5, 10 times～increased.

[b)] Blank parts mean "no data available yet".

*FT-IR*

Figure 8 shows FT-IR spectra of the obtained plasma obtained films. The structure of the films from SX are mainly polysiloxane judging from the main absorption due to $Me_3SiO_{1/2}$ (840 and 750 $cm^{-1}$) and the sub absorption due to $Me_2SiO$ (790 $cm^{-1}$) (see Fig.8-(a)). In the FT-IR spectrum for the film from SZ (Fig.8-(b)), the structures of $Me_3SiO_{1/2}$ and $Me_2SiO$ are seen like in the film from SX. Additionally absorption peaks at 920 and 600 $cm^{-1}$ assigned as stretching vibrations due to Si-N bonds are seen. The absorption peaks at 1180 $cm^{-1}$ due to the Si-NH-Si (silazane) backbone vibration and at 3450 $cm^{-1}$ due to the N-H stretching vibration which were seen in the spectrum of the SZ monomer disappeared in the spectrum of its plasma polymerized film.

In the FT-IR spectrum for the film from F-SX (Fig.8-(c)), absorptions at 1210 $cm^{-1}$ due to the C-F stretching vibration and at 2900 – 2950 $cm^{-1}$ due to the C-H stretching vibration assigned to $-CH_2-$ are seen.

In the FT-IR spectrum for the film from F-SZ (Fig. 8-(d)), any absorption due to organic groups was not seen, instead an absorption peak at around 620 $cm^{-1}$ probably due to the SI-N stretching vibration is seen. It is difficult to assign the other peaks.

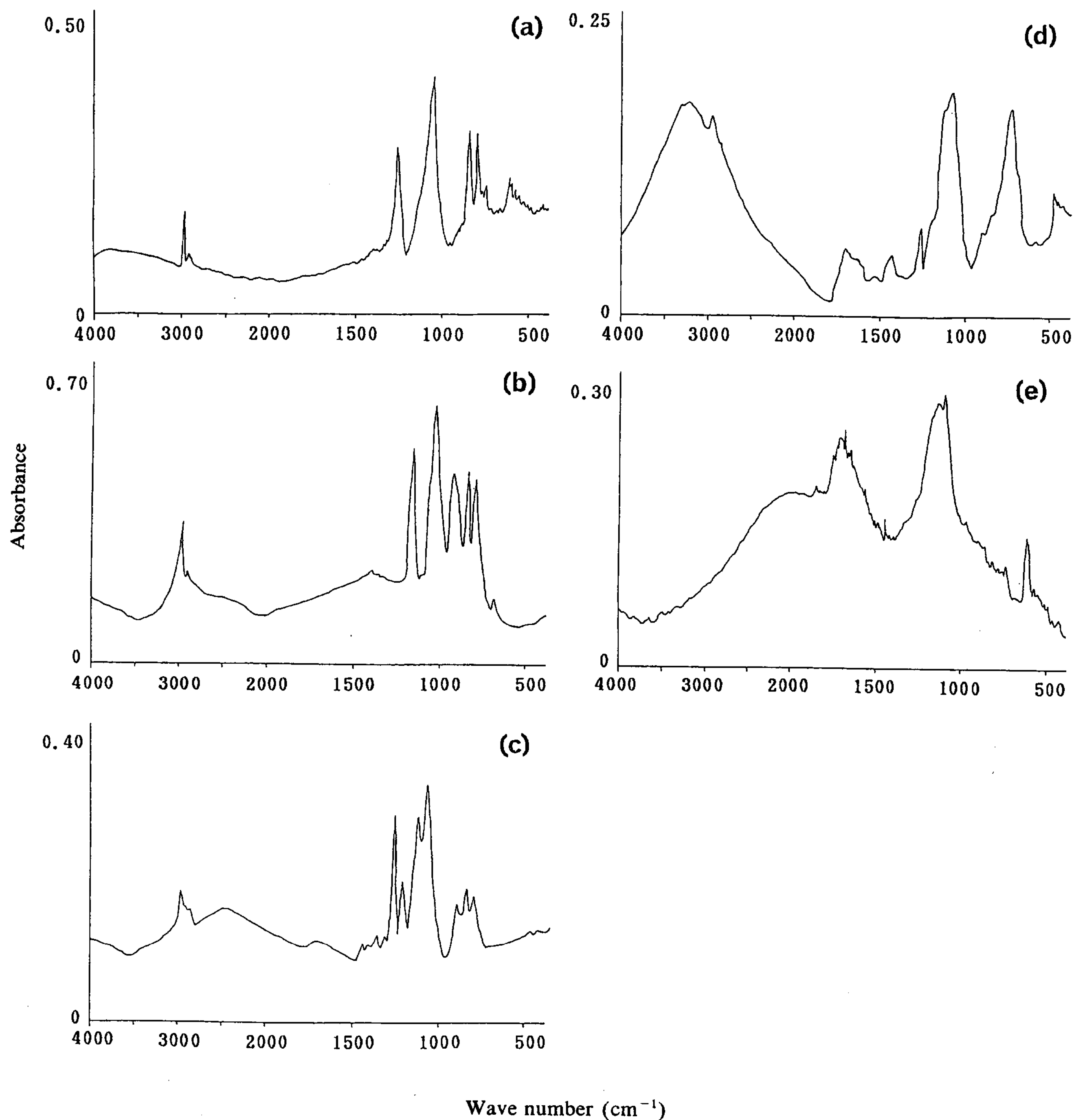


**Fig. 8.** FT-IR spectra of plasma polymerized films on silicon wafers from monomers of (a) SX, $(Me_3Si)_2O$; (b) SZ, $(Me_3Si)_2NH$; (c) F-SX, $(CF_3CH_2CH_2SiMe_2)_2O$; (d) F-SZ, $(CF_3CH_2CH_2SiMe_2)_2NH$; (e) CF, $CHF_3$. Film thickness $=3\,\mu m$

In the case of F-SZ, the structure of the obtained film was not polymeric but inorganic.

The spectrum for the film from CF had an absorption at 1100 – 1200 $cm^{-1}$ due to C-F stretching vibrations (see Fig.8-(e)).

*Permeability of water vapor, oxygen*

Results of the measurement of permeability of water vapor or oxygen are shown in Table 6. SX showed a relatively high value of water vapor permeability, whereas other films showed similar values.

Table 6. Water–vapor transmission ratio and oxygen transmission rate for plasma polymerized films

| Monomer | Water–vapor transmission ratio ($g/m^2 \cdot 24$ h) (JIS Z-0208) (Film thickness = 10 $\mu$m) |
|---|---|
| SX | $2.4 \times 10^2$ |
| SZ | $3.5 \times 10^1$ |
| F-SX | $4.1 \times 10^1$ |
| F-SZ | $3.0 \times 10^1$ |
| CF | $3.2 \times 10^1$ |

| Monomer | Oxygen transmission rate ($cm^3(STP)/cm^2 \cdot s \cdot cmHg$) (Film thickness = 3 $\mu$m) |
|---|---|
| SX | $1.1 \times 10^{-4}$ |
| SZ | $7.3 \times 10^{-6}$ |
| F-SX | $7.0 \times 10^{-6}$ |
| F-SZ | $7.7 \times 10^{-5}$ |
| CF | $2.9 \times 10^{-4}$ |

## 3.4 Discussion

*Increase of resistivity due to deposition*

The increase of resistivity due to the formation of the passivation film from F-SZ suggests that some reaction occurred between the plasma radicals and Y-system resulting in a formation of a third layer in the interface region.

*FT-IR*

The structure of the film polymerized from SZ is supposed to be a hybrid of silicone polymer and inorganic SiN. The presence of oxygen in the polymerized film is believed to be from the process and/or the starting material.

The structure of the polymerized film from F-SX is proposed to be polymer like that retains $(CF_3CH_2CH_2SiMe_2)_2O$ being kept from the monomer, and are with the reduction of $CF_3CH_2CH_2$ group and the formation of $Me_2SiO$ units.

The active species in the plasma for F-SZ may not be a kind of species that forms polymers or may be hard to stick to the substrate. In the former case the behavior of the active species is interesting.

The structure of the film for CF is suggested to be mainly Teflon like. The absorption at around 1700 $cm^{-1}$ is hard to be assigned.

*Permeability of water vapor, oxygen*

Considering that the structure of the film from CF is Teflon like, the values could be said to be very small in polymer films. However, the order of $10^1$ $g/m^2 \cdot 24h$ is not very low compared to the values for bulk materials that have been reported. More correctly, the comparison should be done by considering the effect of thickness and density.

The speed of oxygen permeability was relatively high for CF and low for SZ and F-SX.

*Passivation effects*

To conclude, the plasma polymerized films showing good passivation effects

under water vapor or oxygen free ambient at the high temperature showed relatively low values of peameability of water vapor and oxygen. This can explain the mechanism of the passivation effect.

Since the films had no cracks or physical defects, the results of the passivation effect can be explained the chemical structure of the films.

The passivation effects obtained in this study are not sufficient at practical applications. More studies are needed.

### 3.5 Conclusion

1) CVD conditions for plasma polymerization of the four model monomers were optimized to keep the basic chemical structures of the monomers. Passivation effects of these films on ceramic superconductors were examined.

2) Silicone (-$SiMe_2O$-) based films were found to be inert to the superconductors, ie, the deposition of these films gave no negative impact on superconducting properties.

3) Simple silicone structures of film did not show sufficient passivation effects, since water vapor and oxygen are permeable through these films.

4) It was effective for intercepting water vapor and oxygen to introduce dense structures such as SiN or fluoroalkyl groups to the film.

5) Therfore, for sufficient passivation effects, having both silicone and dense structures is essential.

6) Totally, the film prepared from SZ (hexamethyldisilazane) showed the best passivation effect among the four model starting monomers. The film had mixed structures of cross-linked dimethylsiloxane (SiO bond order = $2+\delta$) and SiN (0). Having such a hybrid bonding dimension is essential for passivation of ceramic superconductors.

**References**

1) S. Kanbe, T. Hasegawa, M. Aoki, T. Nakamura, H. Koinuma, K. Kishio, K. Kitazawa, H. Takagi, S. Uchida, S. Tanaka and K .Fueki, *Jpn. J. Appl. Phys.*, **26**(5), L613 (1987)
2) H. Koinuma, T. Hashimoto, T. Nakamura, K. Kishio, K. Kitazawa and K. Fueki, *Jpn. J. Appl. Phys.*, **26**(5), L761 (1987)
3) S. Morohashi, H. Tamura, A. Yoshida, S. Hasuo, *Technical Report of IEICE*, 31(1988)
4) K. Sato, S. Omae, K. Kojima, T. Hashimoto and H. Koinuma, *Jpn. J. Appl. Phys.*, **27**, L2088(1988)
5) S. Morohashi, H. Tamura, A. Yoshida and S. Hasuo, *Appl., Phys. Lett.*, **52**, 1897(1988)
6) S. Morohashi, K. Yoshikawa, A. Yoshida, H. Tamura, K. Goto, N. Fujimaki and S. Hasuo, *Technical Report of IEICE*, 19(1988)

# Chapter 4

## Siloxane/PEO based polymer electrolytes for lithium battery


4.1 Introduction 65

4.2 Experimental part 67

4.3 Results 72

4.4 Discussion 78

4.5 Conclusion 79

## 4.1 Introduction

The function discussed in this chapter is in more macro level. Lithium ion conductivity is studied from a polymer level standpoint.

Solid polymer electrolyte (SPE) is a key material for advanced devices that are thin, light and flexible. One of the most advanced and expected devices is lithium battery. Scheme 1 illustrates a principle of rechargeable lithium battery. In the lithium battery applications, high conductivity of lithium ion, flat temperature dependency of properties and film toughness and flexibility are required on SPE. Several crosslinked polymers having polyethyleneoxide (PEO) units with lithium salts dispersed have been proposed as one of good candidates for SPE[1-4)]. Their ionic conductivity was mostly in the range of $10^{-6}$ to $10^{-4}$ $S \cdot cm^{-1}$. Ideally the order of $10^{-3}$ $S \cdot cm^{-1}$ or lower is desirable for lithium battery applications. In those cases mobile ions are lithium ion and its counter anions, so that they are so called "double ion" type SPE's. For lithium battery applications, "single ion" type SPE (ie, only lithium ion is mobile) is desirable since it gives constant currents. Even if the ionic conductivity is low, "single ion" type SPE is valuable for application for special devices such as heart pace maker. The PEO based SPE's have other problems. Their conductivity was drastically dropped at low temperature due to the presence of Tg (glass transition temperature) for the PEO segments. Ionic conductivity may rise if the polymer matrix has a more flexible main chain, a lower glass transition temperature and many promotion sites for solvation and transportation of cationas.

Polysiloxane having the Si-O-Si backbone has been suggested for the matrix of SPE[5-7)], since its main chain is flexible and it has a low Tg at around −120 ℃. Polysilixane also has excellent stabilities chemically and physically and could be chemically modified variously that will be able to design the SPE matrix with high functions.

In this chapter novel siloxane/PEO based polymer electrolytes of either single or double ion type are introduced and the feasibility of application of these materials for lithium batteries are discussed. Those two types of SPE could be prepared from same prepolymers and different lithium salts. Any single ion type SPE with a siloxane matrix had never reported before.

RECHARGEABLE LITHIUM BATTERY (LOCKING-CHAIR TYPE)

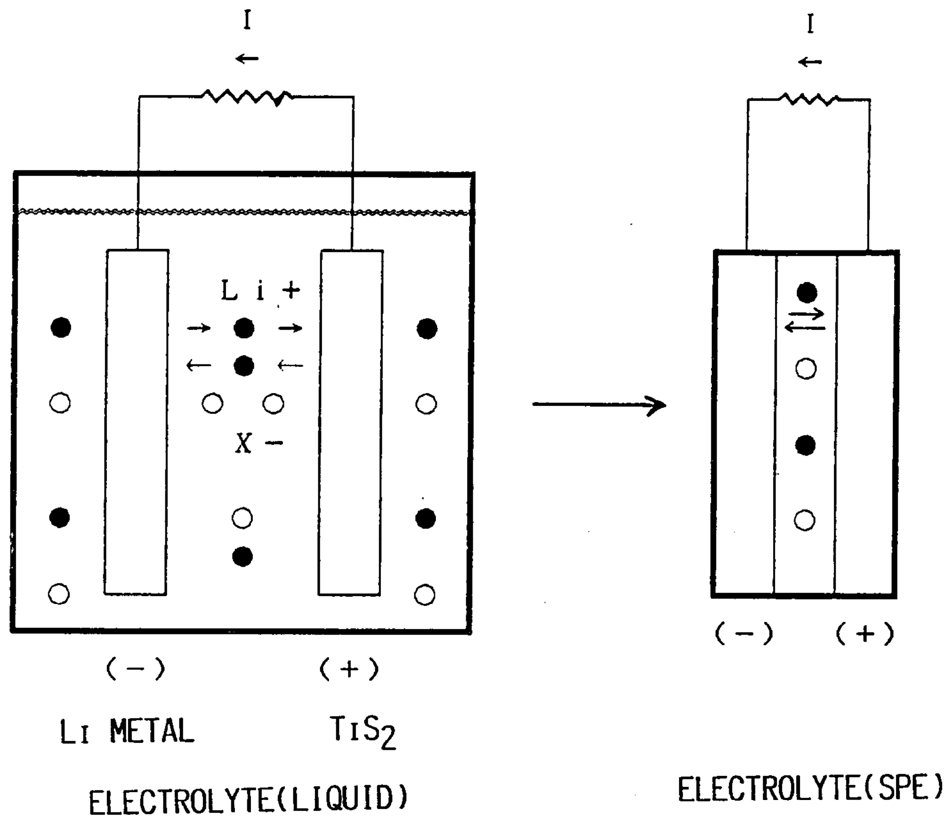

$$(-)\ Li \rightleftharpoons Li^{+} + e^{-}$$

3.0V

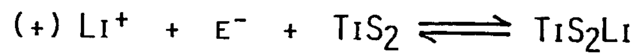

$$(+)\ Li^{+} + e^{-} + TiS_2 \rightleftharpoons TiS_2Li$$

SPE = ION DISPERSED POLYMER NETWORK

Scheme 1. Principle of rechargeable lithium battery.

## 4.2 Experimental part

Scheme 2 shows the structure of the prepolymers, the synthetic procedures and the schematic structure of the SPE's of single or double ion type. The prepolymers have poly(dimethylsiloxane) chains as the backbone and as sidechains one has carboxy groups (PP1) and another, hydroxyl groups (PP2). PP1 was prepared by the procedure shown in a published paper[8]. PP2 was used as a commercial product of Dow Corning Toray Silicone Co., Ltd. PP3 was purchased from Nihon Yushi Co., Ltd. The polymer crosslinked network was formed by ester formation between the carboxyl groups and hydroxyl groups on the prepolymer side chains. In the case of the single ion type, a part of the carboxyl groups on the prepolymer side chains behave as immobile counter anions in the polymer matrix. $LiClO_4$ and LiOH were purchased from Kanto Chemical Inc. and dried under high vacuum at 120 ℃ for 24 h before use. Lithium foil with 0.2 mm thickness purchased from Kyokuto Kinzoku Co., Ltd. was used as a non-blocking electrode for DC current and transference number measurements.

Typical preparation details of the SPE's were as follows.

Single ion type: 1.23 g of PP1 (4.45 mEq of COOH), 1.32 g of PP2 (1.93 mEq of OH), 0.41 g of PP3 (1.10 mEq of OH) and 37.1 mg of lithium hydroxide (1.55 mmol) were mixed with a small amount of water and tetrahydrofurane to make a homogeneous solution. After being poured on a casting plate made of either Teflon or stainless steel, it was heated under high vacuum (1 Torr) at 140 ℃ for 48 h for complete crosslinking. The sample number for the obtained SPE is named as S-1.

Double ion type: A mixture of 0.98 g of PP1 (3.54 mEq of COOH), 1.54 g of PP2 (2.26 mEq of OH), 0.47 g of PP3 (1.26 mEq of OH), 0.77 mmol of lithium perchlorate and 0.1 M hydrogen chloride/methanol solution (0.01 ml) as the catalyst was poured on a casting plate made of either Teflon or stainless steel, and was heated under high vacuum (1 Torr) at 140 ℃ for 48 h for complete crosslinking. The sample number for the obtained SPE is named as D-1.

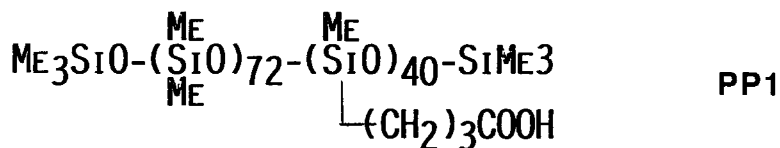


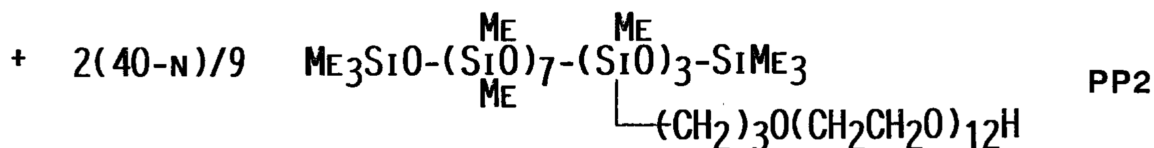


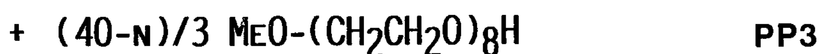


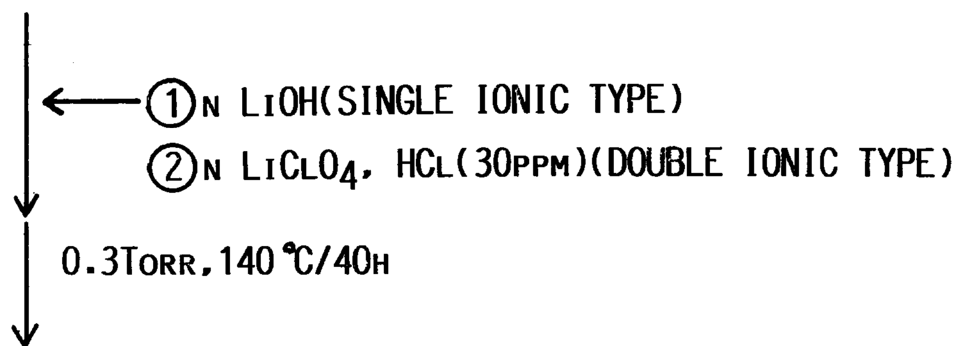


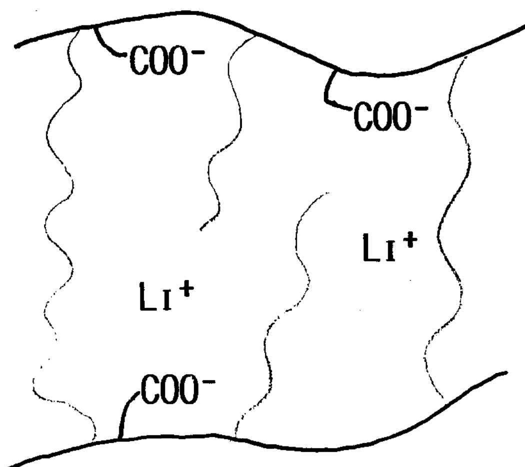


SINGLE IONIC TYPE

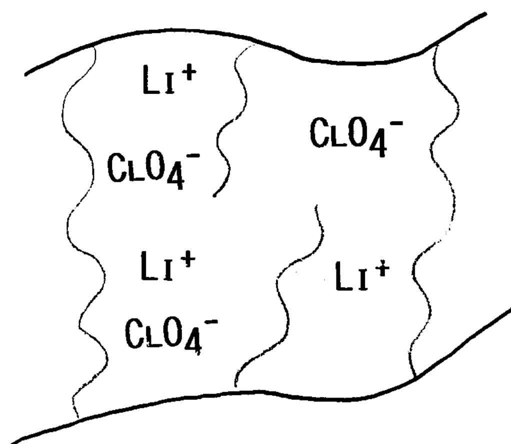


DOUBLE IONIC TYPE

Scheme 2. Synthesis of siloxane/PEO based solid polymer electrolytes (SPE).

Characterization of the resulting films were carried out in Dow Corning Toray Silicone Co., Ltd. except that IR analysis was carried out by Tsutsumi et al. at Yamaguchi University. The following equipment was used for film characterizations. IR: Shimadzu FTIR-4200, DSC (differential scanning calorimeter): Seiko I&E SSC580DS. Ionic conductivity ($\sigma_i$) and dielectric constant ($\varepsilon_s$) of the films were measured with a LCR meter (Yokogawa Hewlet Packard 4192A) with stainless steel electrodes by scanning the frequency from 1 Hz to 10 MHz and having Cole-Cole plots. Scheme 3 illustrates the principle of the measurement of $\sigma_i$ and $\varepsilon_s$. DC current and transference number measurements were with a potenio/galvano statt (Hokuto Denko HA-501G). Transference number (ion transform number) (T) in the resulting SPE's was measured by an isothermal transient ionic current method[9] shown in the Scheme 4.

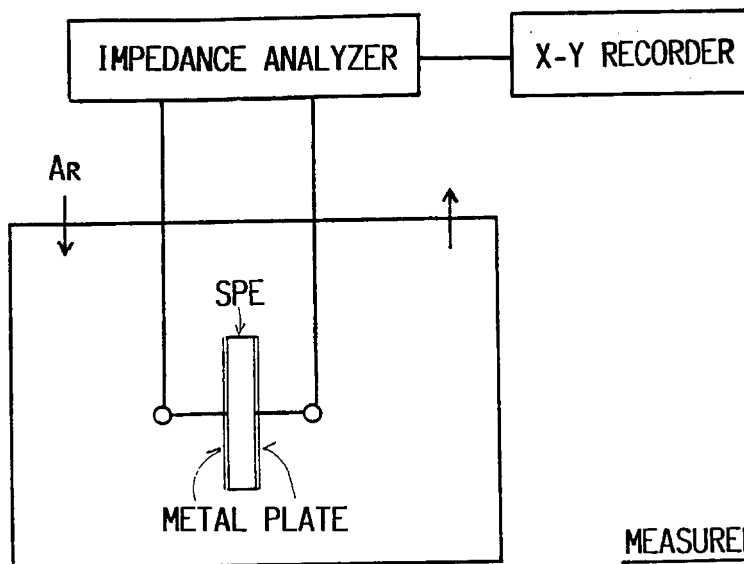


MEASUREMENT SYSTEM

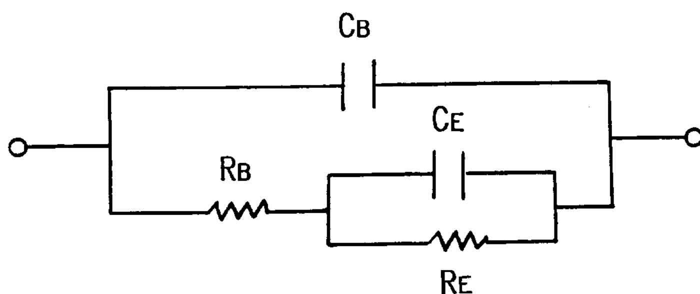


EQUIVALENT CIRCUIT

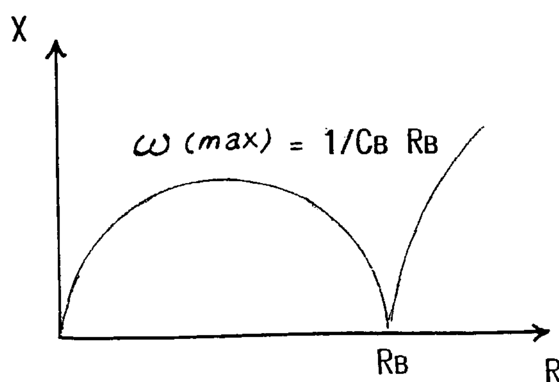


COLE-COLE PLOT

Scheme 3. Principle of the measurement of ionic conductivity ($\sigma_i$) and dielectric constant ($\varepsilon_s$).

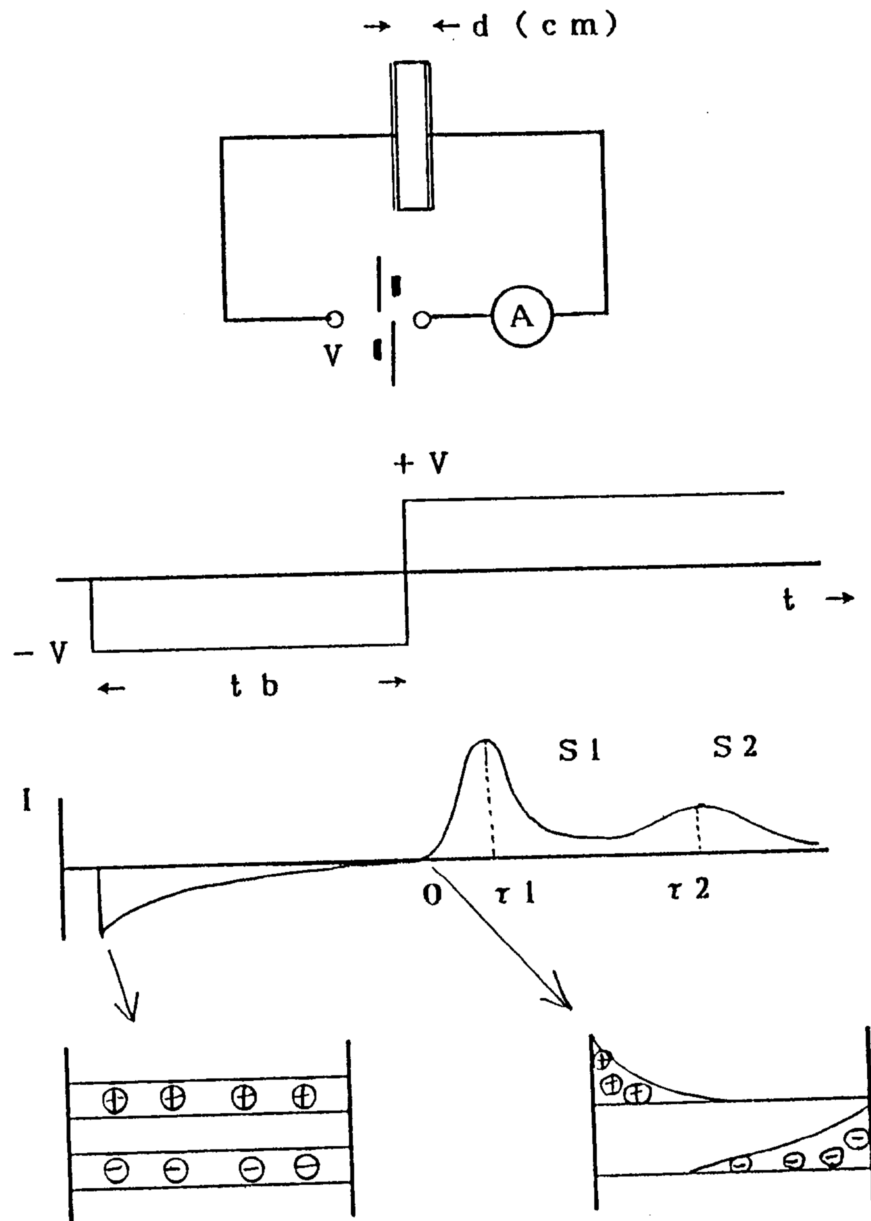


$$\mu = d^2 / \tau V \ (\mathrm{cm^2/Vsec})$$

$$\sigma_i = q n (\mu_+ + \mu_-)$$

$$S = q n$$

$\mu$ ; ION MOBILITY

n ; ION DENSITY

S ; PEAK AREA

→ $Li^+$ TRANSPORT NUMBER $= \mu_+ / (\mu_+ + \mu_-)$

Scheme 4. Schematic explanation for isothermal transient ionic current method.

## 4.3 Results

*Characterization of the SPE's*

After the final thermal treatment (cure), the resulting SPE films were transparent and elastic having a thickness around 0.3 mm. These films did not dissolve in common organic solvents, however, swelled with acetone.

IR spectra of the single and double type SPE's (S-1, D-1) are shown in Fig.1 including the prepolymers PP1-3. Both spectra have an absorption band at 1740 $cm^{-1}$ which is assigned to C=O stretching vibration of ester bonds and a strong band at around 1100 $cm^{-1}$ which is assigned to the siloxane polymer chain. The broad bands at 3400 – 3500 $cm^{-1}$ which are assigned to O-H stretching in PP2 and the band at 1715 $cm^{-1}$ which is assigned to COOH in PP1 disappeared after curing.

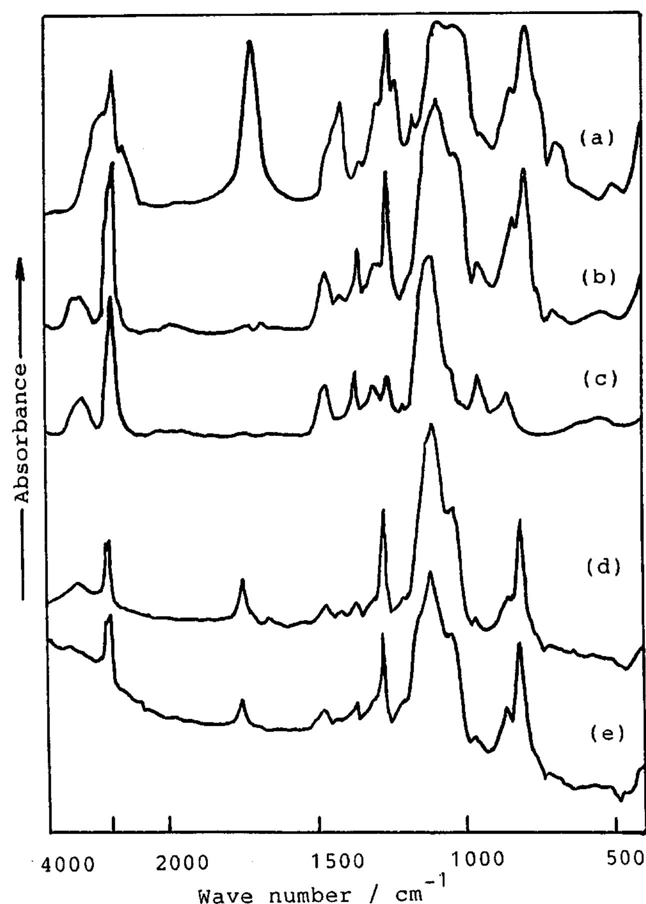


Fig.1. IR spectra of prepolymers, PP1 (a), PP2 (b), PP3 (c), SPE's S-1 (e) and D-1 (d).

Figure 2 shows the DSC curves for S-1 and D-1. Tg of the both SPE's were around −63 ℃.

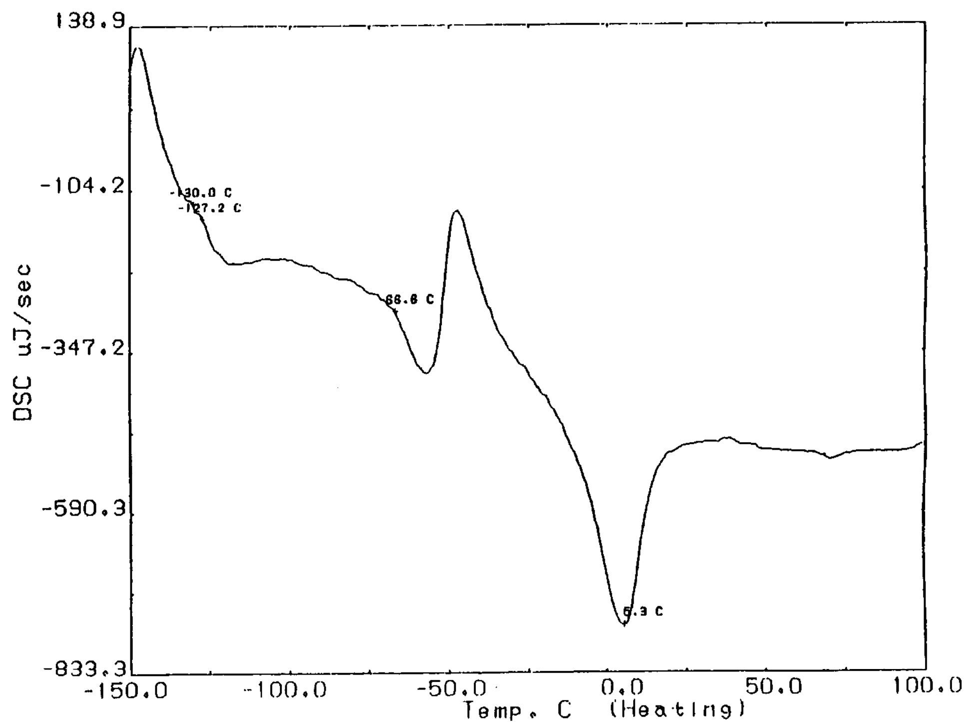


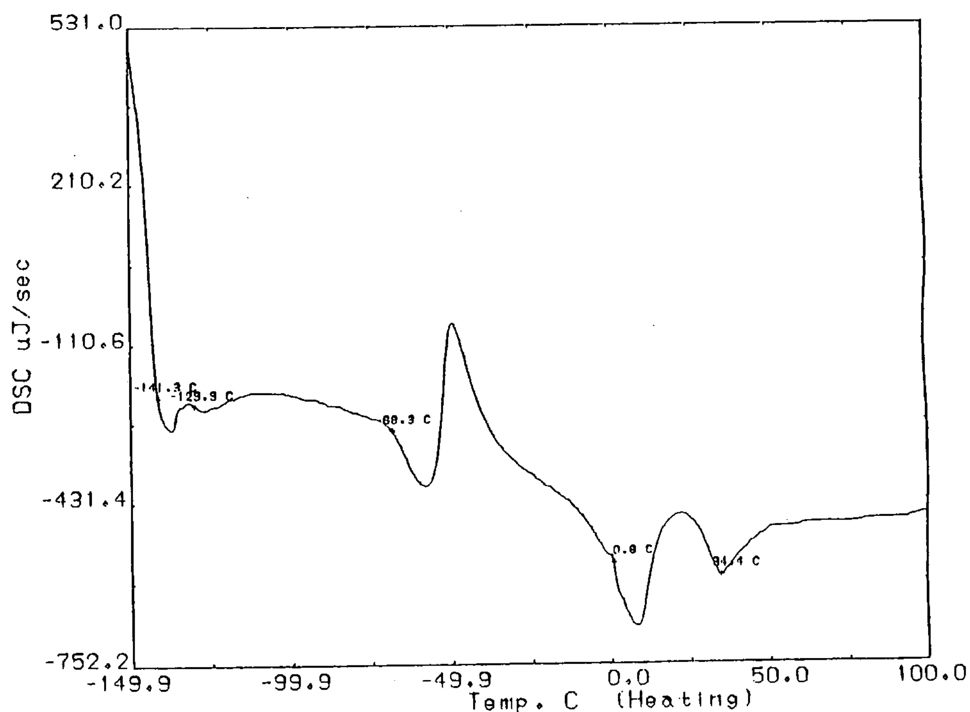


Fig.2. Differential scanning calorimetric curves for S-1 (upper) and D-1 (lower).

*Electrical properties of the SPE's*

Ionic conductivities $\sigma_i$ of S-1 and D-1 at 25 ℃ were $1.0 \times 10^{-7}$ $S \cdot cm^{-1}$ and $1.7 \times 10^{-5}$ $S \cdot cm^{-1}$, respectively. The temperature dependence of conductivity for S-1 is shown in Fig.3. The curve of its conductivity versus 1/T was not linear but convex. The curve for D-1 showed a similar style.

The dielectric constants $\varepsilon_s$ were calculated from capacitance values measured with the LCR meter. $\varepsilon_s$'s of S-1 and D-1 were 5.1 and 3.9 respectively.

Effect of lithium atom content in SPE on $\sigma_i$, $\varepsilon_s$ and Tg was investigated. The lithium content was changed by just changing the amount of LiOH or $LiCiO_4$ in the formulations. The result is shown in Fig.4. The open circuits mean S-1 or D-1. The tendency for the single and double ion type SPE's were similar. The ionic conductivities were highest at S-1 and D-1. Dielectric constant and Tg increased as the lithium atom content increased.

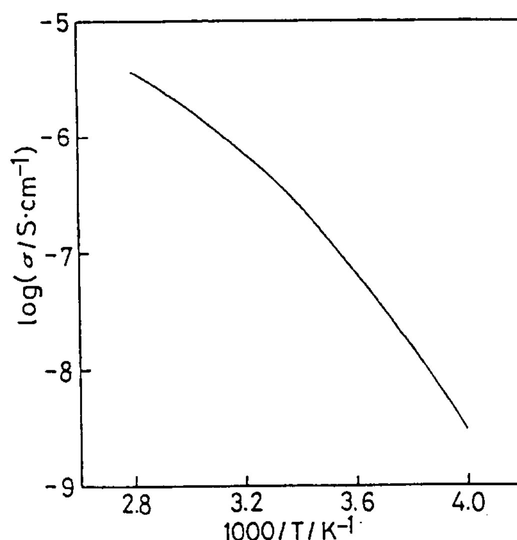


Fig.3. Temperature dependence of ionic conductivity for S-1.

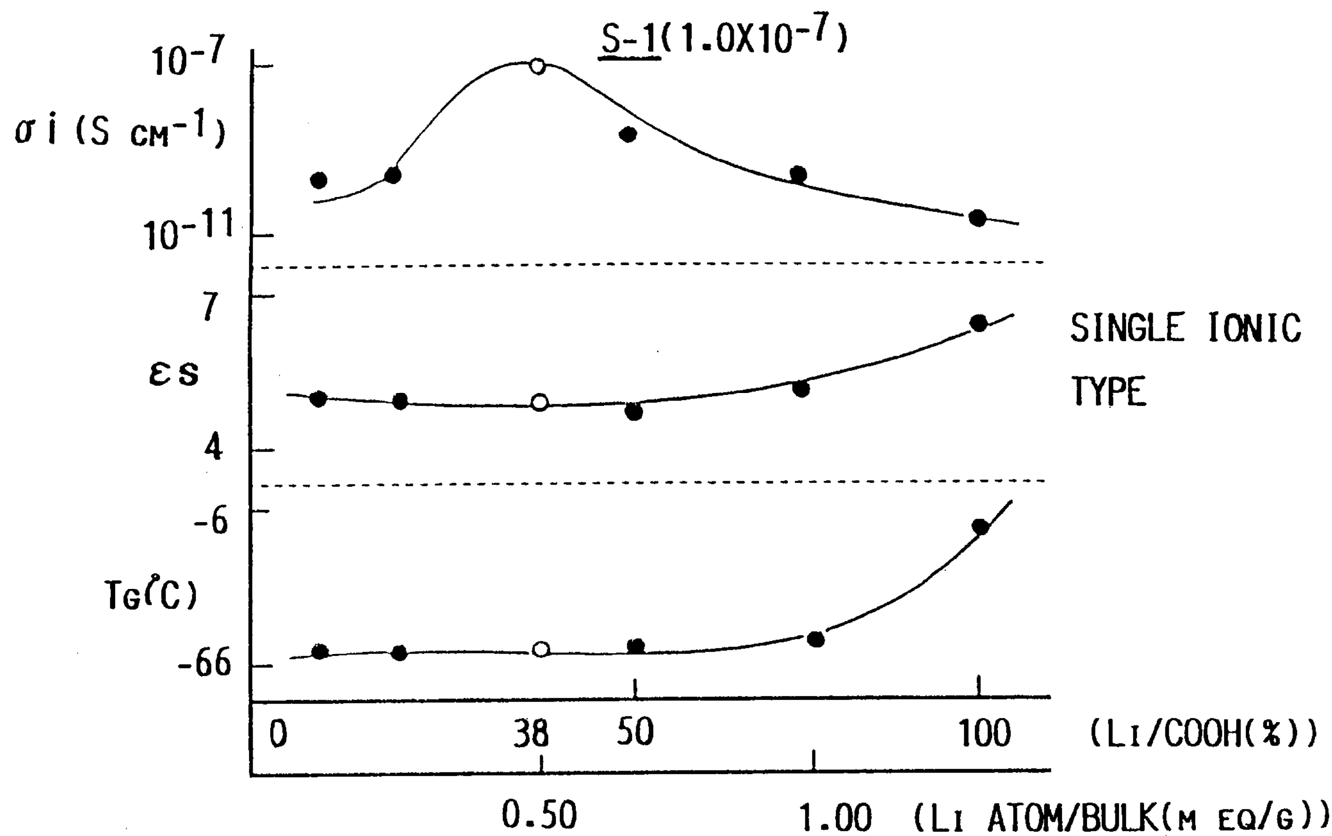


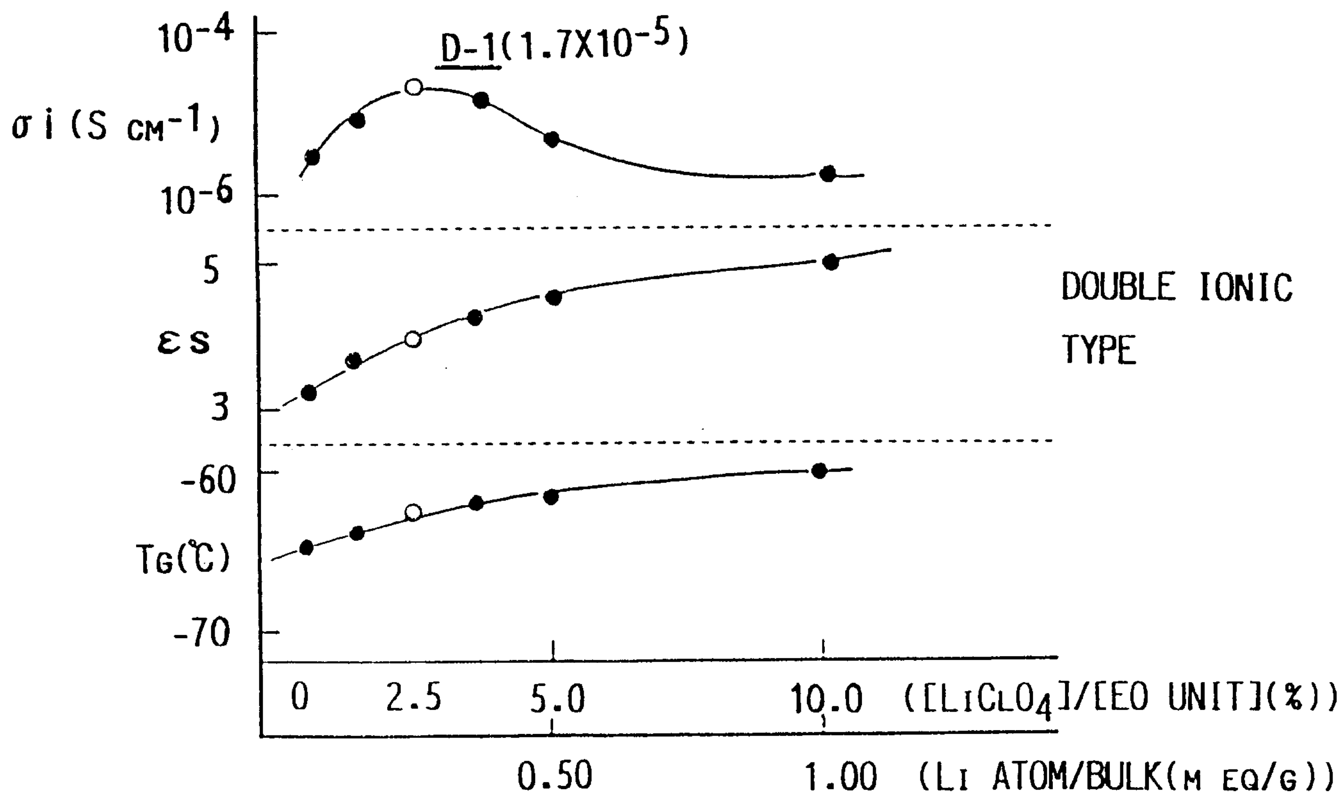


Fig.4. Ionic conductivity, dielectric constant and glass transition temperature for S-1 (upper) and D-1 (lower) as a function of lithium atom content in SPE.

Transition of ionic current under DC electric voltage was investigated. A sandwich structure of the lithium foils and SPE with 0.3 mm thickness was used. DC 1V was supplied to the sandwich structures. Figure 5 shows the result. In the S-1 sample almost the same current was kept although its current was not very high. On the other hand, the current at the D-1 sample decrease with time, although its initial current was high.

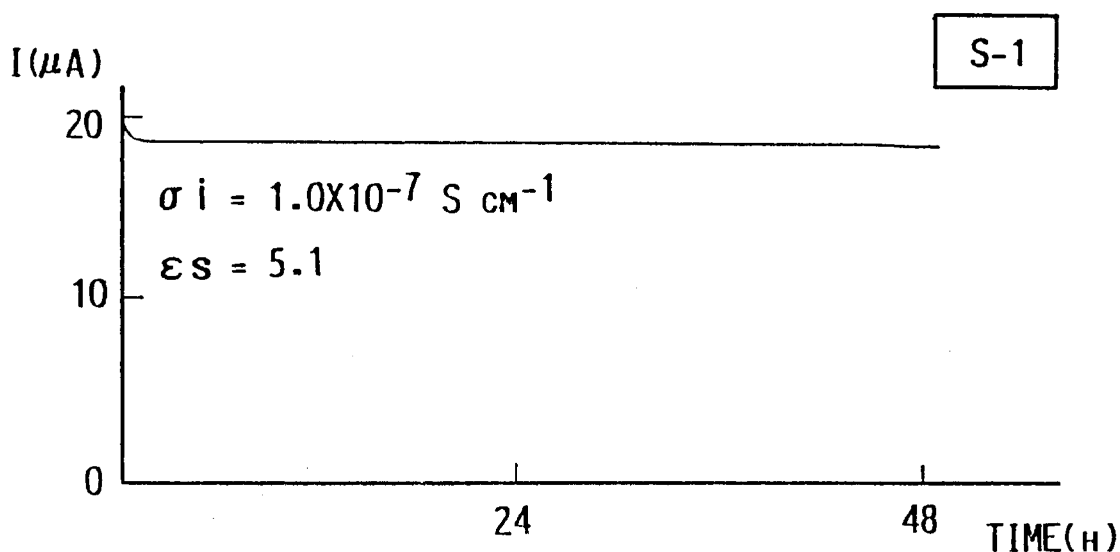


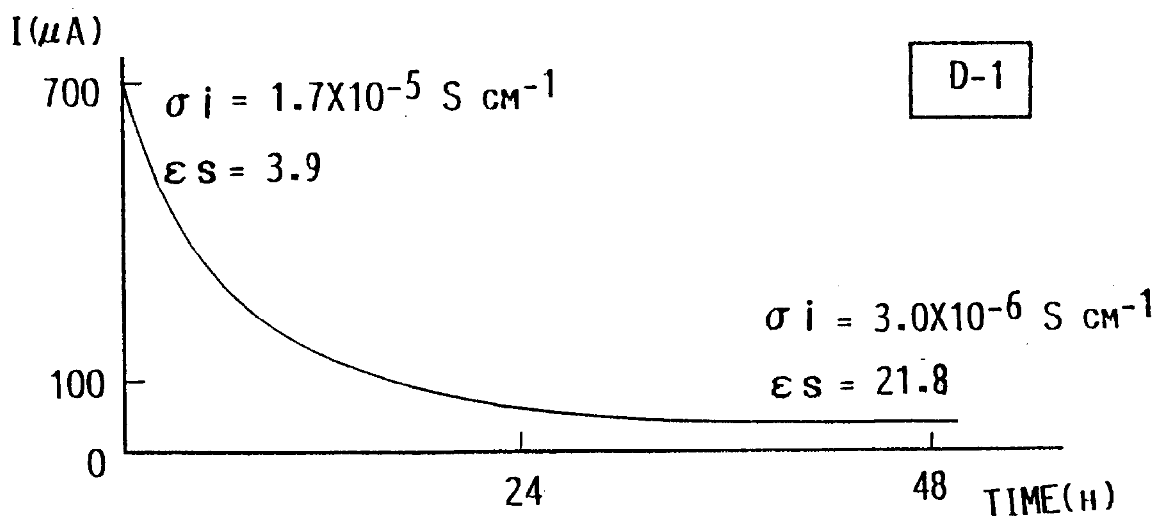


Fig.5. Transition of ionic current under DC electric field for S-1 and D-1.
(SPE thickness: 0.3 mm, Electrodes: Li foil, DC voltage: 1V)

The isothermal transient ionic current (ITIC) method was performed to determine the transference number (T) of the SPE's[9]. This method is based on using an ion-blocking stainless steel electrode and an ion reversible lithium electrode. A sample was sandwiched between the two electrodes and current responses were recorded as schematically explained in Scheme 4.

The results were shown in Table 1. The mobility of the lithium ion for D-1 was one order higher than that for S-1. However, the transference number of lithium ion (T) for S-1 was almost 100 %, whereas that for D-1 was 44.9 %.

Table 1. Electric properties of S-1 and D-1.

| | S-1 | D-1 |
|---|---|---|
| Li CONTENT (m eq/g) | 0.50 | 0.25 |
| $\sigma i$ (S cm$^{-1}$) | $1.0\times10^{-7}$ | $1.7\times10^{-5}$ |
| $\varepsilon s$ | 5.06 | 3.88 |
| DC CURRENT STABILITY | EXCELLENT | DECREASED TO 1/10 |
| $\mu_+$ (cm$^2$/V sec) | $1.0\times10^{-7}$ | $3.5\times10^{-6}$ |
| $\mu_-$ (cm$^2$/V sec) | $5.2\times10^{-11}$ | $4.3\times10^{-6}$ |
| T($Li^+$) (%) | 99.95 | 44.9 |
| N($Li^+$) (number/cm$^3$) | $6.3\times10^{18}$ | $1.3\times10^{19}$ |
| DEGREE OF DISSOCIATION OF Li SALT (%) | 0.90 | 11.8 |

$\mu$ : ION MOBILITY

T : ION TRANSFORM NUMBER

N : ION DENSITY

## 4.4 Discussion

*Characterization of the SPE's*

Judging from the infrared spectra, the polymer matrices have a polysiloxane backbone and crosslinking parts which form with ester bonds between PP1 and PP2. Also PP3 reacted with PP1. The side chains formed played an important role as solvation and transportation sites of the cation, lithium ion, in the polymers.

The Tg's of both the SPE's, around –63 ℃, are below typical temperatures that are actually used for practical device. The presence of the siloxane chain should impact the lowering of Tg.

*Electrical properties of the SPE's*

Since the curves of its conductivity versus 1/T for both single and double ion type SPE's were not linear but convex, the ion conduction mechanism is WLF type[10].

The properties versus the lithium content for both the single and double ion type SPE's can be explained as follows. If the lithium content is high, it is suggested that the mobility of the matrix become high resulting in lower conductivities.

It is suggested that the equiblium state between the metal lithium and the lithium ion be smooth at the both electrodes in the case of S-1, while the anions ($ClO_4^-$) be concentrated in one electrode that interferes smooth mobility of the lithium ions.

Judging from the data on transference number of lithium ion, S-1 is exactly proved to be the single ion conducting SPE that is expectable for specific device applications.

## 4.5 Conclusion

1) Novel siloxane/PEO based solid polymer electrolytes (SPE) of single and double ion types were prepared from same prepolymers. The ionic conductivities of the single ion type and the double ion type were in the order of $10^{-7}$ and $10^{-5}$ $S \cdot cm^{-1}$, respectively.

2) Glass transition temperatures for both the types of SPE were below −60 ℃. It means that these SPE's could be practically applied for lithium batteries. Having the SiO bond order as $2+\delta$, meaning partial cross-linked polydimethylsiloxane, is a key to give good SPE performances.

3) Transference number of lithium ion for the single ion type SPE was almost 100 %. Thus it could be applied for specific devices which require constant lithium ion currents.

4) Both the single and double ion type SPE's showed expectable performances for lithium ion battery and other devices for the future, however, the ionic conductivities for both the types still need improvement. Further studies are required for improvement.

## References

1) P. V. Wright, *Br. Polym. J.*, **319**, 137(1975)

2) M. B. Armand, J. M. Chabagno and M. J. Duclot, *Fast Ion Transport in Solids (Edited by P. Vashista, J. N. Mundy and G. K. Shenoy),* p. 131. *Elsevier, New York*(1979)

3) J. R. MacCallum and C. A. Vicent (Eds), *Polymer Electrolyte Review I. Elsevier Applied Science, London*(1987)

4) J. S. Tonge and D. F. Shriver, *Polymer for Electronic Applications (Edited by J. H. Lai)*, p. 157. *CRC Press, Boca Raton, FL*(1989)

5) H. L. Mei, Y. Okamoto, T. Skotheim and C. S. Harris, *Mol. Cryst. Liq. Cryst.*, **160**, 321(1988)

6) M. Watanabe, S. Nagano, K. Sanui and N. Ogata, *Solid State Ionics*, **28-30**, 911(1988)

7) Z. Ogumi, Y. Uchimoto and Z. Takehara, *J. Chem. Soc. Chem. Commun.*, 358(1989)

8) M. Ohyanagi, H. Kanai, Y. Katayama, K. Ikeda and Y. Sekine, *Polym. Commun.*, **26**, 249(1985)

9) M. Watanabe, M. Rikukawa, K. Sanui and N. Ogata, *J. Appl. Phys.*, **58**, 736(1985)

10) M. L. Williams, R. F. Landel and J. D. Ferry, *J. Am. Chem. Soc.*, **77**, 3701(1955)

# Chapter 5

## Siloxane ionomers for electrorheological fluids

5.1 Introduction 82

5.2 Experimental part and results 84

5.3 Discussion 96

5.4 Conclusion 97

## 5.1 Introduction

This chapter also discusses a polymer level function. The materials introduced here are silicone ionomers that have ions on the silicone segments.

Electrorheological (ER) fluid is one of functional fluids that is expected to be applied for advanced electronic devices such as shock absorbers having high performances. ER fluid can transform power when electric voltage is applied, since its viscosity drastically increases under electric fields. It has also a switching function since the viscosity responds to the on/off of electric filed.

Most common and expectable ER fluid type currently is dispersion which comprises particles dispersed in a electro-insulating fluid as the medium. The first ER fluid of this type was reported by Winslow et al[1]. Silica particles were dispersed in dielectric fluids.

Electric charges or dipole moments on the particles are respond to the electric fields, forming a chain like line along with the electric field direction that is believed to exhibit the increase of viscosity. Very high change in viscosity and response to the electric field are required. Scheme 1 illustrates the electrorheological behavior for the particle dispersion system.

Silicone oil (mostly polydimethylsiloxane) is the most suitable for the medium of ER fluid, since it is excellent in insulating, viscosity and thermal properties and has a wide temperature range for use. From standpoints of chemical/physical compatibility and matching of specific gravity, silicone as the material for particle is expected.

Various types of ER fluid have been reported to combine particles having ability to respond electric field and base oils including silicone oils. However, none of them has shown totally good performances[2-9].

In this chapter the variety of chemical modification in silicon was focused to develop excellent silicon based particles for ER fluid. Novel silicone ionomers comprising of alkali metal salts of either carboxylic acid modified silicone or sulfonic acid modified silicone were developed and examined for the particle for ER fluid.

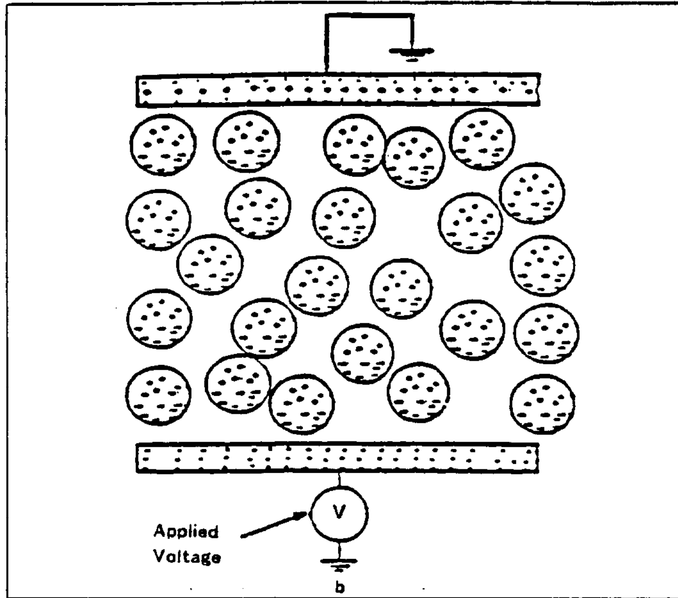


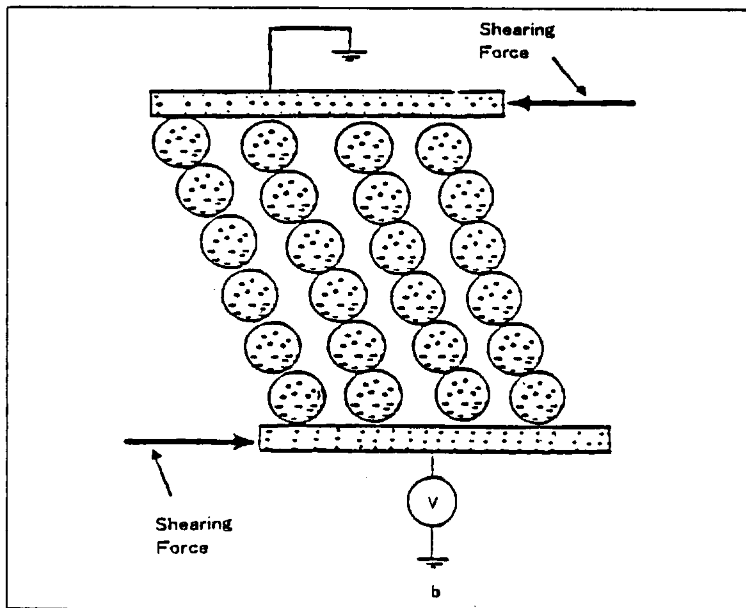


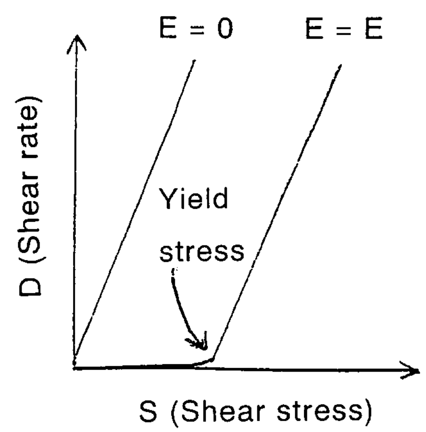


Scheme 1. Electrorheological behavior for a particle dispersion system.

## 5.2 Experimental part and results

*Synthesis of silicone ionomers*

The ionomer, alkali metal salts of carboxylic acid modified silicone, was synthesized through the route shown in Scheme 2. The obtained ionomer was solid and hard when isolated from the solution, probably due to the intermolecular interaction mostly by the aromatic rings. It exhibited no melting point. It was soluble in water, but insoluble in organic solvents.

The ionomer, alkali metal salts of sulfonic acid modified silicone, was synthesized through the route shown in Scheme 3. Lithium salts were not synthesized because of the difficulty of obtaining reagents.

The obtained ionomer was solid and hard when isolated from the solution, probably due that the molecules of the ionomer are crosslinked by polycondensation of silanols.

FT-IR spectra of the carboxylic acid modified silicone and its lithium salt are shown in Fig. 1(a) and (b) respectively. Those of the sulfonic acid modified silicone and its sodium salt are shown in Fig. 1(c) and (d) respectively. Those spectra show that the resultant polymers have expected structures.

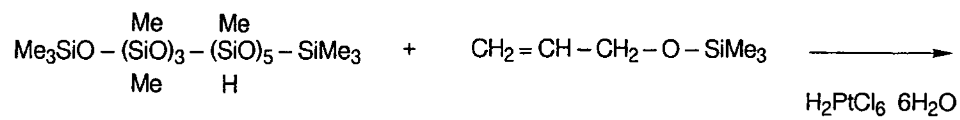


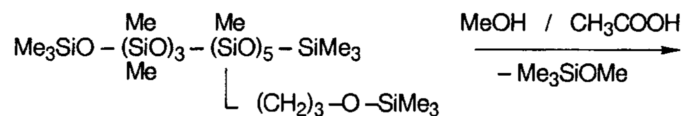


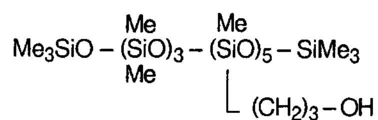


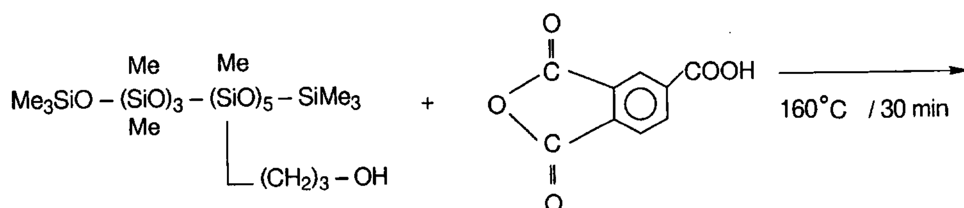


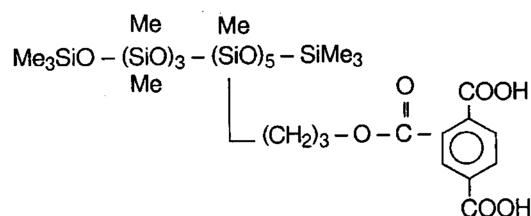


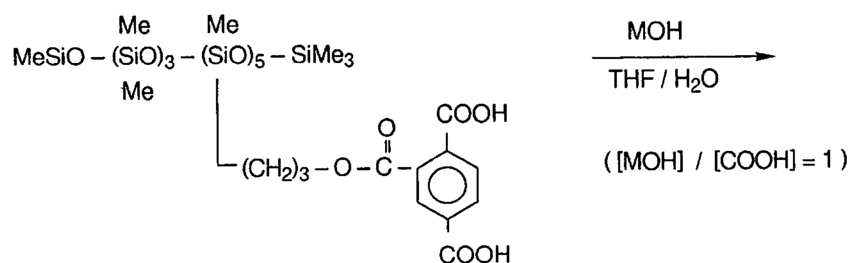


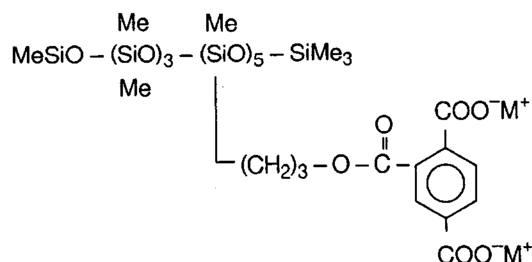


Scheme 2. Synthesis of carboxyl silicone ionomers

$$(MeO)_{3-n}\overset{Me_n}{\overset{|}{Si}}-C_3H_6-O-CH_2-\underset{\diagdown O \diagup}{CH-CH_2} + MHSO_3 \xrightarrow[([MHSO_3]/[\text{epoxide}]=1)]{H_2O\,/\,75\,^{\circ}C}$$

$$(HO)_{3-n}\overset{Me_n}{\overset{|}{Si}}-C_3H_6-O-CH_2-\underset{\underset{OH}{|}}{CH}-CH_2-SO_3^{-}M^{+}$$

Scheme 3. Synthesis of sulfonic silicone ionomers

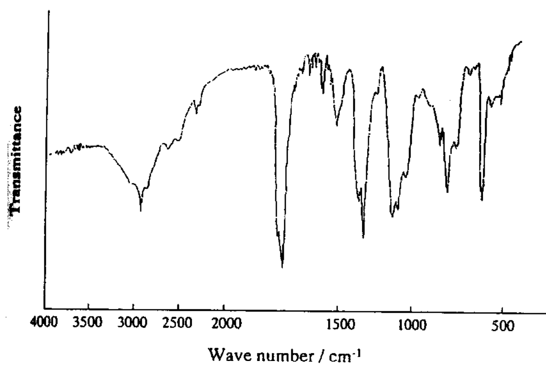


(a) –COOH polymer

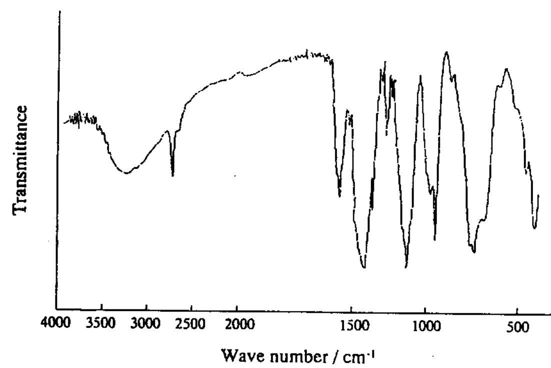


(b) $-COO^{-}Li^{+}$ ionomer

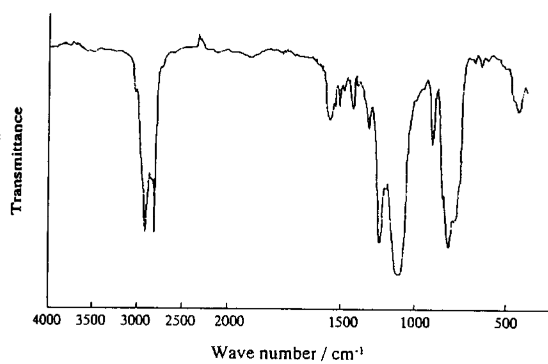


(c) $-SO_3H$ polymer

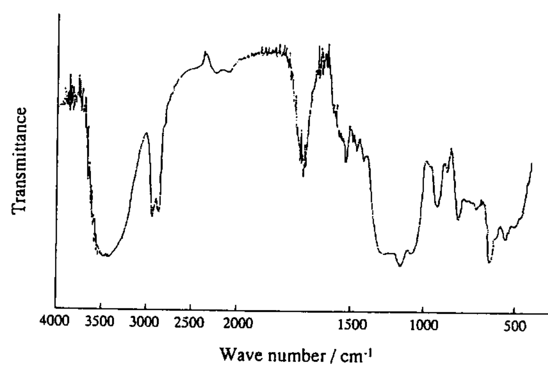


(d) $-SO_3^{-}Na^{+}$ ionomer

Fig.1. FT-IR spectra of silicone ionomers and their starting polymers.

*Particle formation from the ionomers*

Particles of the ionomers were produced by the spray dry method. A Yamato Scientific PALVIS MINI SPRAY GB22 spray drier. 30 % aqueous solutions of the ionomers were supplied to the spray drier. The obtained particles were powder like with white colored in both the ionomer cases. In the case of the sulfonic acid salt type ionomer, the obtained particles were dried at 150 ℃ in vacuum in the form of particle.

Here the ionomer particles are coded as follows.

Alkali metal salts of carboxylic acid modified silicone;

C-M (M = Li, Na, K)

Alkali metal salts of sulfonic acid modified silicone;

S-M-X (M = Na, K)

(X = D(n=1), T(n=0))

The shape of the particles was completely spherical in any type of ionomer. The mean sizes in diameter of the particles were in the ranges of 5 – 10 μm and 2 – 3 μm for C-M and S-M-X, respectively. Photo 1 shows photographs of the silicon ionomer particles by a microscope for C-Li and S-Na-T. The water contents were in the ranges of 6 – 7 %, 8 – 9 % and 2 – 4 % for C-M, S-M-D and S-M-T, respectively. In the case of S-M-T, the solubility in water was drastically reduced and the moisture absorption was very little. The other ionomer particles were soluble in water and had high water absorbing natures except that C-Li had a less water absorbing property.

Table 1 summarizes typical properties of the ionomer particles.

C-Li 10 μm → ←

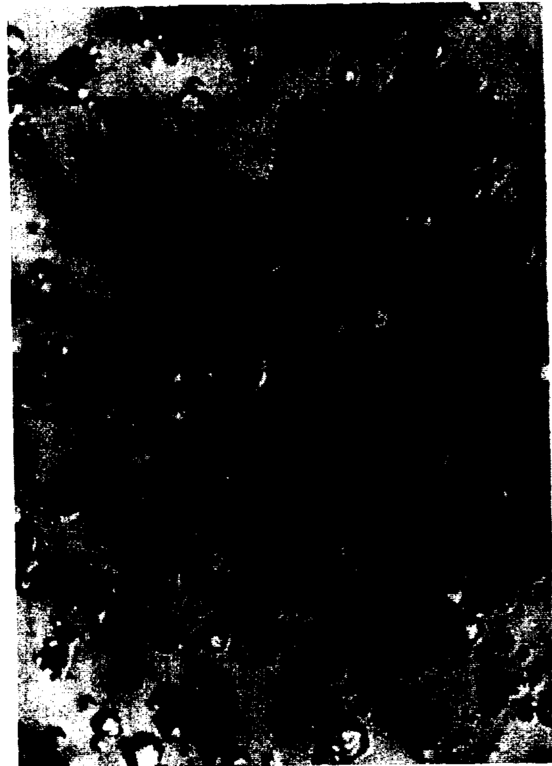

S-Na (T)

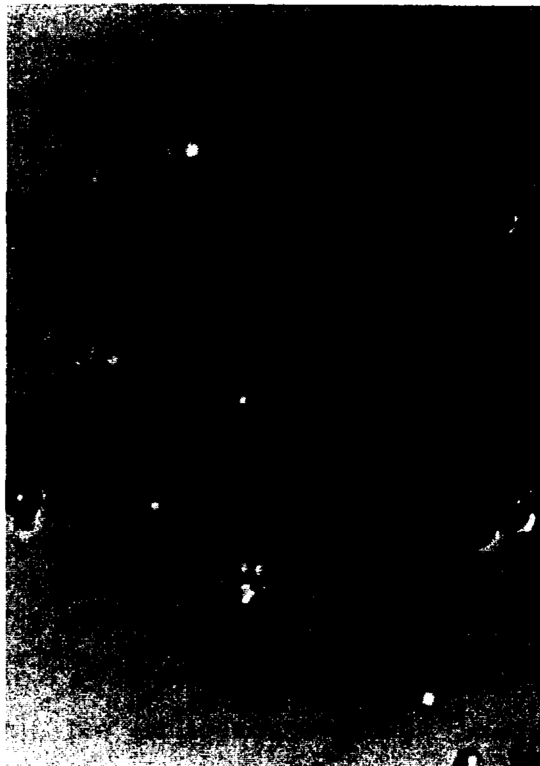

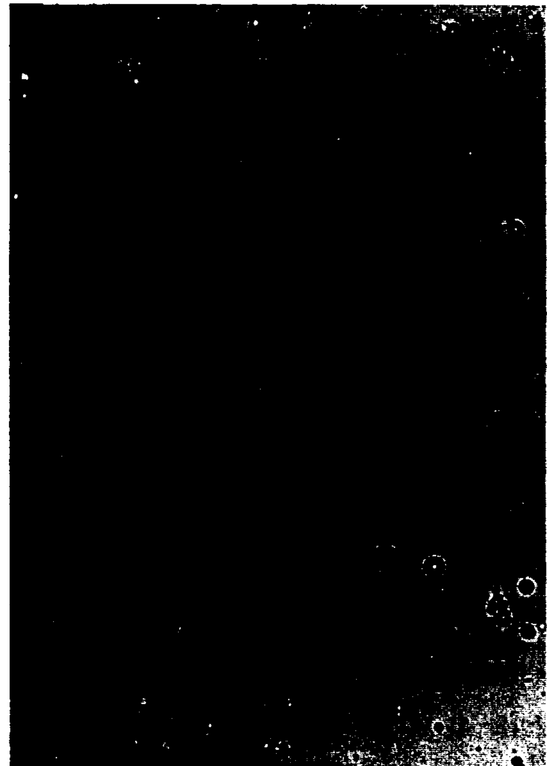

Photo 1. Photographs of silicone ionomer particles by microscope for C-Li and S-Na-T

Table 1. Typical properties of ionomer particles.

| Particle code | Shape | Mean particle diameter (ì m) | Water content (Wt. %) | Solubility in water | Solubility in organic solvents | Moisture absorption |
|---|---|---|---|---|---|---|
| C-Li | Completely spherical | 5 - 10 | 7.0 | Yes | No | Moderate |
| C-Na | Completely spherical | 5 - 10 | 6.5 | Yes | No | High |
| C-K | Completely spherical | 5 - 10 | 6.1 | Yes | No | High |
| S-Na-D | Completely spherical | 2 - 3 | 8.2 | Yes | No | High |
| S-K-D | Completely spherical | 2 - 3 | 8.9 | Yes | No | High |
| S-Na-T | Completely spherical | 2 - 3 | 2.4 | No | No | Low |
| S-K-T | Completely spherical | 2 - 3 | 3.3 | No | No | Low |

*Application of the silicone ionomers for ER fluid*

Right after the final process of particle formation, each kind of ionomer particles shown in Table 1 was dispersed in polydimethylsiloxane oil having a viscosity of 100 CS at 33 wt.% to be tested as ER fluid. The code of the obtaining ER fluid samples is named same as that for the particles as shown in Table 1.

Figure 2 shows the evaluation system and the sample cell for ER fluids. Evaluation of ER properties was carried out using a double cylindrical cell made of aluminum. The size of the rotor was 6 cm (L) x 4 cm ($\phi$). The distance (spacing) between the rotor and the cup was 1 mm. Direct electric voltages were applied between the rotor and the cup. After the cell was filled with an ER fluid, the cup was rotated by a motor in order that the shearing speed (D) increase up to 413 $S^{-1}$ as the maximum for 40 sec then down to zero (ramp mode). Stress (S) was detected with a torque meter that was connected to the rotor. Yield stress was obtained on the D/S plot.

Firstly a screening test was carried out for ER fluid samples with the seven kinds of particle (as shown in Table 1) dispersed. If the break-down voltage was less than 1 kV/mm or a plating (particles are gathered at either side of the electrodes) was seen, the fluid sample failed. Results are seen in Table 2. S-K-X was luck in break-down voltage, and S-M-D showed a plating, thus the two samples failed. The other four samples passed the screening test and were tested for detailed ER properties.

(a)

24V

Timer

5V

+5V

100V

Ramp Buffer

Function Generator

ETC.

V-F Converter

o/c Output

Pulse Input

AC Servo Driver

Toque Transducer Max. 2kg·cm

Strain Amplifier

Max. 9kV

AC Servo Motor Max. 167rpm

X-axis (Shear Stress) max. 2kg·cm

X-Y Recorder

Y-axis (Shear Rate) max. 330/sec

(b)

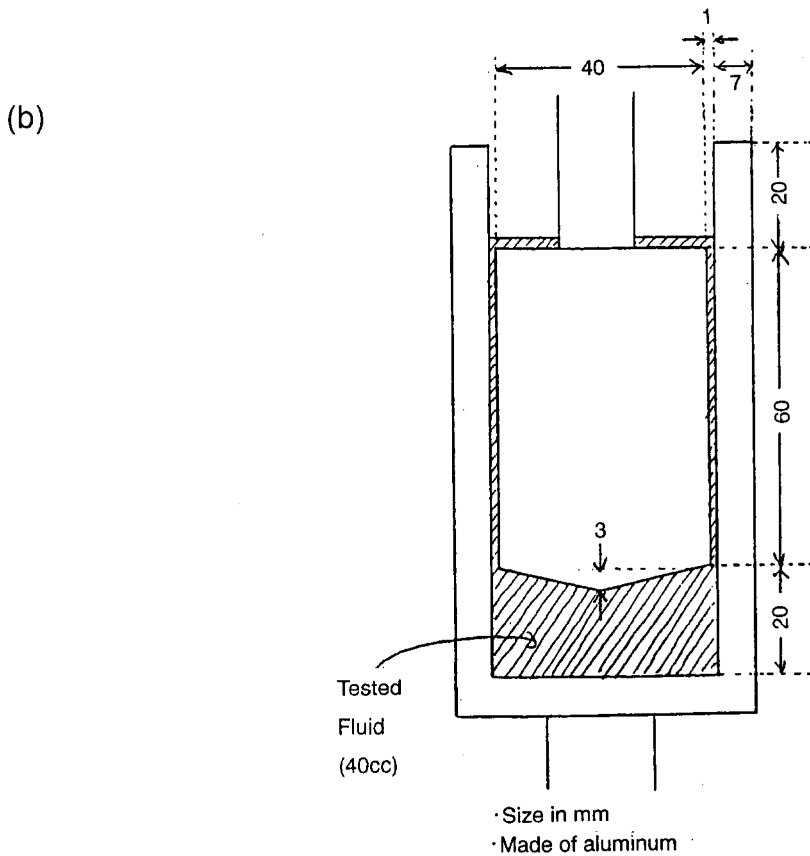


Fig.2. Evaluation system (a) and sample cell (b) for ER fluids

Table 2. Result of screening test

| Code for ER fluid sample | Break down voltage < 1 kV/mm | Plating | Screening test |
|---|---|---|---|
| C-Li | No | No | Passed |
| C-Na | No | No | Passed |
| C-K | No | No | Passed |
| S-Na-D | No | Yes | Failed |
| S-K-D | Yes | Yes | Failed |
| S-Na-T | No | No | Passed |
| S-K-T | Yes | No | Failed |

Figure 3 shows the dependence of yield stress on temperature when the electric filed was fixed as 2 kV/mm. In the case of C-M's (carboxyl acid salts), the yield stress was highest at around 100 ℃, while in the case of S-Na-T, it increase as the temperature increased. Increase of the yield stress versus temperature was in the order for: C-Li < C-Na < C-K. In the case of C-K, the leak current increased as the temperature increased. At 100 ℃ a break-down occurred and the particles were agglomerated at the same time in C-K. Current leakage was little for C-Li. It was stable even after several thermal cycles up to 150 ℃. The champion data of yield stress in this study was 2150 Pa for C-Li at 100 ℃ / 4 kV/mm. The highest yield stress for S-Na-T was 560 Pa at 150 ℃ / 2 kV/mm. The thermal stability for S-Na-T was excellent.

An aging test was carried out to check if the properties of the fluids can be kept. 100 ℃ was applied to the samples. Within a few hours, all the fluids showed good stabilities except C-K. For several days of the aging, only S-Na-T kept its properties, whereas the other fluids showed some agglomeration of the particles or were deteriorated in properties.

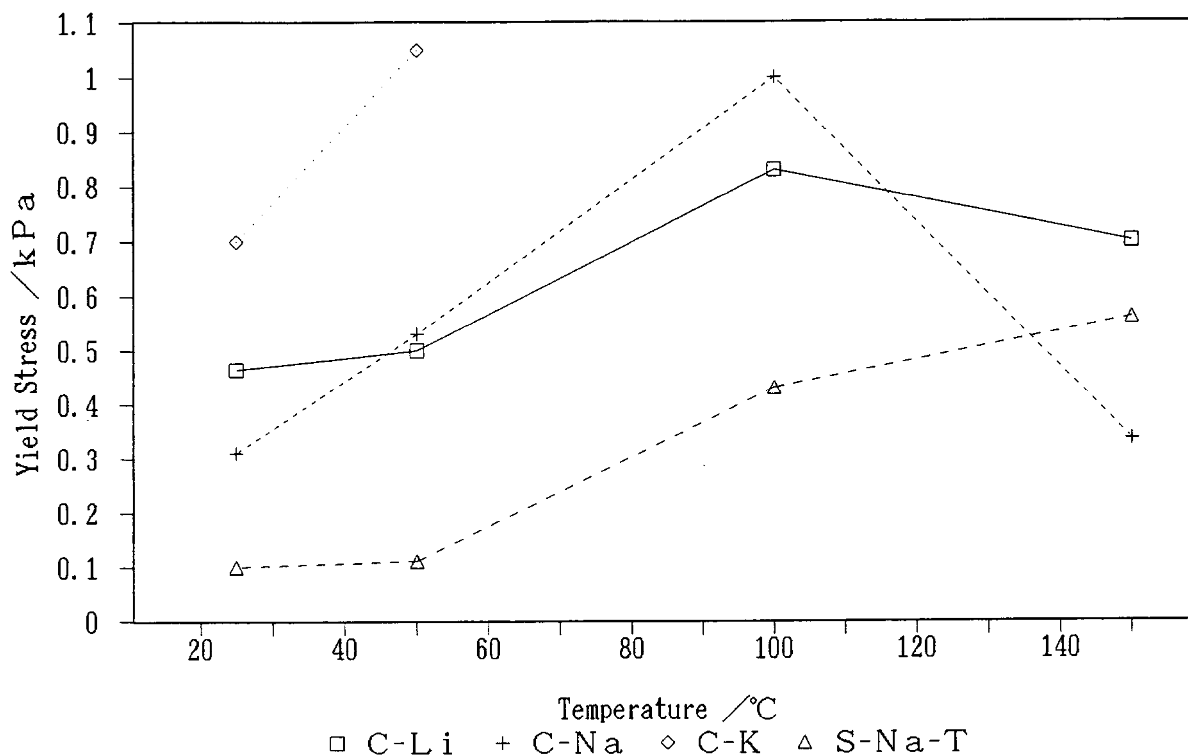


Fig.3. Dependence of yield stress on temperature (electric field = 2 kV/mm)

Fig.4 shows the dependence of leak current on temperature when the electric filed was fixed as 2 kV/mm. In the case of C-M's (carboxyl acid salts), all the samples showed very low levels of leak current at room temperature, however, it increased as the temperature increased. The leak current at a same temperature was in the order for: C-Li < C-Na < C-K. On the other hand, S-Na-T kept very low leak currents in the order of $10^{-9}$ A/cm$^2$ at the whole tested temperature range. The concentration of ions for S-Na-T was almost same as that for C-M's, however, its yield stress was lower.

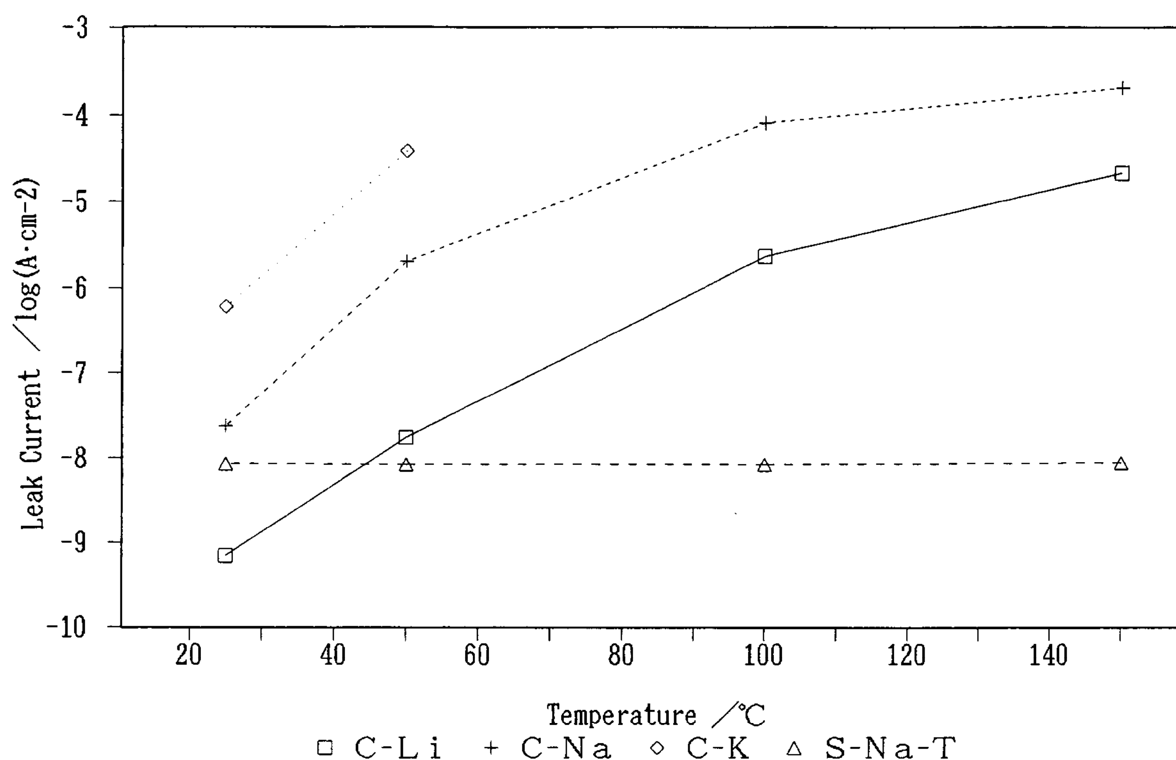


Fig.4. Dependence of leak current on temperature (electric field = 2 kV/mm)

Time lag between the supply of electric voltage and torque increase was evaluated for only C-Li fixing the shearing speed and the electric field as 132 $S^{-1}$ and 1 kV/mm, respectively. The response time was 26 msec.

Storing stability was evaluated by visually checking if a supernatant phase is formed due to the sedimentation of particles. The life was in several weeks for C-M's, whereas that was in several days for S-Na-T.

Also, re-producibility was checked for the four kinds of ER fluid. All the four fluids showed excellent re-producibilities.

Summary of the ER properties for the four kinds of ER fluid samples is shown in Table 3.

Table 3. Summary of ER properties

| Code for ER fluid sample | Basic viscosity (CS) | Yield stress (Pa) 25℃-2kV/mm | Yield stress (Pa) Maximum | Leak current (A/cm, @2kV/mm) 25℃ | Leak current (A/cm, @2kV/mm) 100℃ |
|---|---|---|---|---|---|
| C-Li | 560 | 465 | 2150[2)] | $6.8 \times 10^{-10}$ | $2.3 \times 10^{-6}$ |
| C-Na | 370 | 310 | 1000[3)] | $2.3 \times 10^{-8}$ | $8.0 \times 10^{-5}$ |
| C-K | 340 | 700 | 1500[4)] | $6.0 \times 10^{-7}$ | -[6)] |
| S-Na-T | 320 | 100 | 560[5)] | $8.4 \times 10^{-9}$ | $8.2 \times 10^{-9}$ |

| Code for ER Fluid sample | Stability at high temperatures[1)] Within several hours | Stability at high temperatures[1)] Within several days | Time for supernatant formation |
|---|---|---|---|
| C-Li | Good | Bad | Several weeks |
| C-Na | Good | Bad | Several weeks |
| C-K | Bad | Bad | Several weeks |
| S-Na-T | Good | Good | Several days |

1) For several hours or several days, re-producubility of the properties.

2) 100 ℃ - 4 kV/mm  3) 100 ℃ - 2 kV/mm  4) 25 ℃ - 4 kV/mm  5) 150 ℃ - 2 kV/mm

6) Break down.

## 5.3 Discussion

*Application of the silicone ionomers for ER fluid*

The ER fluids with the silicone ionomers showed generally high yield stress values, low leakage current values and stability over temperature. The ion pairs in the ionomer particles may be well oriented to the direction of the electric voltage because of the free rotation energy for the SiO bond. The same material of silicon for both particle and dispersing media should contribute to the good ER performances and stability.

The tendencies of yield stress and leakage current versus the kind of alkali metal are probably due to the ionization tendency of the alkali metals.
The flat temperature dependency for the S-Na-T system is very encouraging for ER fluid, however, it is very rare in ER fluids whose particles are ionically charged. It is probably because the mobility of the ions in the particle is limited in a small local area due to the three dimensional (resin) structure of the ionomer. The short life for S-Na-T is probably because of a higher specific gravity of the particles having the resin structure.

### 5.4 Conclusion

1) Novel silicone inomers, alkali metals of carboxyl acid modified silicone and those of sulfonic acid modified silicone, were developed and particles of those ionomers were made. ER fluids were prepared by dispersing these ionomer particles in a silicone oil. ER properties were examined.

2) It is generally concluded that the ER fluids comprising of the siloxane ionomers showed high levels of yield stress, stable performances at high temperatures and good dispersing stability, compared to other types of ER fluid.

3) ER properties are summarized as follows with regard to the following parameters.

| | Salt type | Alkali metal | SiO bond order |
|---|---|---|---|
| Potential response to electric field | $SO_3M$ > COOM | K > Na > Li | (High) 2 > 3 |
| Actual yield stress | COOM > $SO_3M$ | K > Na > Li[1)] | -[2)] |
| Leak current | $SO_3M$ > COOM | K > Na > Li | 2 > 3 (better) |
| Thermal stability | COOM > $SO_3M$ | Li > Na > K | (Better) 3 >> 2 |
| Plating | $SO_3M$ > COOM | K > Na > Li | 2 > 3 (better) |

1) In the case of COOM. 2) Not always determined.

Higher ionic polarity (ie, sulfonic acid salt or K) and lower network flexibility (bond order = 2) gave better potential responses to electric field. However, higher response will cause negative properties such as leak current as well as potential higher yield stresses. Therefore, optimization is needed to balance these properties.

4) An ER fluid comprising of a sulfonic acid salt type ionomer having the SiO bond order = 3 showed a very flat leak current versus temperature. This is a remarkable performance that is required for advanced ER devices.

## Reference


1) W. M. Winslow, *J. Appl. Phys.*, **20**, 1137(1949).

2) K. Yatsuzuka, K. Miura, N. Kuramoto, and K. Asano, *IEEE Trans. Ind. Appl.*, **31**(3), 457(1995).

3) H-Q. Xie, J-G. Guan, and J-S. Guo, *J. Appl. Polym. Sci.*, **58**, 951(1995).

4) A. Inoue and S. Maniwa, *J. Appl. Polym. Sci.*, **55**, 113(1995).

5) Y. Asako, S. Ono, R. Aizawa, and T. Kawakami, *Int. J. Modern Phys. B*, **10**, 3159(1996).

6) T. Hao, Z. Xu, and Y. Xu, *J. Colloid Interface Sci.*, **190**, 334(1997).

7) H. J. Choi, M. S. Cho, and K. To, *Physica A*, **254**, 272(1998).

8) J. W. Kim, S. G. Kim, H. J. Choi, and M. S. Jhon, *Macromol. Rapid Commun.*, **20**, 450(1999).

9) J. Plocharski, M. Rozanski, and H. Wycislik, *Synth. Met.*, **102**, 1354(1999).

# Chapter 6

## Polyhydrogensilsesquioxane thin films for inter layer dielectric applications


6.1 Introduction 100

6.2 Dynamic viscoelastic behaviors of HSQ resin at high temperatures 106

- 6.2.1 Experimental part 106
- 6.2.2 Results 109
- 6.2.3 Discussion 110
- Appendix (Fig. 2 - 17) 112

6.3 Oxidative curing of hydrogen silsesquioxane resin films enhanced by electron beam at ambient temperature and characterization of the cured films 120

- 6.3.1 Experimental part 120
- 6.3.2 Results 122
- 6.3.3 Discussion 130

6.4 Formation of HSQ based low-k films 133

- 6.4.1 Experimental part, results and discussion 133

6.5 Conclusion 134

## 6.1 Introduction

Polyhydrogensilsesquioxane (HSQ, $(HSiO_{3/2})_n$) resin is widely used as a precursor for silica films for interlayer dielectric (ILD) applications. HSQ can gap fill and planarize the patterned substrate excellently since it has a sharp melting point at around 180 ℃. It is a completely inorganic material, so that it will give affinity and cost benefit to the integration processes for IC devices. Also the cured HSQ film has a low dielectric constant of around 3.0 that is much lower than that of conventional $SiO_2$ based films.

The synthesis method for HSQ was first reported by Frye and Collins[1] as shown in Scheme 1.

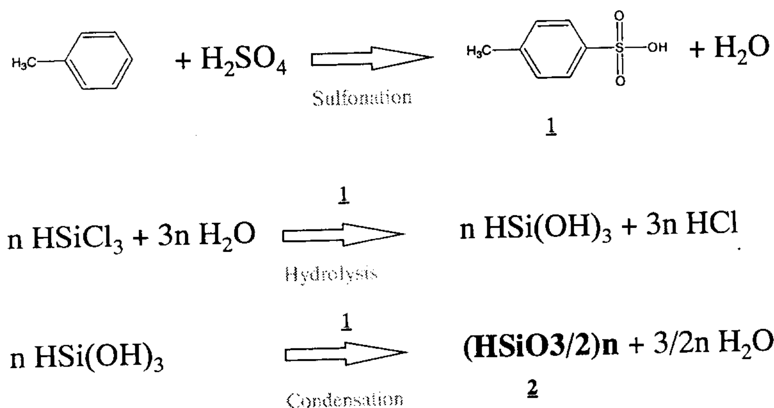


**2 : Polyhydrogensilsesquioxane (HSQ resin)**

Scheme 1. Synthesis route for poly hydrogensilsesquioxqne (HSQ) resin

Since the HSQ resin can be spun onto substrates through solutions to form thin films and be cured (ie, converted to silica) by oxidation mostly with heat, efforts had been made to establish an electronics grade of HSQ resin and its practical application processes. Commercial products and their application processes were establish in 1990's[2,3]. The standard process sequence was as follows: 1) Spun into thin films via organic solution. 2) Pre-bake at 150 – 350 ℃ for gap fill and planarity. 3) Cure in a furnace at 400 ℃ for 1 h with nitrogen flow. It is schematically shown in Scheme 2.

| Spincoat | Flow | Cure |
|---|---|---|
| 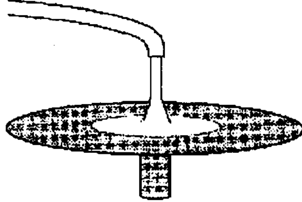 | 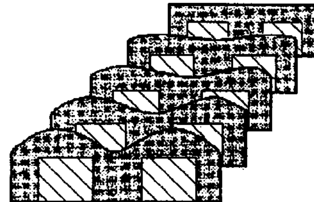 | 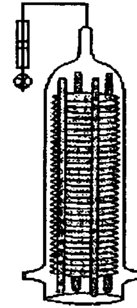 |
| Apply HSQ film with conventional SOG spin coater | Melt and flow with hot plate processing | Cure film in quartz tube furnace |
| Thickness= 0.2 - 1.2 (um) | (150/200/350 °C/ 1min) | (400 °C/$N_2$/1h) |

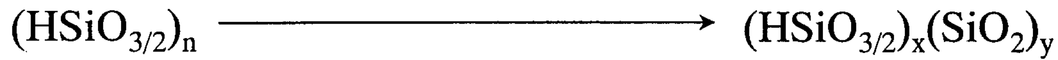


Scheme 2. Application process for HSQ resin.

Table 1. A typical roadmap for interlayer materials for advanced LSI's

| | Design rule (μm) | | | | |
|---|---|---|---|---|---|
| | 0.25 | 0.18 | 0.13 | 0.10 | 0.07 |
| Volume production start (Yr.) | 1995 | 1998 | 2001 | 2005 | 2009 |
| Required k | $\lesssim$ 3.5 | $\lesssim$ 3.3 | $\lesssim$ 2.7 | $\lesssim$ 2.5 | $\lesssim$ 2.0 |
| Best material | HSQ, Fluorinated $SiO_2$ | HSQ, Fluorinated $SiO_2$ | Organic materials | Low k and inorganic material | Low k and inorganic material |

Scheme 3 shows a drawing of the cross section of an LSI device being currently produced and explanations about materials for semiconductor fabrication. HSQ is currently used for the ILD application using the SOD (spin-on dielectrics) technology. HSQ is believed to be applied to other applications.

Table 1 shows a typical roadmap for interlayer materials for advanced LSI's. As well known, the required k (dielectric constant) becomes lower as the device generation proceeds (ie, as the design rule becomes smaller). Now IC manufacturers are going to develop fabrication processes with fixing an interlayer material for the 0.10 $\mu$m design rule generation. At the same time the industry and research institutes are collecting materials having k = 2.0 or lower. In general, organic materials can achieve lower k values more easily than inorganic materials. However, future LSI devices require tough and adhesive materials like $SiO_2$. There has never been such materials having both high SiO bond order (close to 4) and low k. In this study, the author targets these materials.

Scheme 4 summarizes possible reactions of HSQ resin. Figure 1 shows an infrared spectrum of a typical HSQ resin and the relationship between the structure and the absorption bands. There are mainly four kinds of reactions. One is a bond rearrangement reaction mainly from the cage-like structure to the network structure without changing the elemental composition. This reaction is promoted dominantly by heat. Typically it occurs at over 350℃ with or without oxygen. This reaction gives the HSQ film tougher due to the increase of molecular weight. The next one is an oxidation reaction. Oxygen attacks SiH bonds in HSQ resin. In most cases the SiH bonds are converted to silanols by oxygen, then the silanols are condensed to form $SiO_2$ structures. This means that both oxidation and cross-linking (cure) reactions take place. We call it "oxdative cure" in this thesis. This reaction is promoted by either temperature or oxygen concentration in the atmosphere. It is empirically known that this reaction occurs at over about 300℃ in air, on the other hand it occurs very easily under a very small oxygen concentration if the temperature is around 400 ℃ or higher.

The oxidative cure is the major reaction that takes place on HSQ films at typical interlayer dielectric applications. It is believed that the oxidative reaction is more dominant than the bond rearrangement.

There are two other possible reactions, hydrolysis by water and redistribution.

However, these reactions are believed not to take place very dominantly at the typical application processes on HSQ resin.

Practically the oxygen concentration in the furnace is typically controlled as in the range of 10 to 100 ppm. This small concentration of oxygen is believed to take a significant role for the oxidative cure of HSQ resin. At the step 3) HSQ is partially converted to Silica. The remaining % SiH concentration in the cured film is in the range of 60 to 90 typically that gives the total best film performances.

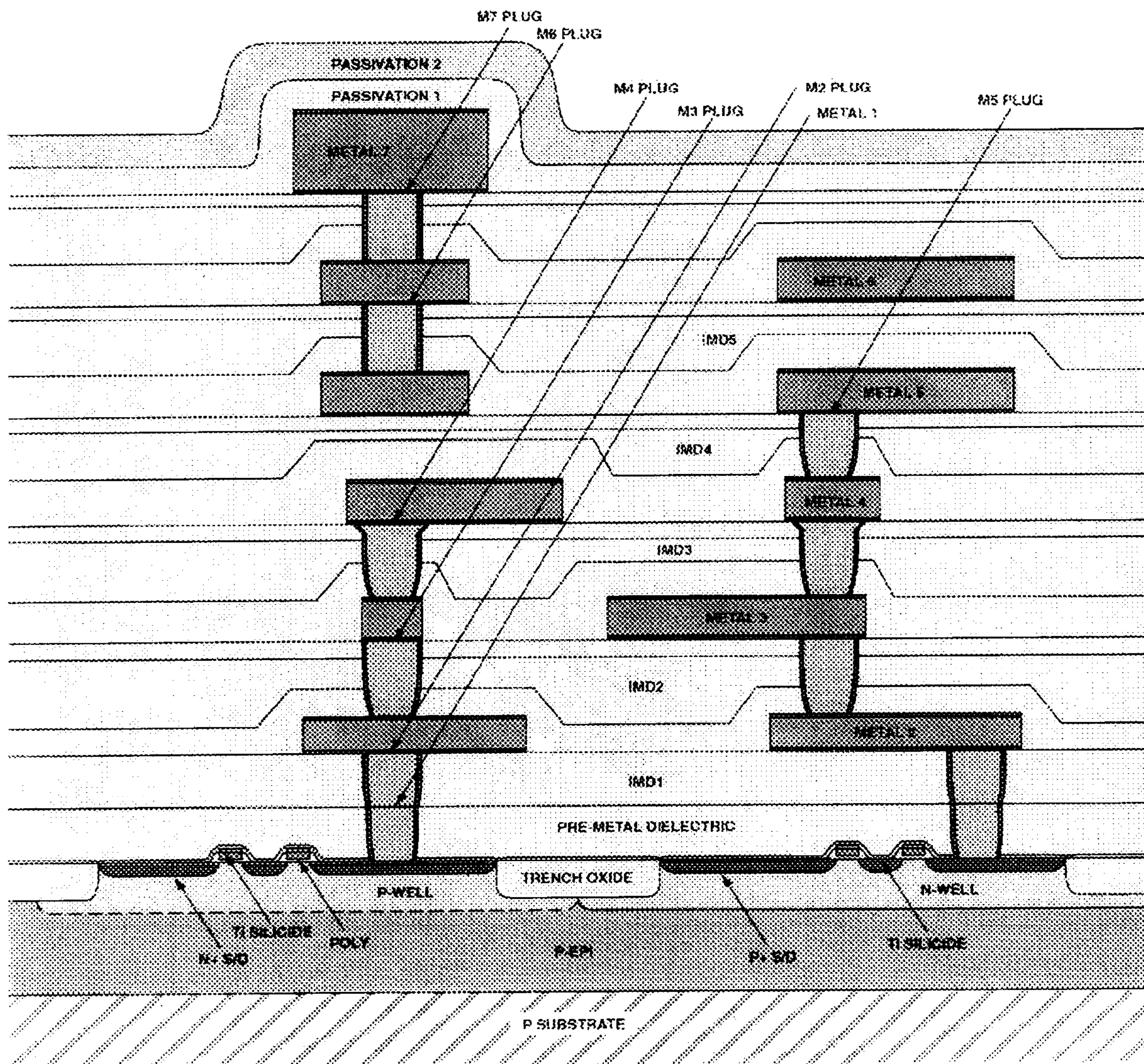


Scheme 3. Drawing of cross section of LSI device being currently produced and explanations about materials for semiconductor fabrication.

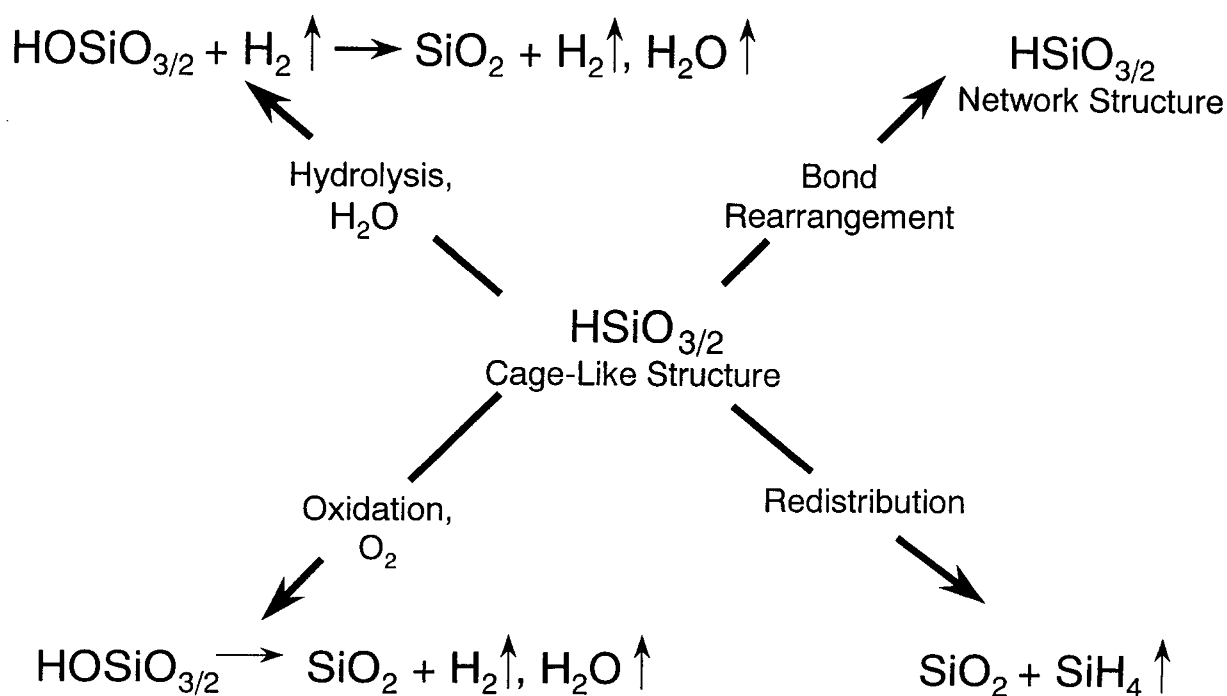


Scheme 4. Possible reactions of hydrogen silsesquioxane resin

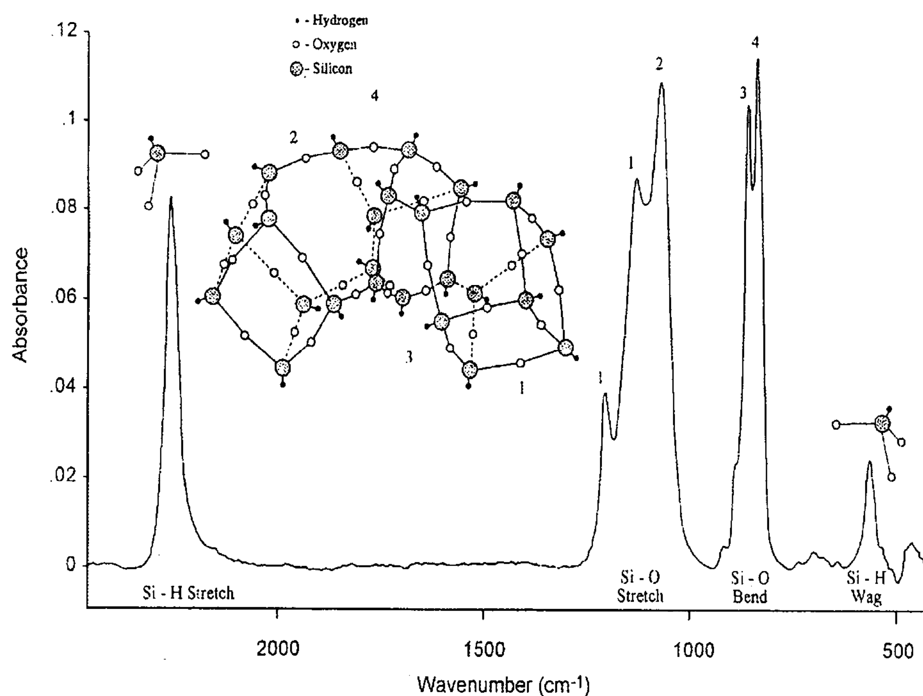


Fig.1. Typical FT-IR spectrum of hydrogen silsesquioxane resin

The cured HSQ films have been reported to have a cracking threshold near 1.2 μm[2,3]. Next generation microelectronics devices will require cure processes that demonstrate cost and throughput improvements over thermal cures. Also, lower cure temperatures and higher crack-free thicknesses will be required. Very little study has been carried out to understand the cure mechanism and dynamics.

The current process conditions have been established empirically expecting that melting and flowing on hot plates and oxidative curing in furnaces. The curing temperature 400℃ was established since it was very productively available.

None of scientific approaches have been made to understand the behaviors of HSQ resin and to established processes for improved performances of HSQ films.

In Section 6.2 a schematic analysis of dynamic viscoelasticity on HSQ resin at high temperatures is described to catch to understand thermal and oxidative behaviors of HSQ resin and improve the cracking threshold.

Cure of HSQ films enhanced by electron beam has been reported in several papers[4,5]. Electron beam is believed to enhance the reaction of SiH groups in HSQ resin.

In the study introduced in Section 6.3, electron beam was applied to HSQ films at ambient temperature and pressure to cure HSQ oxidatively into silica and basic characterizations were performed on the cured films. Crack resistance behaviors were also investigated.

HSQ resin gives low-k (k; dielectric constant) films as low as around 3.0 if the remaining SiH % is moderately controlled. This is one of big advantages for interlayer dielectric applications. However, for future LSI's, especially for logic IC's, lower k is required to achieve more advanced performances such as high speed. For instance, k as 2.0 or lower is required for devices having 0.10 μm design rules which will be actualized in around 2005.

In Section 6.4, a supplemental study on HSQ is introduced to show updated studies by the author et al. One of useful technical approach to achieve low k is to form porous materials since the k for pore is 1.0 (very low). In this section a novel process is discussed to have porous HSQ based films.

## 6.2 Dynamic viscoelastic behaviors of HSQ resin at high temperatures

### 6.2.1 Experimental part

HSQ resin was synthesized by the manner which was reported by Frye and Collins[1] and was fractionated by molecular weight in a dual solvent system using toluene and acetonitrile. Number average molecular weight and weight average molecular weight of the fractionated resin were 3,360 and 10,360 respectively. The obtained fraction was white and power like.

Analyses were taken on a Rheometric Scientific ARES dynamic analyzer using 25 mm φ aluminum parallel plates as the test fixture. Vibrations with 1 Hz frequency was applied to samples at temperature range of 200 to 400 ℃ in either nitrogen or air atmosphere. Fixed and variable conditions for measurement are shown in Tables 2 and 3, respectively.

Table 2. Fixed conditions for dynamic viscoelastic measurement of HSQ resin

| Item | Condition |
|---|---|
| Test fixture | : Parallel aluminum plates, 25 mm φ |
| Frequency | : 6.28 rad/sec (1 Hz) |
| Strain | : 3.0 % |
| Auto tension direction | : Compression |
| Auto tension sensitivity | : 20.0 gm |
| Initial static force | : 10.0 gm |
| When sample modulus < | : 1.0 dyne/cm$^2$ |
| Auto strain | : On |
| Max applied strain | : 197.0 % |
| Max allowed torque | : 1000.0 gm·cm |
| Min allowed torque | : 2.0 gm·cm |
| Strain adjustment | : 20.0 % of current strain |
| Initial temperature | : 200 ℃ |
| Preheat of sample on plate | : 200 ℃ for ca. 1 min |
| Time from 200 ℃ to holding temperature (on Runs # 5 – 12) | : 200 sec |

Table 3. Variable conditions for dynamic viscoelastic measurement of HSQ resin

| Run # | Atmosphere | Temperature mode | Figures # |
|---|---|---|---|
| 1 | $N_2$ | 3℃/min ramp up (200 → 400℃) | 2, 3 |
| 2 | Air | 3℃/min ramp up (200 → 400℃) | 4, 5 |
| 3 | $N_2$ | 200℃ -(ramp up/100sec) → 300℃ | 6, 7 |
| | | -(ramp down/100sec) → 200℃ | |
| | | → 200℃ hold/100sec | |
| | | → 3℃/min ramp up (200 → 400℃) | |
| 4 | $N_2$ | 200℃ -(ramp up/100sec) → 350℃ | 8, 9 |
| | | -(ramp down/100sec) → 200℃ | |
| | | → 200℃ hold/100sec | |
| | | → 3℃/min ramp up (200 → 400℃) | |
| 5 | $N_2$ | 350℃ hold/2000sec | 10 |
| | | -(ramp down/100sec) → 200℃ | |
| | | → 3℃/min ramp up (200 → 400℃) | |
| 6 | Air | 250℃ hold/2000sec | 11 |
| 7 | $N_2$ | 300℃ hold/2000sec | 12 |
| 8 | Air | 300℃ hold/2000sec | 13 |
| 9 | $N_2$ | 350℃ hold/2000sec | 14 |
| 10 | Air | 350℃ hold/2000sec | 15 |
| 11 | $N_2$ | 400℃ hold/2000sec | 16 |
| 12 | $N_2$ | 400℃ hold/2000sec | 17 |

Scheme 5 shows the equipment and the test fixture for dynamic viscoelastic measurement.

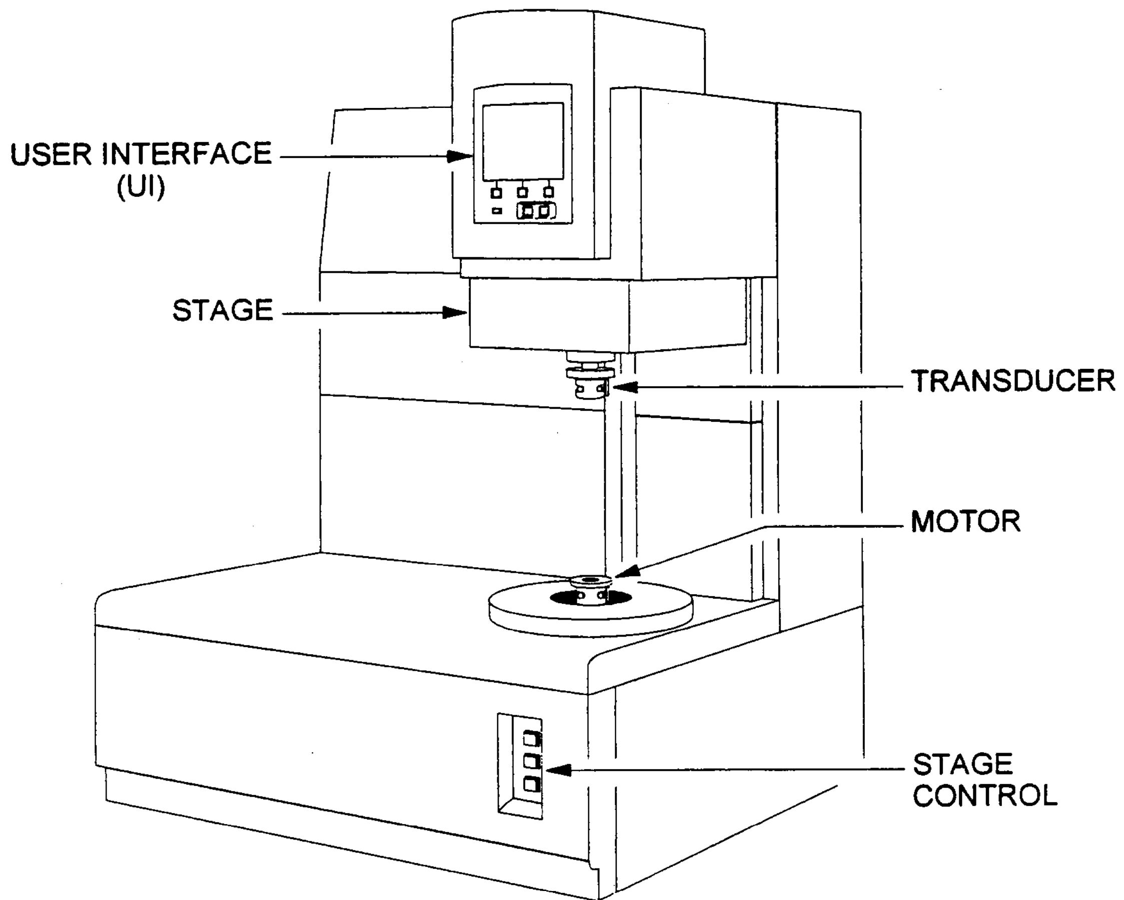


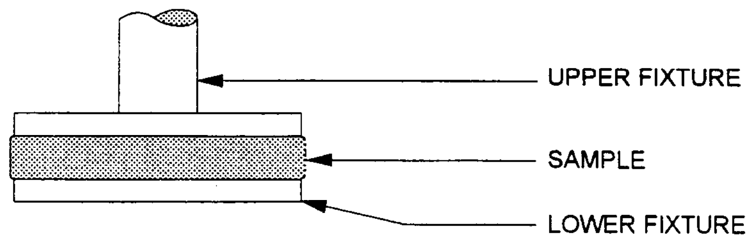


Scheme 5. Equipment and test fixture for dynamic viscoelastic measurement.

Temperature mode was chosen as ramp up or hold, or their combination. In Runs # 3 and 4, short time ramps (peak temp: 300 and 350 ℃, respectively) were programmed before a standard ramp up in nitrogen. In Run # 5, a ramp was followed by a 350 ℃ hold in nitrogen to see the effect of the bake at 350 ℃ more in detail.

Sample powders were preheated before the measurement between the parallel plates at 200 ℃ for about 1 minute in order to form a continuous phase of HSQ resin and enough adhesive forces between HSQ resin and the plates. At this temperature HSQ resin is believed to be rarely oxidized and melt in nitrogen or air, since its melting point is usually around 180 ℃. Sample weight and gap (distance between the plates) were not exactly constant for each run. The gap was actually 1 mm or a little narrower. Oxygen concentration in the sample chamber when nitrogen was flowed was not detectable, however, the flow rate was constantly controlled.

To process data, G' (storage modulus) and G" (loss modulus) were output.

### 6.2.2 Results

Sixteen figures (Figs.2 – 17) were made by plotting G' , G" and/or temperature versus time or temperature. The figures are in Appendix (p. 112 - 119).

Looking overview of the data, G" decreased to an undetectable low value drastically and clearly at a specific point as either temperature ramped up or time proceeded at a holding temperature. This point is called $G"_c$ in this study. Whereas the elastic factor G' increased gradually as either temperature ramped up or time proceeded at holding temperatures. Generally $G"_c$ appeared at shorter time or at a lower temperature in air than in nitrogen. G' increased more rapidly in air than in nitrogen.

In nitrogen G' was minimum at 285 ℃ and $G"_c$ was at 377 ℃ (Fig.3). G' increased gradually up to the $10^8$ dyne/cm$^2$ order as the temperature ramped up from 300 through 400 ℃. Whereas in air, G' was minimum at 250 ℃ and $G"_c$ was at 290 ℃ (Fig.5), and G' was saturated at around 310 ℃. However, the patterns of G' and G" for in nitrogen and in air were similar (compare between Figs.3 and 5).

Next, the effect of preheat at either 350 ℃ or 350 ℃ in nitrogen prior to the standard ramp up (Runs # 3 – 5, Figs. 6 – 10) is reviewed. In Runs # 3 and 4, the figures showed small thermal histerisis, so it is recommended for the holding time at 200 ℃ after the preheat to be longer. However, the following observations may be

introduced from the figures. To look at Figs. 6 and 7, the effect of the small preheat at 300 ℃ on the pattern of G' and G" was not very significant. Whereas the effect of the preheat at 350 ℃ with short time (Figs. 8 and 9) on the successive curing behavior was significant, ie, the change of G' and G" with temperature ramp up was small. When the preheat at 350 ℃ was long (2000 sec) (Fig.10), this effect was more significant.

Lastly, the data with temperature holding modes (Runs # 6 – 12, Figs. 11 – 17) is reviewed. It was particular that $G"_c$ was at very short time at 350 ℃ or a higher temperature for both in nitrogen and in air. On the other hand, the minimum G' value at 300 ℃ was almost same as that at 350 ℃. In air at 300 ℃ (Fig.13), the curing speed was fast and the minimum G' value was low. In air at 250 ℃ (Fig.11), the curing speed was moderate, however, the standard G' value was over $10^9$ dyne/cm$^2$, higher than that in nitrogen at 400 ℃ (Fig.16). Furthermore, G' at $G"_c$ in air at 250 ℃ was almost $10^9$ dyne/cm$^2$, whereas that in nitrogen at 400 ℃ was $10^8$ dyne/cm$^2$. However, the minimum G' value at 250 ℃ was higher than those at higher temperatures.

### 6.2.3 Discussion

Above $G"_c$ HSQ resin could be believed to be rigid. This may suggest that HSQ resin changes its mechanical property very drastically during a conversion to silica.

The data suggests that HSQ resin could be cured more easily in air than in nitrogen. Since the patterns of G' and G" for in nitrogen and in air were similar it is, to roughly say, that the figure for in air is simply compressed in the x-axis direction of the figure for in nitrogen.

The data on the preheat at 350 ℃ may suggest that the matrix of resin structure is mostly determined at 350 ℃. Anyway, some critical point with regard to structure determination may exist at between 300 and 350 ℃.

Judging from the data on the temperature holding modes, HSQ resin seemed to be liquid at the initial time. Therefore, the phase of HSQ resin changed very drastically with short time at these temperatures. In nitrogen at 300 ℃ (Fig.12), the curing speed was very slow.

The cure reaction on HSQ resin in air at 250 ℃ could be suggested to be mild with keeping certain viscosity and complete until getting more strength of films than in nitrogen at higher temperatures.

Overall, temperature and oxygen seems to play different roles on the cure of HSQ resin, although it has already been shown that temperature and oxygen content are alternative factors to each other in terms of SiH consumption. According to the results in this study, oxygen seems to act as an accelerator for the curing reaction, whereas temperature, in the other words "heat energy", seems to determine intrinsic viscoelastic behaviors of HSQ resin.

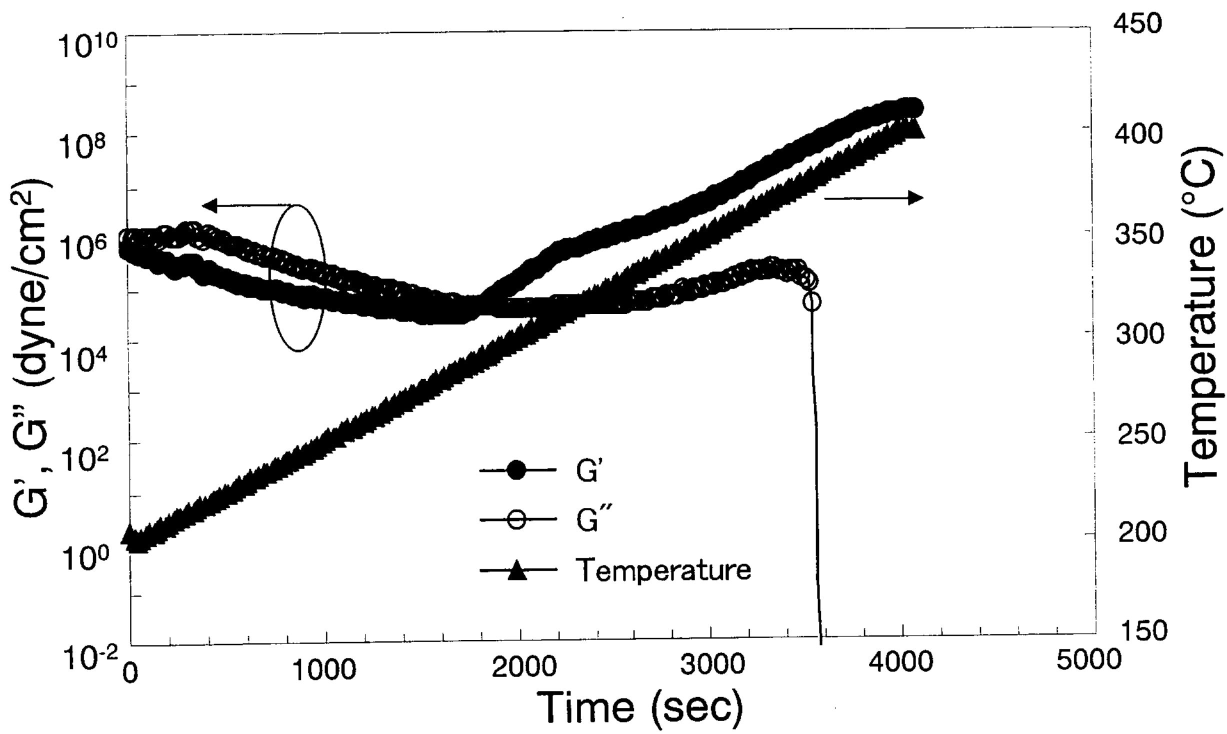


Fig.2. Dynamic viscoelastic behaviors of HSQ resin (in N2, 1 Hz)(Run#1)

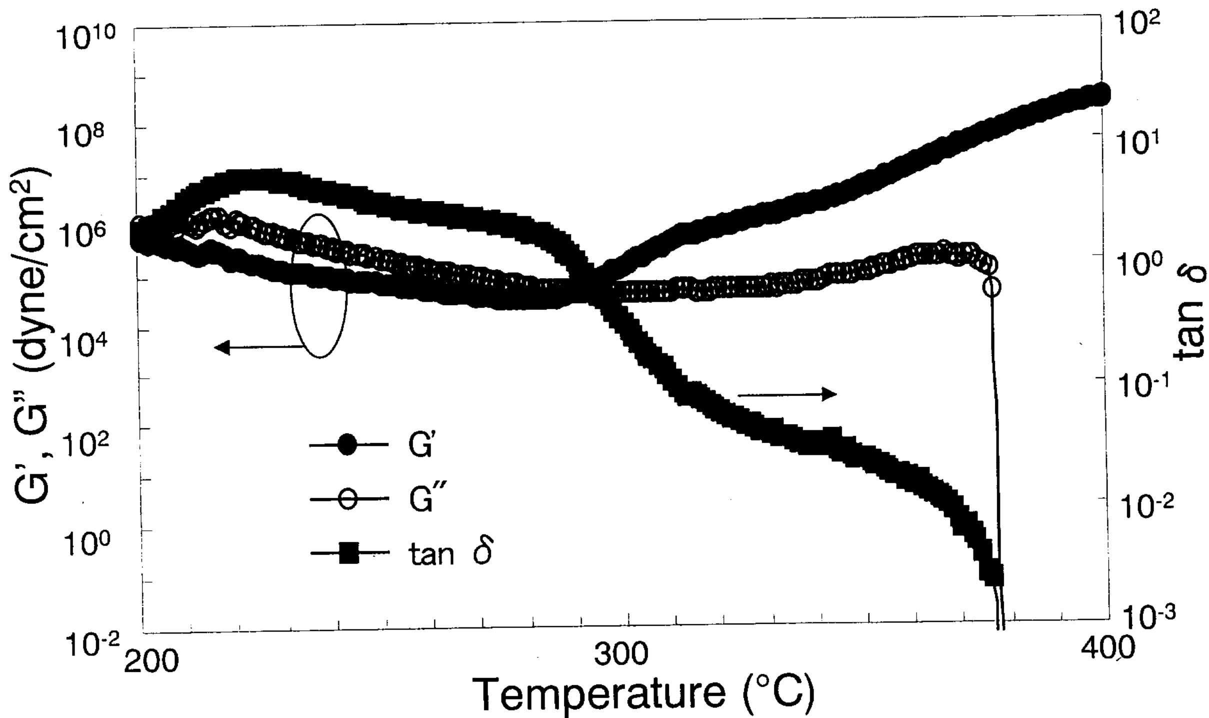


Fig.3. Dynamic viscoelastic behaviors of HSQ resin
(in N2, 3 °C/min, 1 Hz)(Run#1)

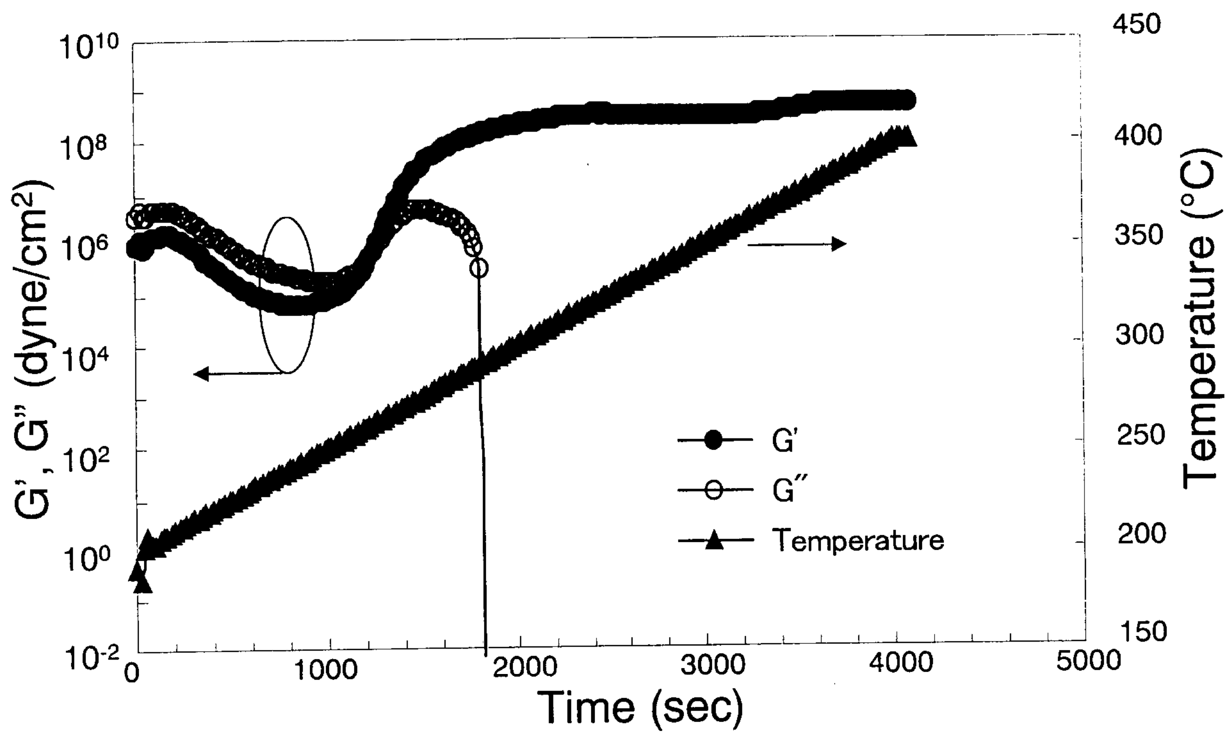


Fig.4. Dynamic viscoelastic behaviors of HSQ resin (in air, 1 Hz)(Run#2)

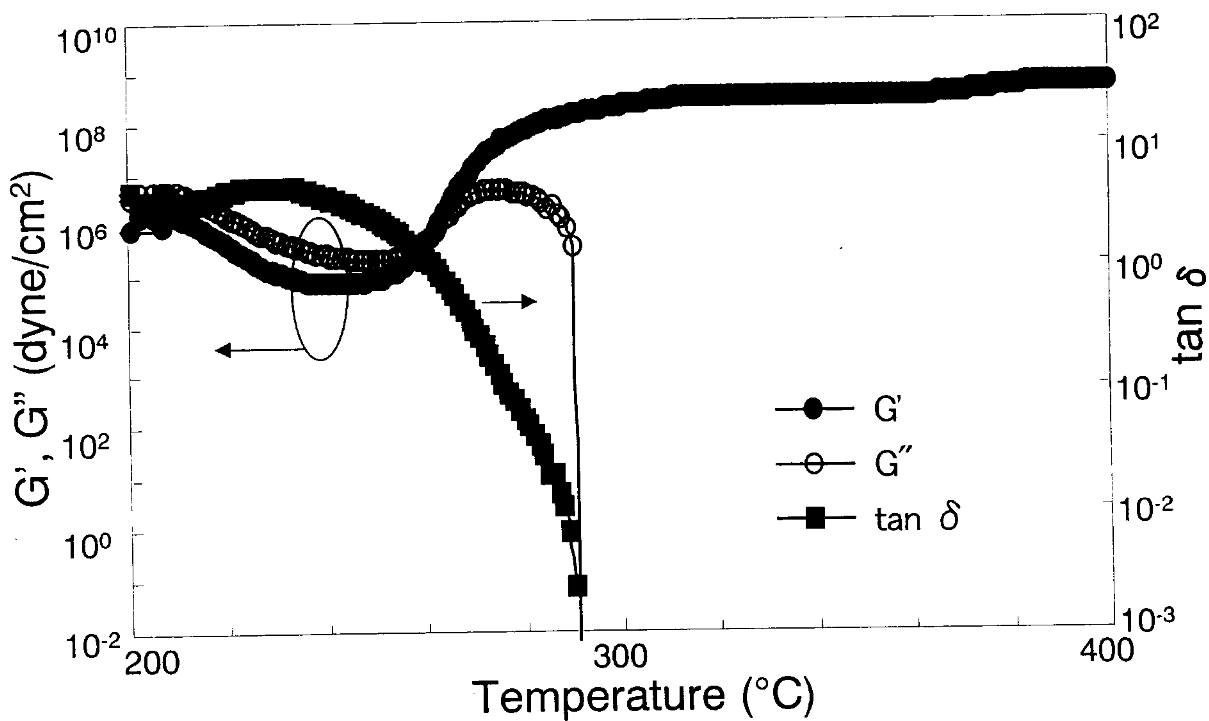


Fig.5. Dynamic viscoelastic behaviors of HSQ resin
(in air, 3°C/min, 1 Hz)(Run#2)

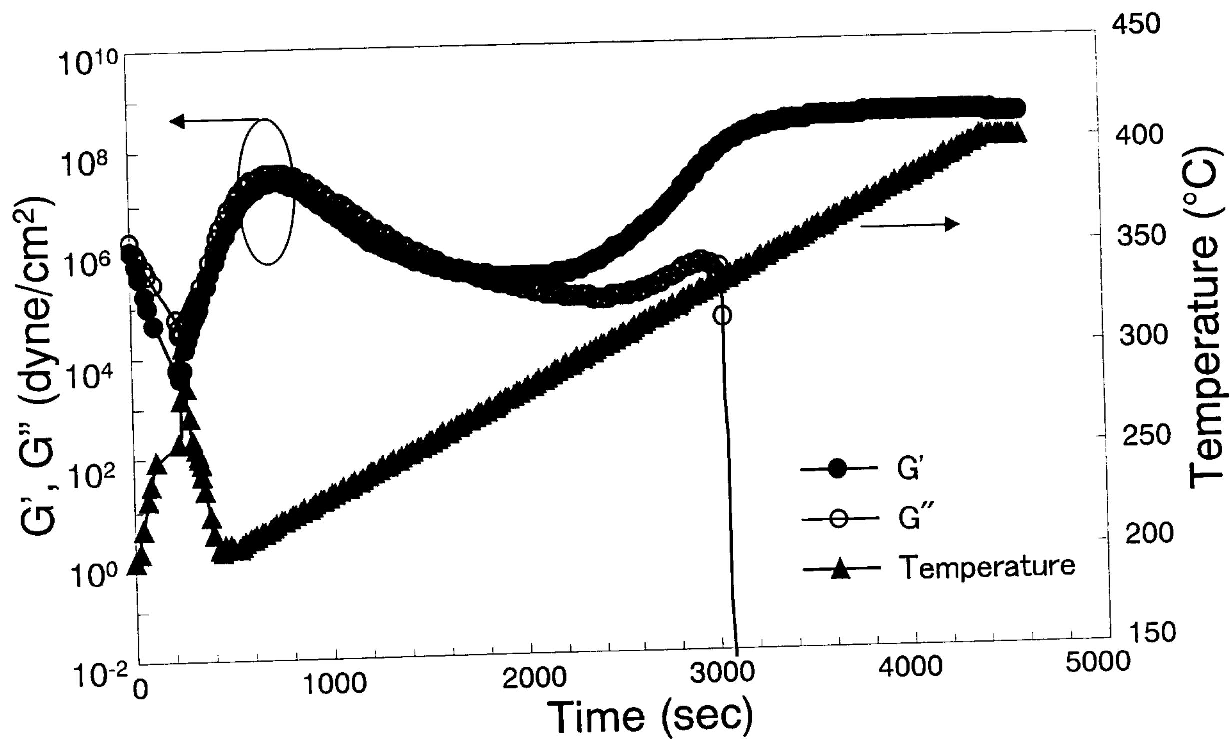


Fig.6 Dynamic viscoelastic behaviors of HSQ resin (in N2, 1 Hz)(Run#3)

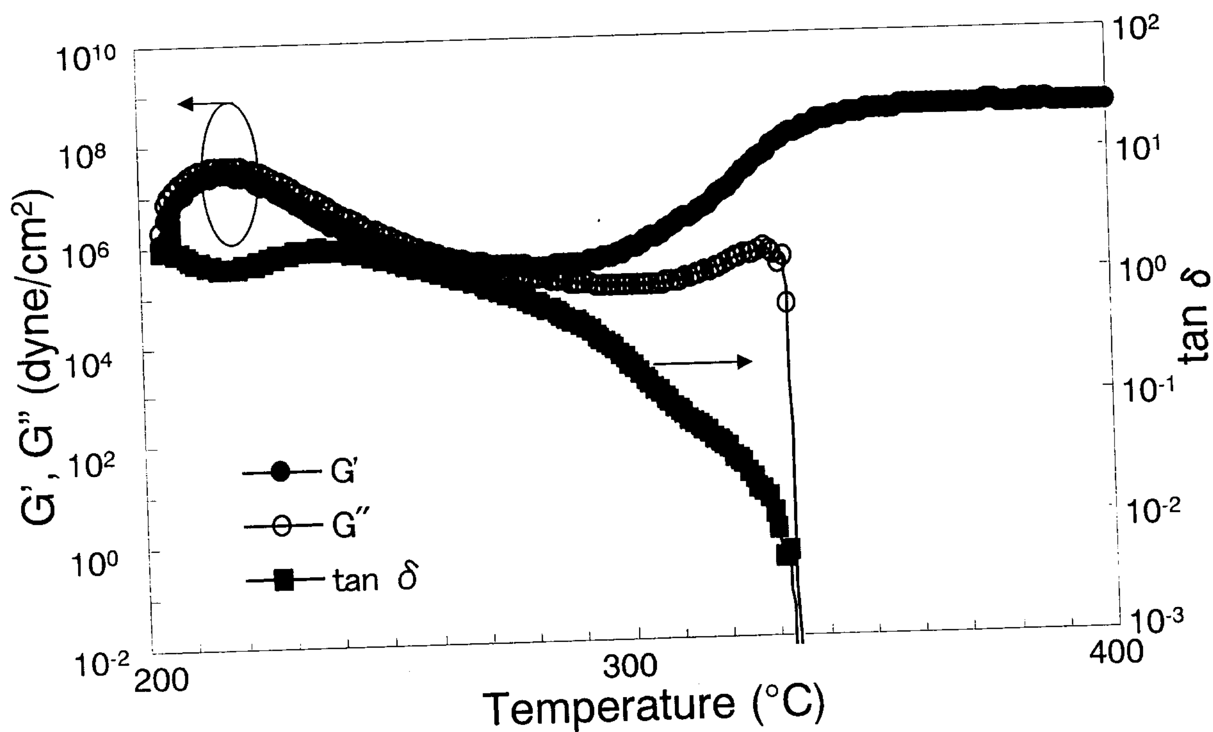


Fig.7. Dynamic viscoelastic behaviors of HSQ resin (in N2, 3 °C/min, 1 Hz)(Run#3)

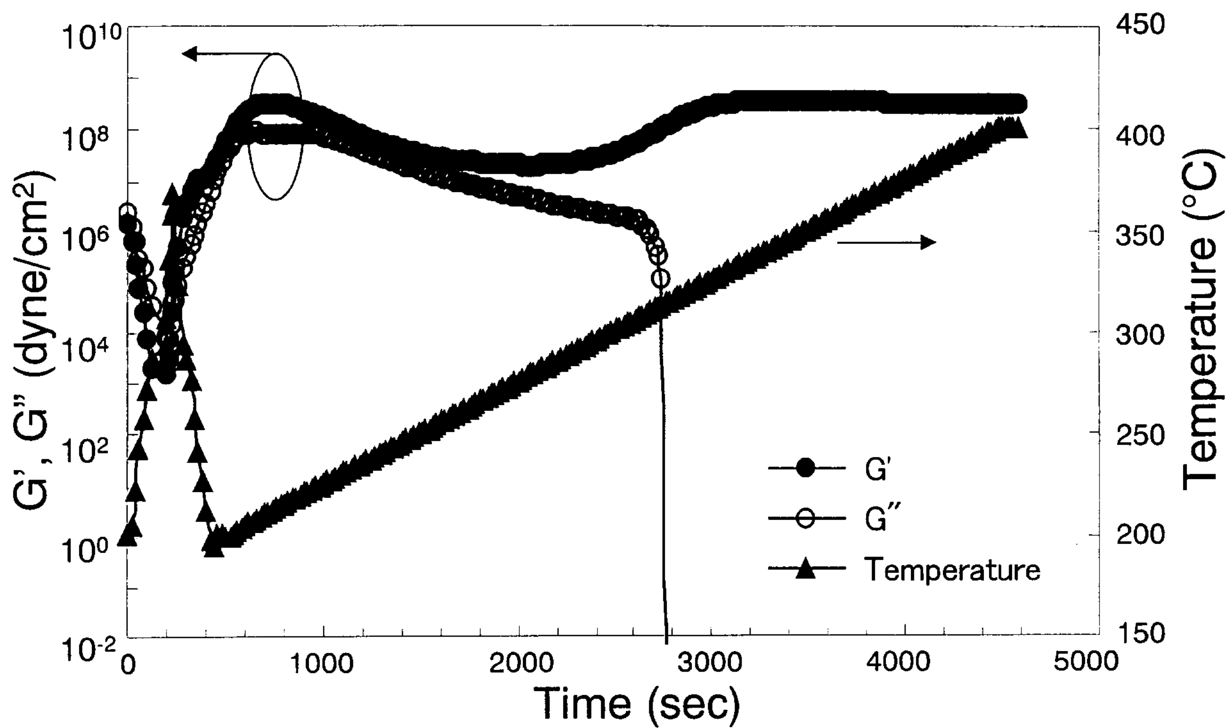


Fig.8. Viscoelastic behaviors of HSQ resin (in N2, 1 Hz)(Run#4)

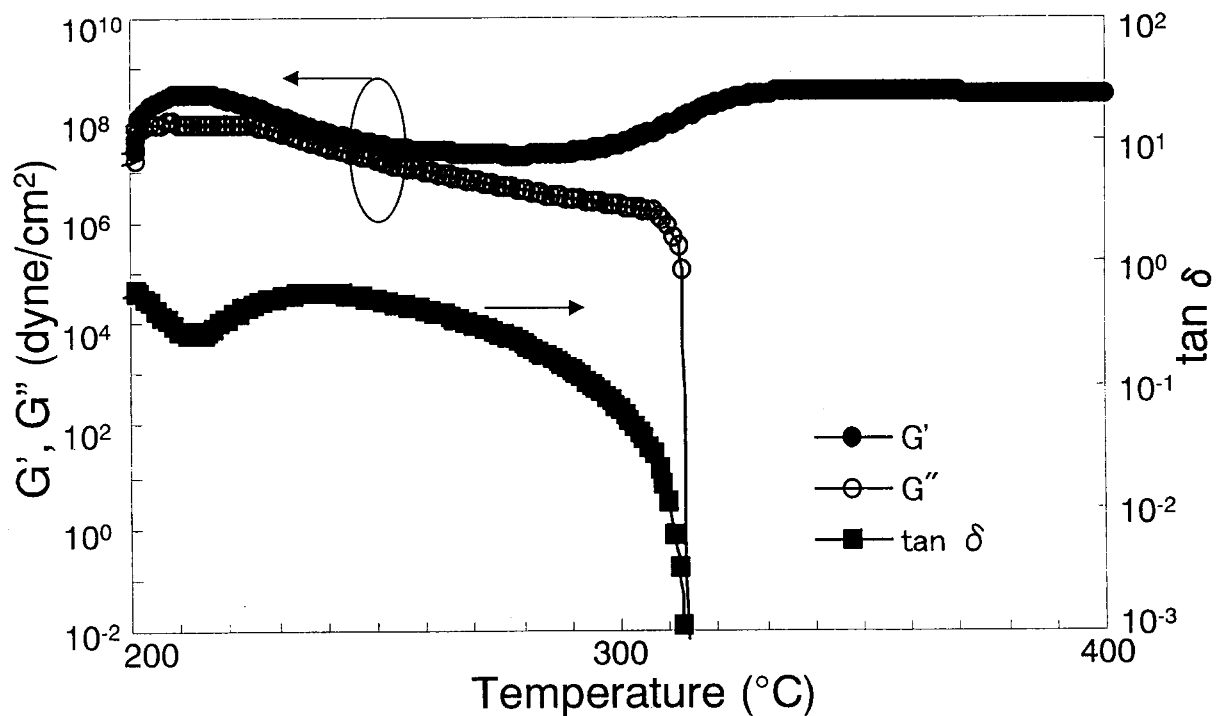


Fig.9. Dynamic viscoelastic behaviors of HSQ resin (in N2, 3 °C/min, 1 Hz)(Run#4)

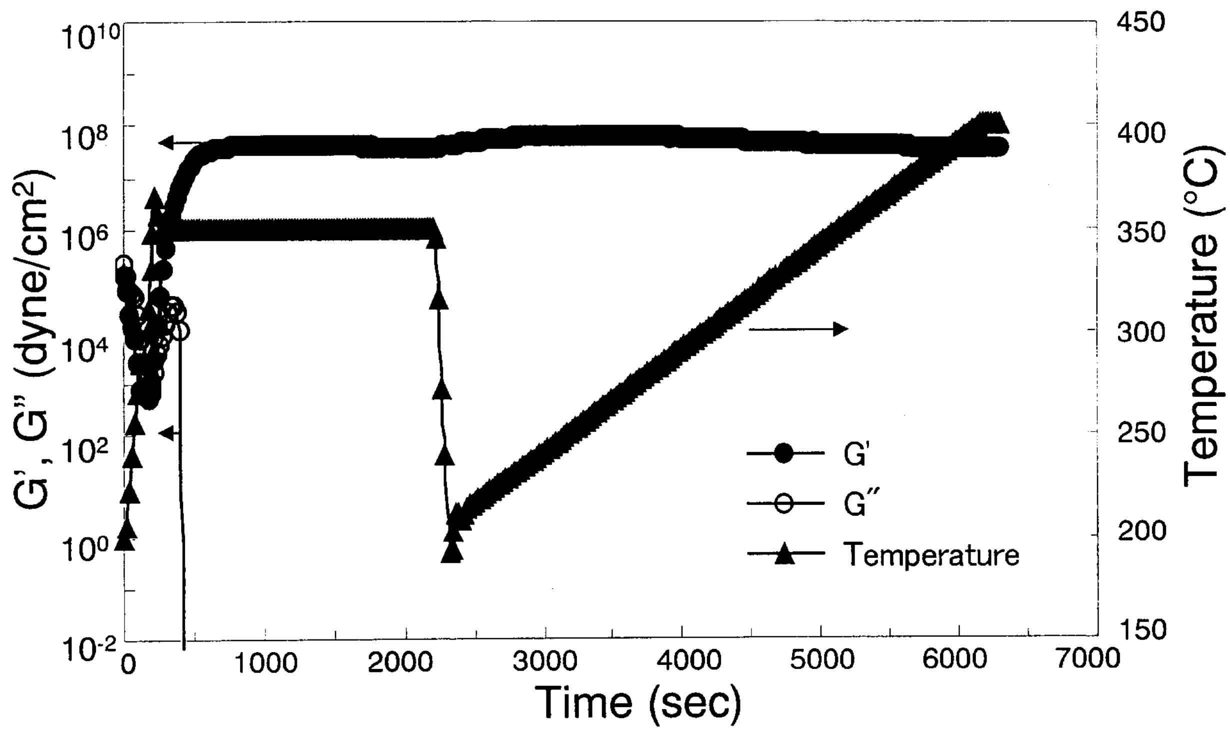


Fig.10. Dynamic viscoelastic behaviors of HSQ resin (in N2, 1 Hz)(Run#5)

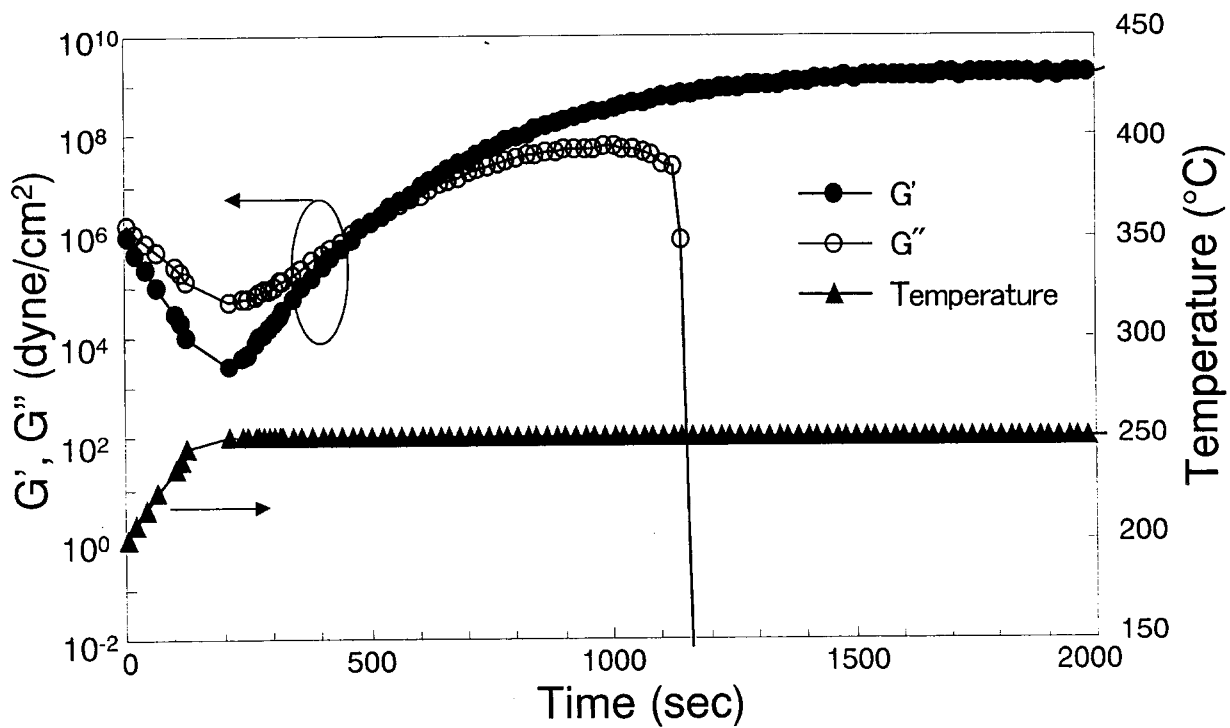


Fig.11. Dynamic viscoelastic behaviors of HSQ resin (in air, 1 Hz)(Run#6)

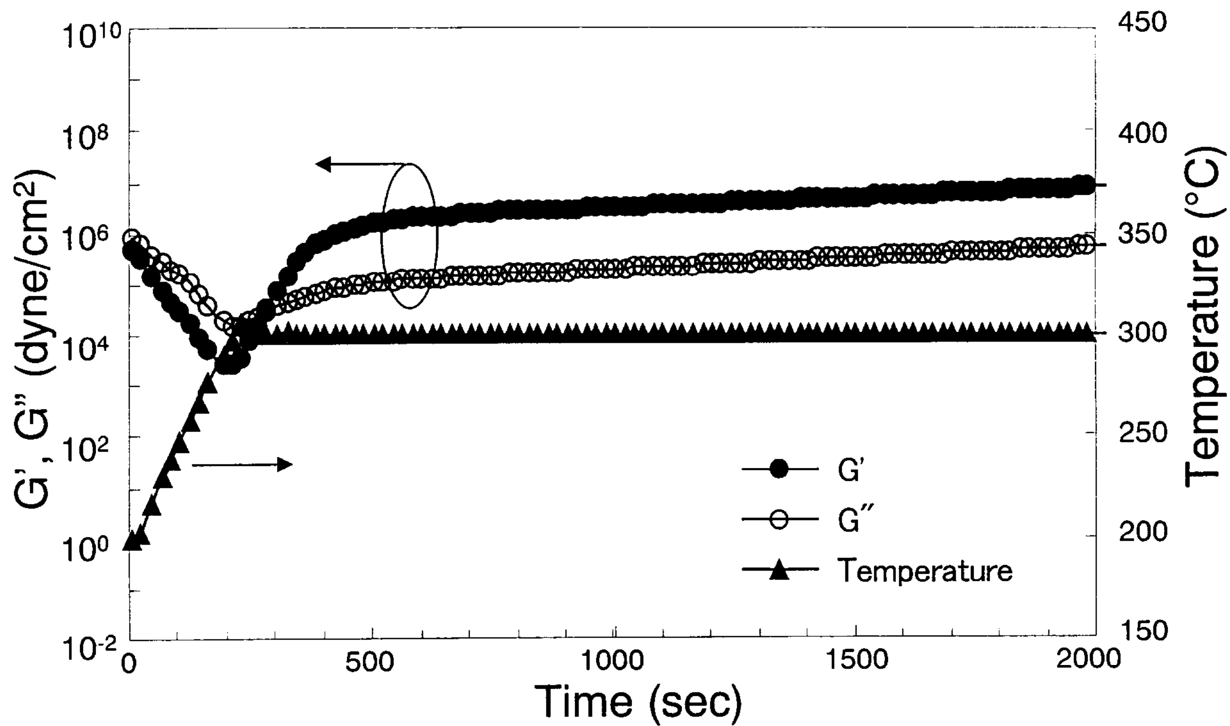


Fig.12. Dynamic viscoelastic behaviors of HSQ resin (in N2, 1 Hz)(Run#7)

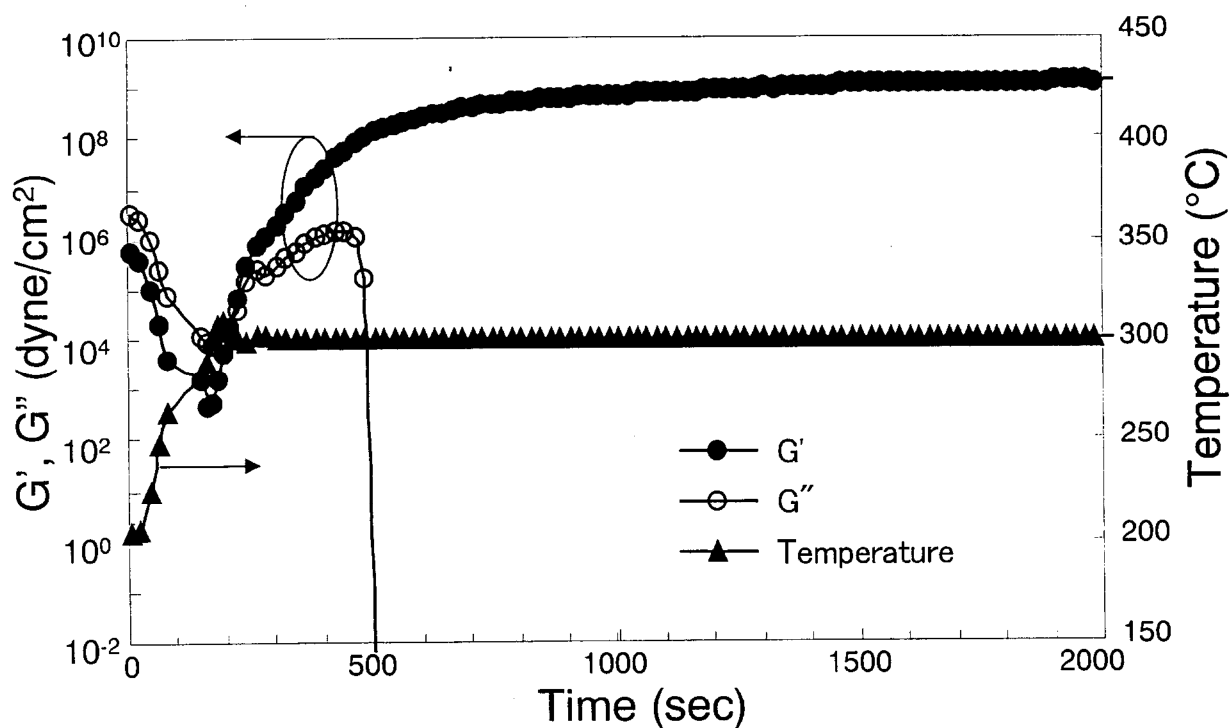


Fig.13. Dynamic viscoelastic behaviors of HSQ resin (in air, 1 Hz)(Run#8)

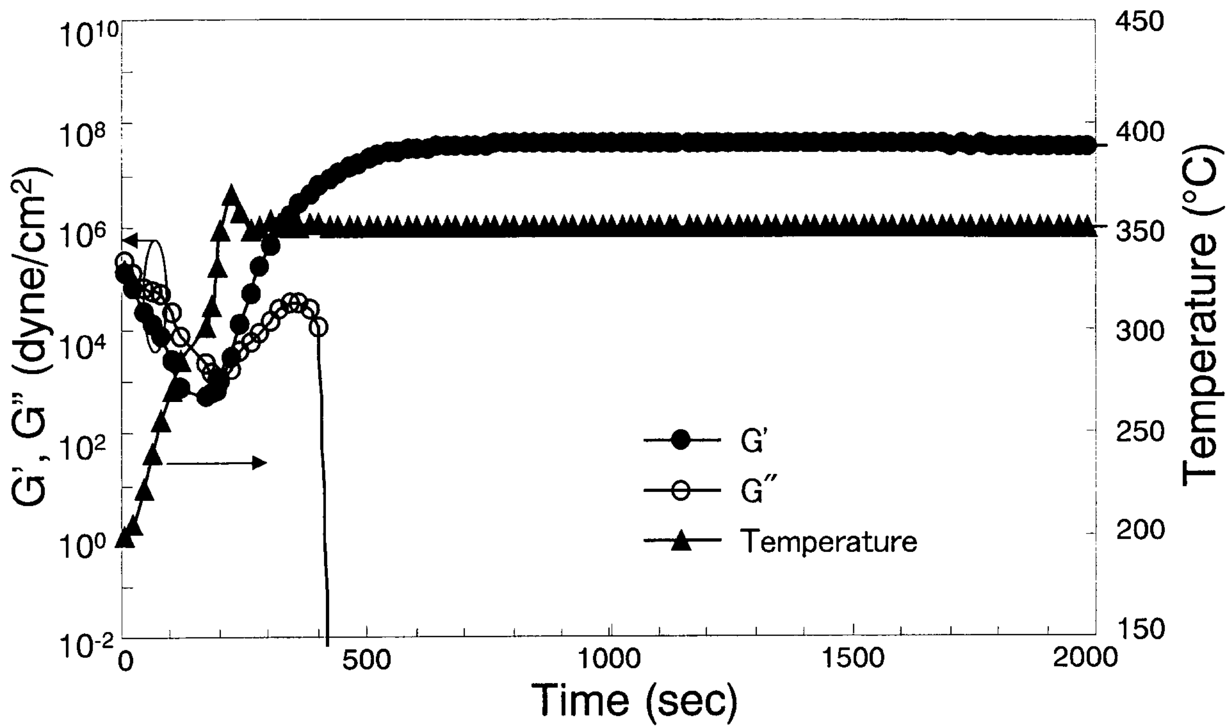


Fig.14. Dynamic viscoelastic behaviors of HSQ resin (in N2, 1 Hz)(Run#9)

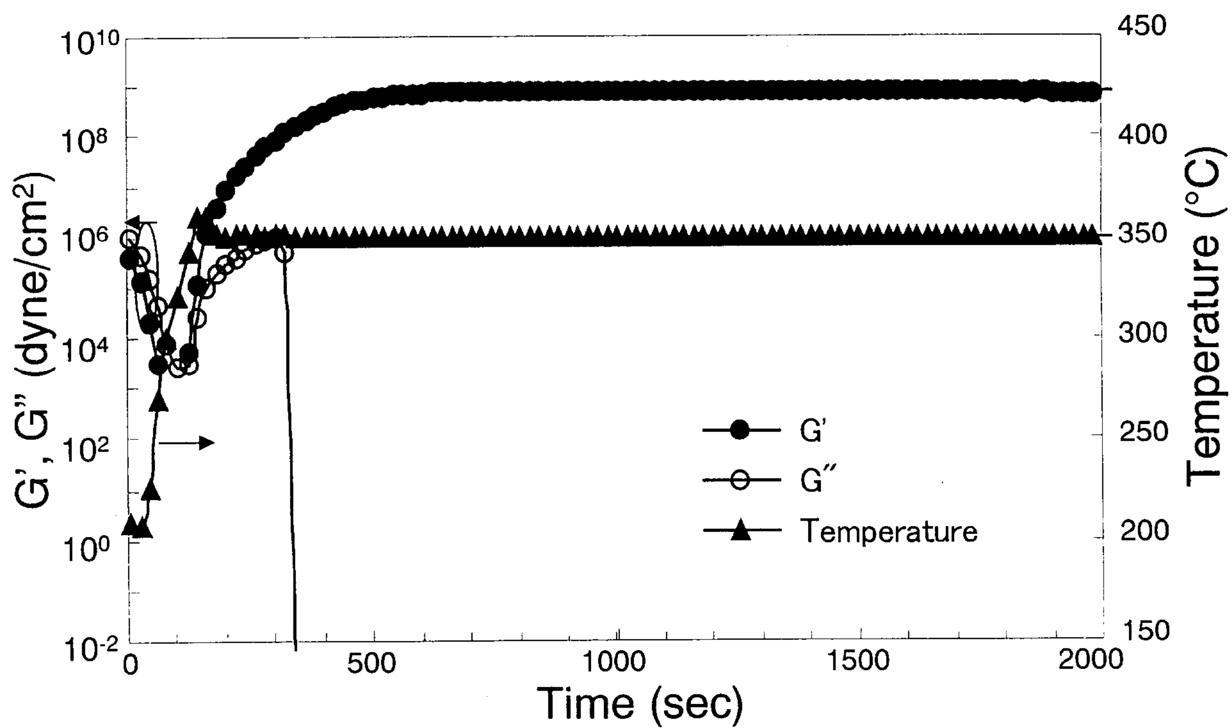


Fig.15. Dynamic viscoelastic behaviors of HSQ resin (in air, 1 Hz)(Run#10)

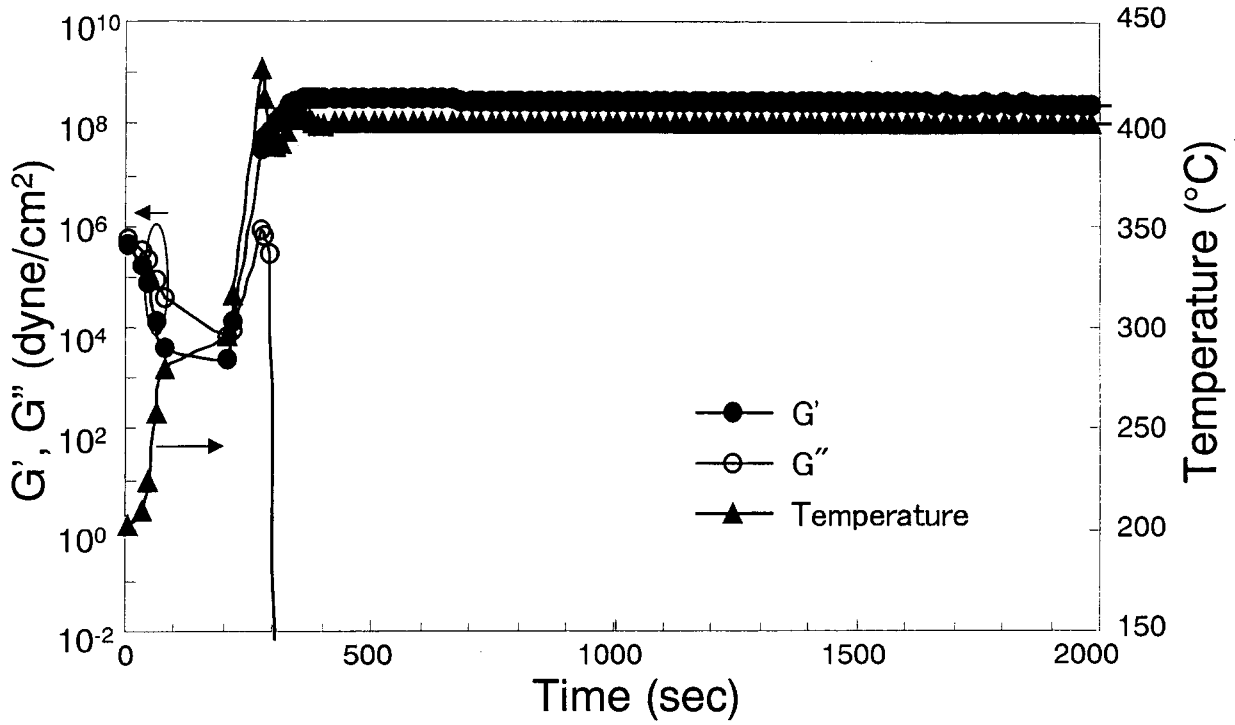


Fig.16. Dynamic viscoelastic behaviors of HSQ resin (in N2, 1 Hz)(Run#11)

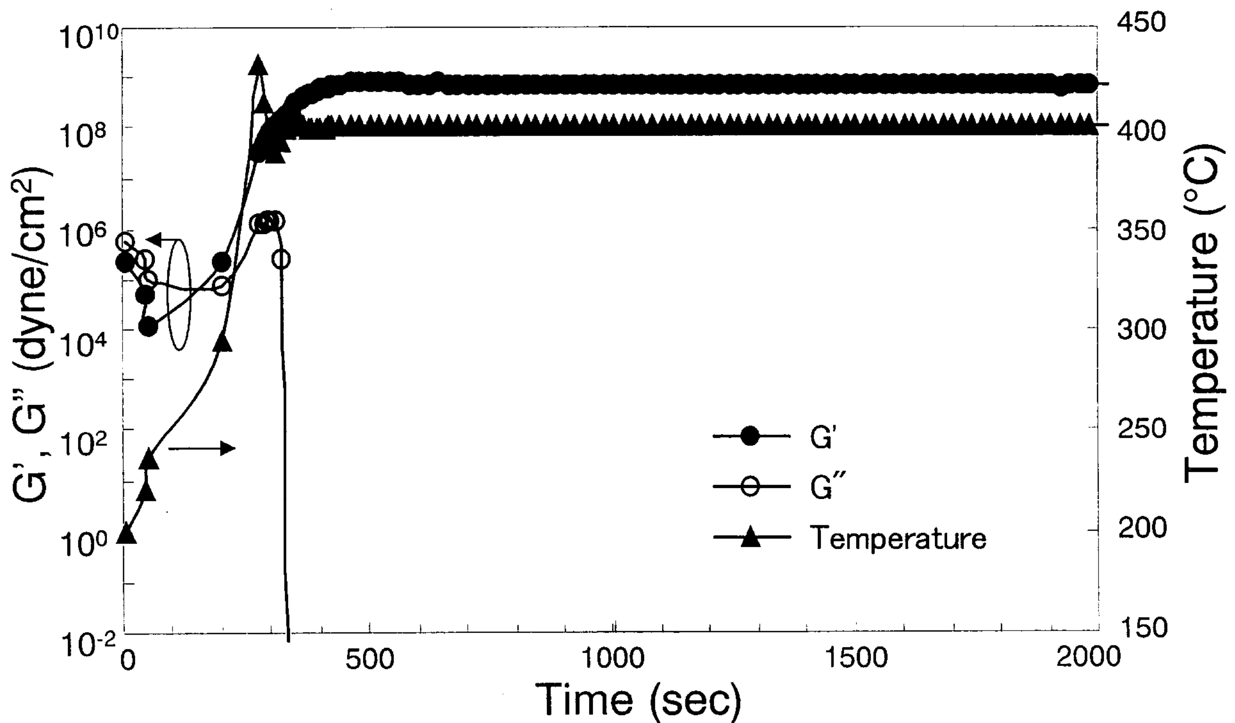


Fig.17. Dynamic viscoelastic behaviors of HSQ resin (in air, 1 Hz)(Run#12)

## 6.3 Oxidative curing of hydrogen silsesquioxane resin films enhanced by electron beam at ambient temperature and characterization of the cured films

### 6.3.1 Experimental part

*Film formation*

The HSQ resin used here was prepared by exactly the same manner described in Section 6.2.1 and had the same molecular weight. The resin was dissolved in methylisobutylketone (MIBK) with 35 wt % concentration and filtered through a 0.2 μm filter. The solution was spun onto six-inch silicon wafers with a Dainippon Screen D-spin 636 spincoater for film formation.

As spun film thickness values were 1.0, 1.25, 1.5, 2.0, 2.5, 3.0 and 3.5 μm.

*Irradiation of electron beam and successive annealing*

Irradiation of electron beam onto the HSQ films was made with Iwasaki Electric CB/250/30/180L apparatus. This apparatus supplies electron beam to the ambient atmosphere through a very thin (0.13 μm) titanium foil[6]. With this apparatus samples were carried on a conveyer through a "curtain" of electron beam at ambient temperature and pressure. Scheme 6 shows a core part of the electron beam supplying apparatus focusing on the "curtain".

Oxygen concentration on the sample was controlled by the flow rate of nitrogen. Though the temperature of the sample stage (tray, 30 cm sq.) was not controlled, it was in the range of 40 to 50 ℃ due to the heat generated by the irradiation. Dosage of electron beam was determined by the combination of beam current, speed of the conveyer and the number of passing through the "curtain".

In this study the voltage and current of electron beam was fixed as 150 kV / 10 mA. The oxygen concentration in the irradiation area was fixed as 50 ppm by controlling the flow rate of nitrogen gas. The dosage of electron beam onto the HSQ films was 5 MGy at maximum.

In order to see the effect of successive heating on properties of the films cured with electron beam, nitrogen annealing at 400 ℃ for 1 h (oxygen concentration was around 10 ppm) and successive annealing in air at 400 ℃ for 1 h was performed with a Koyo Lindberg μTF-6 furnace.

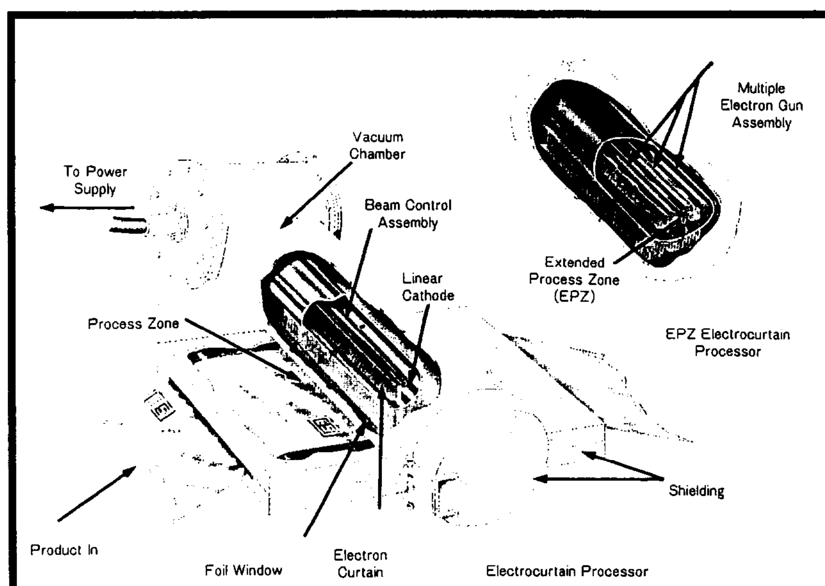


Scheme 6. Core part of electron beam supplying apparatus ("curtain").

For comparison, thermal cure was applied on HSQ films instead of the irradiation of electron beam with the μTF-6 quartz tube furnace. Temperature for cure was 400 ℃ as a standard and was varied in the range of 350 to 450 ℃ to see the relationship between refractive index and SiH concentration. Atmosphere for cure was air or 10 ppm oxygen concentration in nitrogen flow. Time for cure was 1 h for all conditions.

*Film characterization*

Film thickness and RI were measured with an AXIC Tyger thin film analyzer. Values were calculated by the average of 9 points measurements on the wafer. Concentration of SiH group in the film was analyzed with FTIR spectra. FTIR measurement was performed in a transmission mode using a Nicolet Protege 460 spectrometer. Remaining % SiH was calculated with the height of the absorption peak at 2250 $cm^{-1}$, assigned as SiH stretching mode, calibrated by film thickness versus that of the as spun film on the assumption that the as spun film has 100 % remaining SiH group. Presence of cracks in the films was checked by observation with an optical microscope after the films were stored in air for 24 h at room

temperature after cure.

TDS (Thermal desorption spectroscopy) was performed on an ESCO EMD-WA1000KS spectrometer at ESCO, Ltd. Temperature was ramped up from room temperature to 800 C. Table 4 summarizes conditions for the TDS analysis. Total pressure in the sample chamber was detected. Amount of hydrogen molecule desorbed from sample films were calculated by quantitatively detecting the M/Z = 2 species.

Table 4. Conditions for TDS analysis

| | | |
|---|---|---|
| Equipment : | Detector : | QUADREX-200 (quadrupopole mass) |
| | Temperature range : | RT - 800 ℃ |
| | Ramp up speed : | 1℃ / sec |
| | Back pressure : | 1 x $10^{-9}$ Torr |
| Sample : | Size : | 8 mm x 8 mm |
| | Thickness : | 1.0 μm |
| | Substrate : | Silicon wafer |

### 6.3.2 Results

*Cure of HSQ films*

Figure 18 shows remaining %SiH versus dosage of electron beam for 1.0 μm thick films. Remaining %SiH decreased as the dosage increased. Films irradiated with 0.5 MGy dosage of electron beam or more were insoluble to organic solvents such as toluene and MIBK. The remaining %SiH for the film irradiated with 4 MGy dosage of electron beam was 63 that is close to 62, that for the film which was cured thermally at 400 ℃ under nitrogen flow with the oxygen concentration of 10 ppm. Figure 19(a) shows FTIR spectra for the as spun film with 1.0 μm thickness, a film cured at 400 ℃ under nitrogen flow with the oxygen concentration of 10 ppm and film irradiated with 4 MGy dosage of electron beam at room temperature. The major peaks in the SiO stretching and rocking modes in the spectrum for the as spun film are at 1130 $cm^{-1}$ and 860 $cm^{-1}$ being assigned as the $SiO_{3/2}$ cage structure[1]. The other major peak at 2250 $cm^{-1}$ is assigned as the SiH stretching mode. Therefore, the film has a $HSiO_{3/2}$ structure. In either spectrum for films cured with heat or electron beam, the peak height calibrated by thickness was smaller and the relative peak height at 1075 $cm^{-1}$ being assigned as the $SiO_2$ structure versus that at 1130 $cm^{-1}$ was higher than those for the as spun film. The total spectra for the thermally cured film and the electron beam cured film are very similar.

% SiH Remaining value for the thermally cured film was 75 at highest when the curing temperature was 350 ℃ and 47 at lowest when it was 450 ℃, respectively.

Remaining %SiH decreased after the nitrogen annealing (6 % reduction in the case of 4 MGy irradiation). Figure 19(b) shows FTIR spectra of films cured with 4 MGy dosage of electron beam and after the nitrogen annealing at 400 ℃ for 1 h.

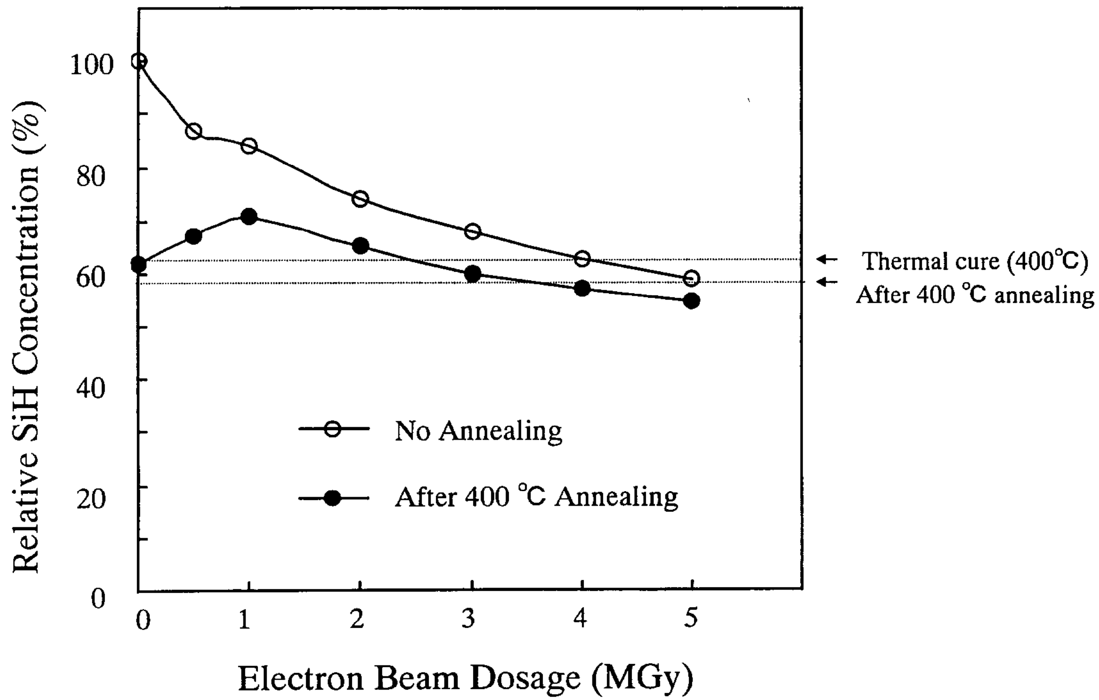


Fig.18. Effect of electron beam dosage on relative SiH concentration for films with thickness 1.0 $\mu$m

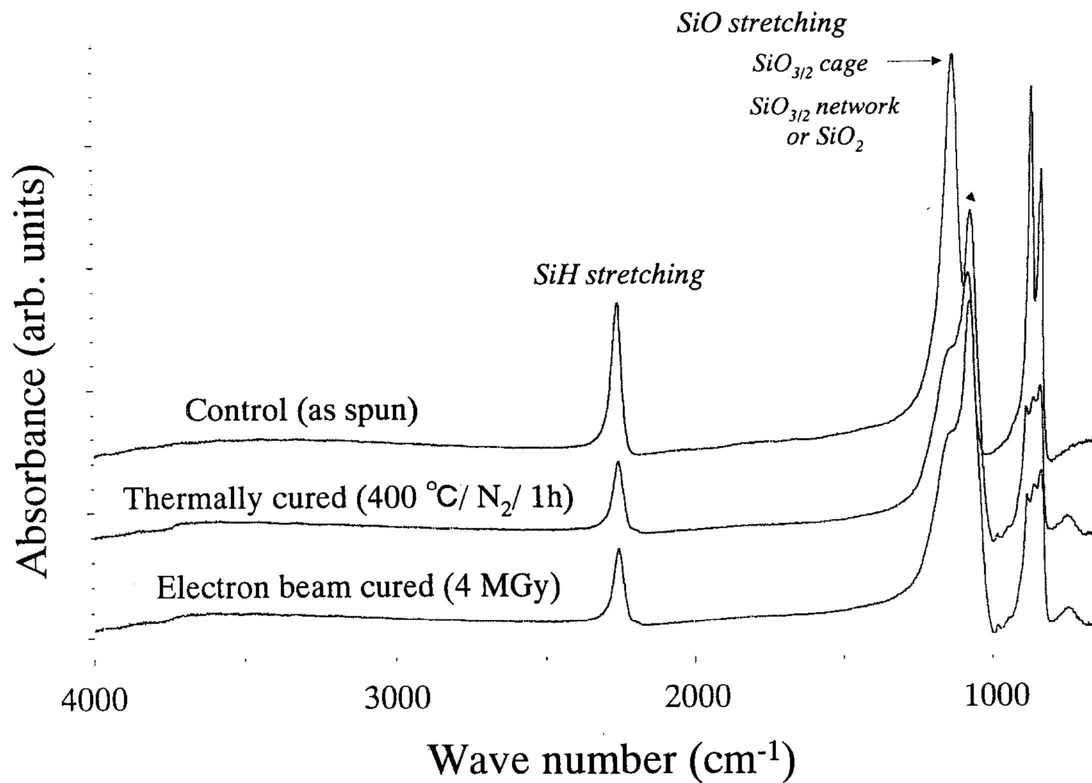


Fig.19(a). FT-IR spectra for films with thickness 1.0 $\mu$m (1)

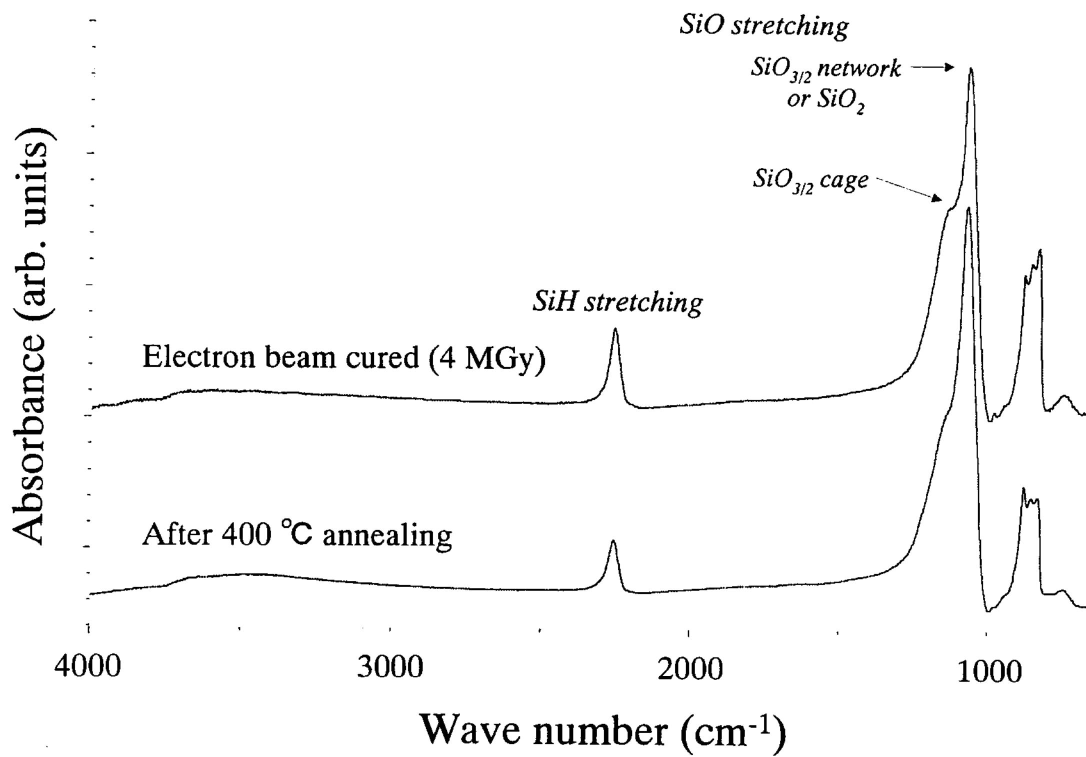


Fig.19(b). FT-IR spectra for films with thickness 1.0 μm (2)

*RI and shrinkage*

Figure 20 shows the relationship between RI and electron beam dosage. RI values for the electron beam cured films were around 1.41 with little relation to the dosage. RI values in all the experiments with either electron beam cure or thermal cure are plotted versus remaining %SiH in Fig. 21. With thermal cure, the RI values are in the range of 1.37 to 1.38 and show a minimum at around 70 % SiH, whereas those for the electron beam cured films are flat at around 1.41.

After the nitrogen annealing, the RI values decreased if the dosage was low, whereas the RI increased if the dosage was high.

Figure 22 shows film shrinkage as a function of the dosage of electron beam. Shrinkage due to irradiation of the electron beam was in the range of 1 to 3 %. Additional shrinkage due to nitrogen annealing was 1.6 % for the film that was electron beam cured with 4 MGy, very close to that for the thermally cured film (the dotted lines in Fig.22). Thickness for the film that was electron beam cured with 1 MGy increased after the annealing.

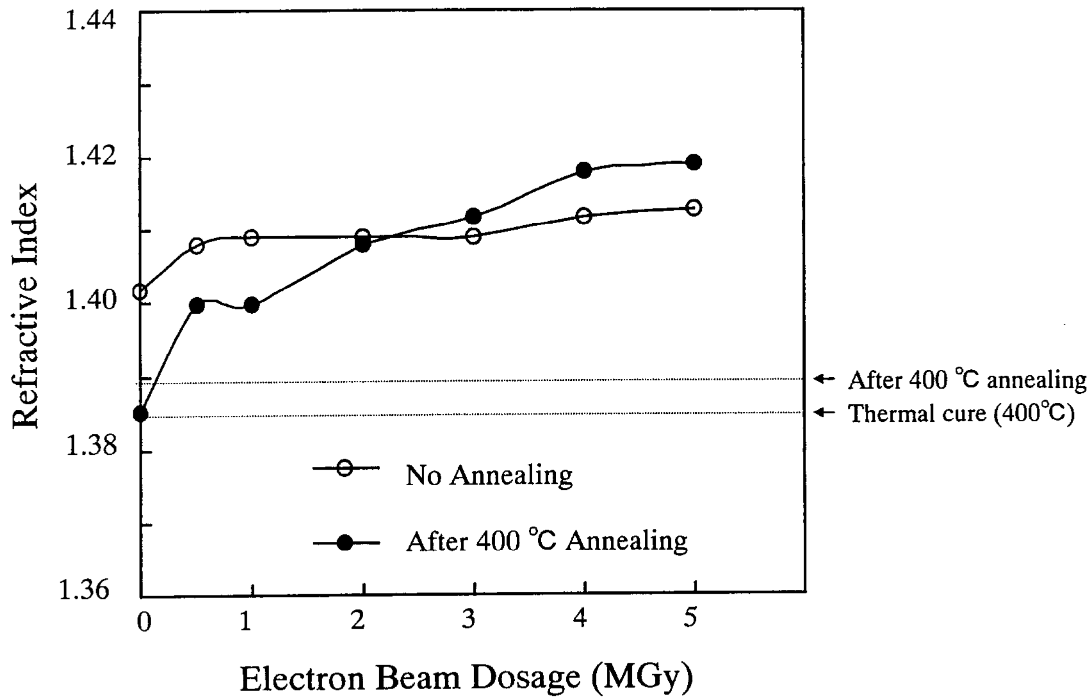


Fig.20. Effect of electron beam dosage on refractive index for films with thickness 1.0 $\mu$m

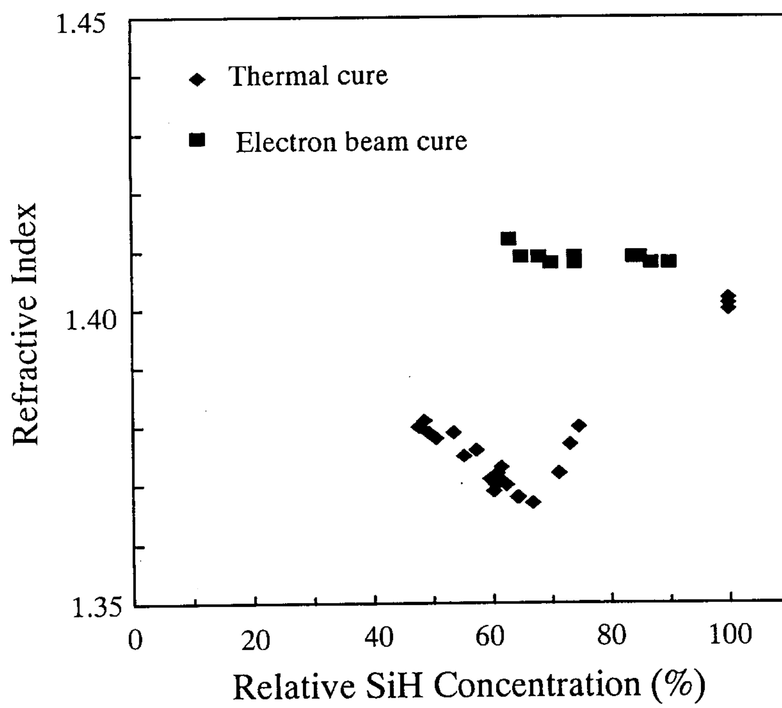


Fig.21. Relationship between refractive index and relative SiH concentration

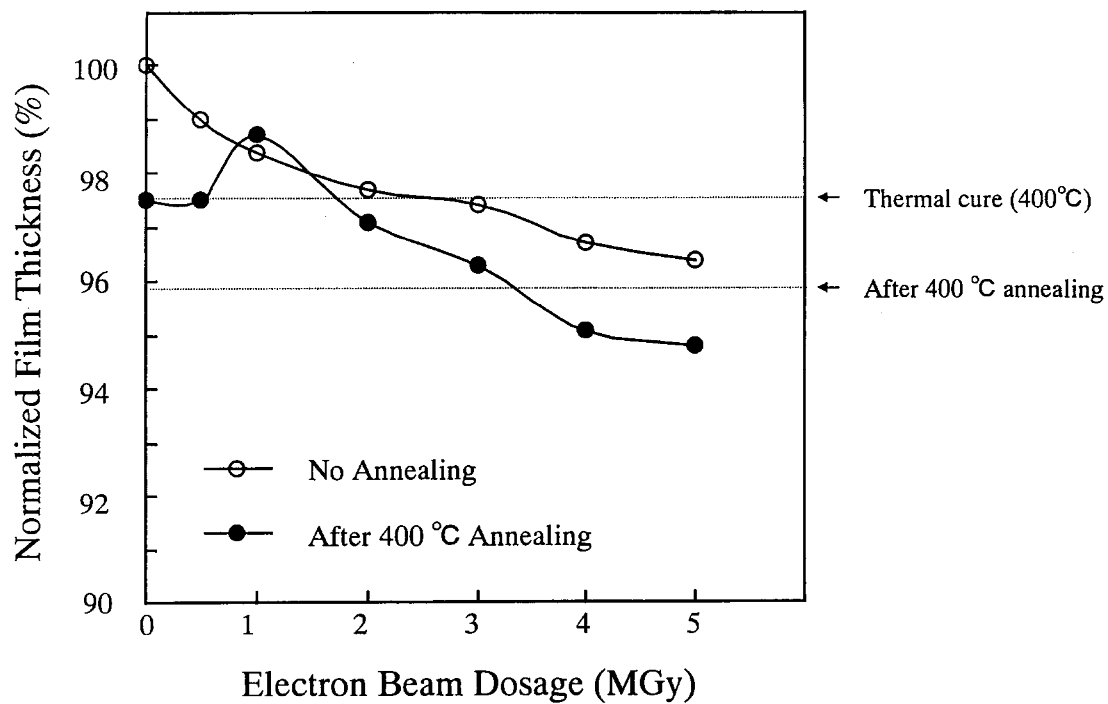


Fig.22. Effect of electron beam dosage on thickness for films with thickness 1.0 $\mu$m

*Cracking resistance*

Table 5 summarizes a comparison of cracking resistance between thermally cured films and electron beam cured films. The films collected in Table 4 have similar % SiH remaining values after cure, ie, in the range of 62 to 65, in order to compare cracking resistance correctively.

In thermal cure, the film with 1.25 μm showed small cracks, whereas in electron beam cure, the film with 3.0 μm showed no cracks. For the 2.5 μm films cured with electron beam, cracks were not seen even after the nitrogen annealing.

Table 5. Comparison of cracking resistance between thermally cured films and electron beam cured films.

| | Thickness (μm) | | | % SiH Remaining[1] | Presence of cracks[2] |
|---|---|---|---|---|---|
| | Targeted thickness | Measured thickness | | | |
| | | As spun | After cure | | |
| Thermal cure[3] | 1.0 | 0.967 | 0.943 | 62 | N |
| | 1.25 | 1.248 | 1.217 | 62 | C |
| | 1.5 | 1.526 | Not measurable | Not measurable | CC |
| Electron beam cure[4] | 1.0 | 0.965 | 0.933[5] | 63 | N |
| | 1.5 | 1.526 | 1.481[5] | 65 | N |
| | 2.0 | 2.086 | 1.957[5] | 62 | N |
| | 2.5 | 2.557 | 2.429[5] | 63 | N |
| | 3.0 | 3.155 | 2.955[6] | 63 | N |
| | 3.5 | 3.666 | 3.428[6] | 63 | C |

1) By FT-IR. As spun film = 100 %

2) By microscope, after 24 h storage under air at RTafter cure.

Ranking; N : No cracks, C : Small cracks, CC : Heavy cracks

3) 400 ℃ / nitrogen flow (oxygen = 10 ppm) / 1 h

4) Electron beam = 4 MGy or 4.5 MGy, Oxygen = 50 ppm

5) Electron beam = 4 MGy

6) Electron beam = 4.5 MGy

### 6.3.3 Discussion

*Cure of HSQ films*

The data suggest that HSQ is oxidatiively cured by the 50 ppm oxygen enhanced by electron beam at room temperature. Therefore, it is concluded that electron beam enhanced oxidative cure of HSQ films and the degree of cure could be controlled by dosage of electron beam.

Degree of cure is also controllable by temperature in thermal cure.

As seen in Fig.18, practical remaining % SiH levels, 60 - 90 %, can be controllably obtained with the electron beam cure at ambient temperature and pressure which are comparable to %SiH levels typically achieved by thermal cure of HSQ films. Total time for electron beam irradiation was only a few seconds. With improvement in equipment greater throughput will be obtained than that for the thermal cure since time for electron beam irradiation with around 4 MGy is within a minute level (depending on the equipment). As shown, it is concluded that electron beam can continuously control the dimension (bond order) between 3 to 4 with changing dosage level.

After the electron beam cure with 4 MGy, the conversion to silicon oxide continued with the nitrogen annealing. The SiH groups remaining in the film processed with electron beam still appear to be reactive at the high temperature, while the remaining SiH groups in the thermally cured films show a very similar reactivity (the dotted lines in Fig.18). Although little change in film structure or properties are expected at annealing steps, the electron beam cured films are believed to have acceptable levels in change for practical use since that of thermally cured films are being practically used.

*RI and shrinkage*

In general, higher RI value indicates higher film density. With thermal cure, it is believed that film expansion due to volatalization of small molecules or thermal elongation occurs in parallel with the densification of the film due to the oxidative cross-linking of SiH groups. On the contrary, the film with electron beam appears to maintain its density before and after the cure.

Thickness for the film that was electron beam cured with 1 MGy increased after the annealing. This nature seems to be related to the RI behaviors.

*Cracking resistance*

The results clearly indicate that cure with electron beam can improve the maximum crack-free thickness. It is generally believed that cracks in the film are caused by stress formation due to densification or elongation of film and/or weak film strength. Electron beam cure can potentially decrease the occurrence of cracking compared to thermal cure of HSQ films.

*Mechanism for electron beam cure*

Low molecular weight species having cage structures such as $T_8^H$, $T_{10}^H$, etc. are sublimated at 300 or higher temperatures[1)]. In thermal cure, those species are believed to be partly evaporated from the film during cure leaving vacancies in the film, and thermal expansion of the film is also believe to occur. On the other hand, in electron beam cure, only densification due to oxidation is suggested to take place during cure involving low molecular weight species to be thoroughly cured without evaporation. This is well explained by the fact that the electron beam cured film with the 4 MGy dosage showed very similar behaviors during the 400 ℃ annealing to the thermally cured film.

To confirm it further, Table 6 summarizes the result of the TDS analysis. Amount of hydrogen molecule desorption was in the following order: As spun film > Thermally cured film > Electron beam cured film (4 MGy). The TDS can detect species having M/Z numbers less than 200. Low molecular weigh HSQ species can not be detected directly by the mass detector of TDS, however, if they are present in the TDS chamber, they will be fragmented into small molecules including hydrogen and also contribute to increasing total pressure in the chamber. Total pressure in the TDS chamber in the temperature range from 200 to 400 ℃ was in the following order: As spun film > Thermally cured film $\geq$ Electron beam cured film (4 MGy). Therefore, it is suggested that the electron beam cured film with the dosage of 4 MGy release an equal or less amount of low molecular weight species during annealing compared to thermally cured films.

Reviewing the figures, it is suggested that curing with electron beam at approximately 2 MGy or less is not sufficiently done, ie, the cured films should have certain amounts of volatiles. Those films may act as similarly during annealing to the thermal cure.

Table 6. Hydrogen desorption amount for hydrogen silsesquioxane films.

| Film status[1)] | % SiH Remaining[2)] | Hydrogen desorption amount[3)] (atom/cm$^3$) |
|---|---|---|
| As spun | 100 | $2.58 \times 10^{21}$ |
| Thermally cured[4)] | 62 | $1.48 \times 10^{21}$ |
| Electron beam cured[5)] | 63 | $4.97 \times 10^{20}$ |

1) Film thickness : 1.0 ì m

2) By FT-IR.

3) By TDS.

4) 400 ℃ / nitrogen flow (oxygen = 10 ppm) / 1 h

5) Electron beam = 4 MGy

The great improvement in cracking resistance in electron beam cure is probably due to the less thermal cycle than in thermal cure.

*Commercial availability of electron beam for cure of HSQ*

The author believes that electron beam cure of HSQ is potentially applicable for commercial use since it enables the cure conditions much simpler (ie, lower temperature and shorter time than those for the conventional thermal cure). Issue is that there is no appropriate equipment for electron beam irradiation which could be combined with the popular spincoaters. A joint study is needed among a lamp manufacturer, a spincoater manufacturer and a material supplier to develop commercially available equipment for electron beam cure of HSQ. If successful, it will bring both upgrade of HSQ film properties and cost reduction for HSQ processing.

## 6.4 Formation of HSQ based low-k films

### 6.4.1 Experimental part, results and discussion

An HSQ solution with a high-boiling-point solvent (a different kind of solvent from the main solvent) formulated was spun onto silicon wafers. The film containing the high-boiling-point solvent which is well dispersed in the film was exposed to a wet ammonia gas flow at room temperature. SiH bonds in the HSQ films were found to be reacted by the wet ammonia to form a SiOSi gel with the high-boiling-point solvent incorporated. The film was finally cured in a furnace at 450 ℃ where the solvent was removed, resulting in the formation of pores in the film. The process is summarized in Scheme 7.

K for the obtained films could be controlled the amount of the high-boiling-point solvent. K lower than 2.0 was obtained[7,8].

At present electron beam is being applied to have low-k HSQ based films. Current data suggest that dosage level of electron beam controls the dimension of cured HSQ film, ie the ratio of HSQ/$SiO_2$, without changing the pore structure. K is controllable with setting the ratio of high boiling solvent / HSQ.

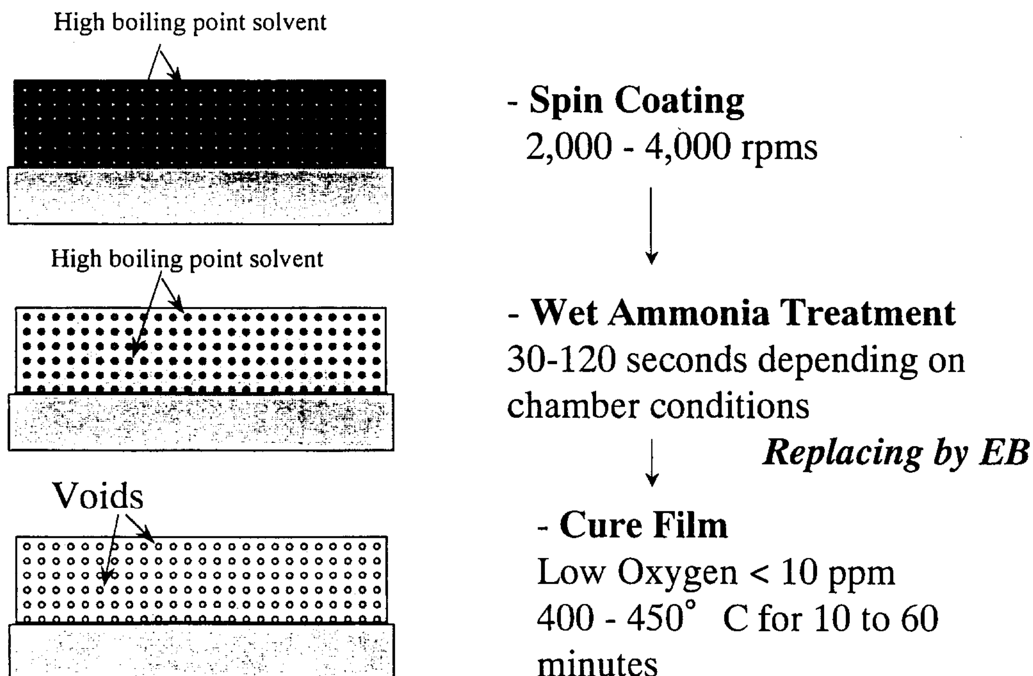


Scheme 7. Process for low-k HSQ based films

### 6.5 Conclusion

Ⅰ. Dynamic viscoelastic behaviors of HSQ resin were investigated using a dynamic analyzer at the temperature range of 200 to 400 ℃ in either nitrogen or air atmosphere. By analyzing data about G' and G", the following conclusions were obtained.

1) In any condition, G" decreased to an undetectable low value drastically and clearly at a specific point during either a heating step or a temperature holding step. (This point is called $G"_c$.)
2) In nitrogen G' was minimum at 285 ℃ and $G"_c$ was at 377 ℃. G' increased gradually up to the $10^8$ dyne/cm$^2$ order as temperature ramped up from 300 through 400 ℃. Whereas in air, G' was minimum at 250 ℃ and $G"_c$ was at 290 ℃, and G' was saturated at around 310 ℃. The graph patterns for in nitrogen and in air were similar.
3) The effect of preheat at 350 ℃ in nitrogen with short time on the successive curing behavior was significant, ie, the change of G' and G" at the successive cure was much smaller than that at a cure without a preheat, whereas that at 300 ℃ was small.
4) It was particular that $G"_c$ was at very short time at 350 ℃ or higher for both in nitrogen and in air.
5) In air at 250 ℃, the curing speed was moderate, however, the saturated G' value was over $10^9$ dyne/cm$^2$, higher than that in nitrogen at 400 ℃. Furthermore, G' at $G"_c$ in air at 250 ℃ was almost $10^9$ dyne/cm$^2$, whereas that in nitrogen at 400 ℃ was $10^8$ dyne/cm$^2$.

As a result, the thermal and oxidative behaviors of HSQ resin were first analyzed and possible process improvement could be suggested for better film properties.

Ⅱ. Oxidative curing of HSQ resin films with electron beam enhanced was attempted.

1) Hydrogen silsesquioxane (HSQ) films were oxidatively cured to silicon oxide enhanced by electron beam at ambient temperature and pressure.

2) Remaining %SiH, a parameter for degree of cure, could be controlled by dosage level down to around 60 % which is typical of thermally cured HSQ films. Refractive index of the films was higher than that of thermally cured films.
3) A film with 3.0 μm thickness does not show any cracks, whereas a thermally cured film with 1.25 μm showed cracks. Furthermore, films with 2.5 μm thickness do not show any cracks even after a nitrogen annealing at 400 ℃ for 1 h.
4) The benefits of the electron beam cure of HSQ, ie, the low temperature cure and the high cracking threshold will expand the usage of HSQ for interlayer dielectric applications.

Ⅲ. Very low dielectric HSQ based films, as low as 2.0, were obtained using a wet ammonia treatment on HSQ films with high-boiling-point solvents dispersed. Through a final heat treatment pores were remain in the HSQ film, contributing the low k.

This technology is believed to fit the LSI roadmap. In this study, the SiO bond order is $3+\delta$ that is close to $SiO_2$. It is very impacting and unique that the high SiO bond order materials have very low k such as 2.0.

## References

1) C. L. Frye and W. T. Collins, *J. Am. Chem. Soc.*, **92**, 5586(1970)
2) D. S. Ballance, K. A. Scheibert and J. V. Tietz, *Proc. VLSI Multilevel Interconnection Conference*, 1992, p. 180.
3) J. N. Bremmer, Y. Liu, K. G. Gruszynski and F. C. Dall, *Proc. Materials Research Society* 1997, Vol. 476, p. 37.
4) H. Namatsu, Y. Takahashi, K. Yamazaki, T. Yamaguchi, M. Nagase and K. Kurihara, *J. Vac. Sci. Technol.*, **B16**, 69(1998)
5) J. Goo, H.-J. Lee, S.H. Kim, J.H. Choi, B.K. Hwang, H.-K. Kang and M.Y. Lee, *Proc. Dielectrics for ULSI Multilevel Interconnection Conference*, 1998 p. 295.
6) S. Kinoshita, *Journal of The Adhesion Society of Japan*, **36**, 201(2000)
7) R. A. Donaton, et al, *Proceedings of International Interconnect Technology Conference 2000 (IEEE)*, p.93
8) A. Kobayashi, K. Sawa, T. Nakamura and K. Mine, *The 4$^{th}$ Symposium of Japan Society of Silicon Chemistry Proceedings* (1999 Nov.), p.44

# Chapter 7

Conclusion 138

Novel amorphous silicon and silicone based thin films and materials were developed and the mechanism understanding of their functions was investigated and discussed. Novel five areas were focused on in terms of dimension of silicon or function of material. Feasibility of their films or materials for electronics applications was also studied. As the result the developed materials showed advanced performances that may be applicable for electronics devices. This wide range of dimension and performances could be coming from the basic nature of silicon.

Followings are the conclusions of this study.

1) Plasma CVD using phenyl substituted silanes as the source gases was first studied in depth. The stricture of deposited films could be varied from inorganic to polymeric being controlled by mainly *rf* power. The polymeric films could be electroconductive with some dopants. Plasma diagnostics data explained the phenomena well.
2) Silicon based thin films were plasma polymerized from several kinds of organosilicon monomers and their passivation effects on ceramic high temperature superconductors were investigated. Some of the films such that prepared from hexamethylsilazane protected the superconductors (kept properties) against water vapor or oxygen-free gas (Ar) at an elevated tempetarure (ie, good passivation effect). The passivation effects were well supported by the data of permeability of water vapor or oxygen.
3) Novel siloxane/PEO based solid polymer electrolytes of single ion type (only lithium ion mobile) or double ion type (both lithium and anion mobile) were synthesized from same prepolymers. The siloxane network is expected to lower the glass transition temperature, that means wide temperature usable range if it is applied for lithium battery. The single ion type was clearly identified that the transportation number of lithium ion was 100 %, that could be applied for advanced devices.
4) Novel siloxane ionomers were developed and their particles (fine powders) were fabricated. Those particles were dispersed in silicone oil and the dispersions were examined as electrorheological fluids. Several fluids showed high yield stresses when high voltages were applied and good stability even at high temperatures.
5) Cure mechanism of polyhydrogensilsesquioxane (HSQ) resin was analyzed by a dynamic viscoelastic methodology in various atmosphere and temperature conditions. The mechanism was well analyzed and good hints to obtain cured films having good properties were suggested. Furthermore, to improve the cracking

resistance of the HSQ films, electron beam was applied. Oxidative cure was proceeded even at room temperature with electron beam and the cured films showed much higher crack free thickness values than those cured thermally.

6) The results indicate that those silicon based materials are potentially applicable for current and future electronics.

From the standpoint of bond dimension, this study can be summarized in Table 1.

Table 1. Summary of this study from the standpoint of bond dimension.

| Application | Function of material | Material | Best dimension: Extending bond order around Si | Best dimension: SiO bond order | Role of silicon |
|---|---|---|---|---|---|
| Solar cell | Optical band gap control | Polisilane alloy - a-SiC / graphite | $(2+\delta)$ - 4 | 0 | Valence state control, $\sigma$ - $\pi$ junction |
| Conductive films | Electrically conductive | | | | |
| Passivation of superconductors | Intercept of $H_2O$ and $O_2$, Inert | Silicone network / SiN | Hybrid $((2+\delta)/4)$ | Hybrid $((2+\delta)/0)$ | Dense bonding, intert |
| Lithium battery | High ion conducting at wide temperature range | Siloxane/PEO network | $2(+\delta)$ | $2(+\delta)$ | Flexible |
| Electrorheological fluid | Respoise to electric field, stability | Siloxane ionomer | 2 -3 (to be optimized) | 2 -3 (to be optimized) | Insulation, Flexible, Combatibility with |
| LSI interlayer | Low k, film strength, integration | $HSQ/SiO_2$ | $3+\delta$ | $3+\delta$ | Insulation, Thermal stability, Rigidity |

The conventional silicon based materials have been just on the dimensional spots at “Si” (Extending bond order around silicon = 4, SiO bond order = 0) or at “silicone” (Extending bond order around silicon = 2, SiO bond order = 2). In this study the concept of these two types of bond dimension was extended and new functions were discovered at novel dimensional spots.

Fig. 1 shows a plane in relation between extending bond order around silicon and SiO bond order, and shows areas in which the best functions of the materials in this study reveal. Possible indications for dominating the extending bond order around silicon and SiO bond order could be “inorganic/organic” and “insulating/conductive”, respectively.

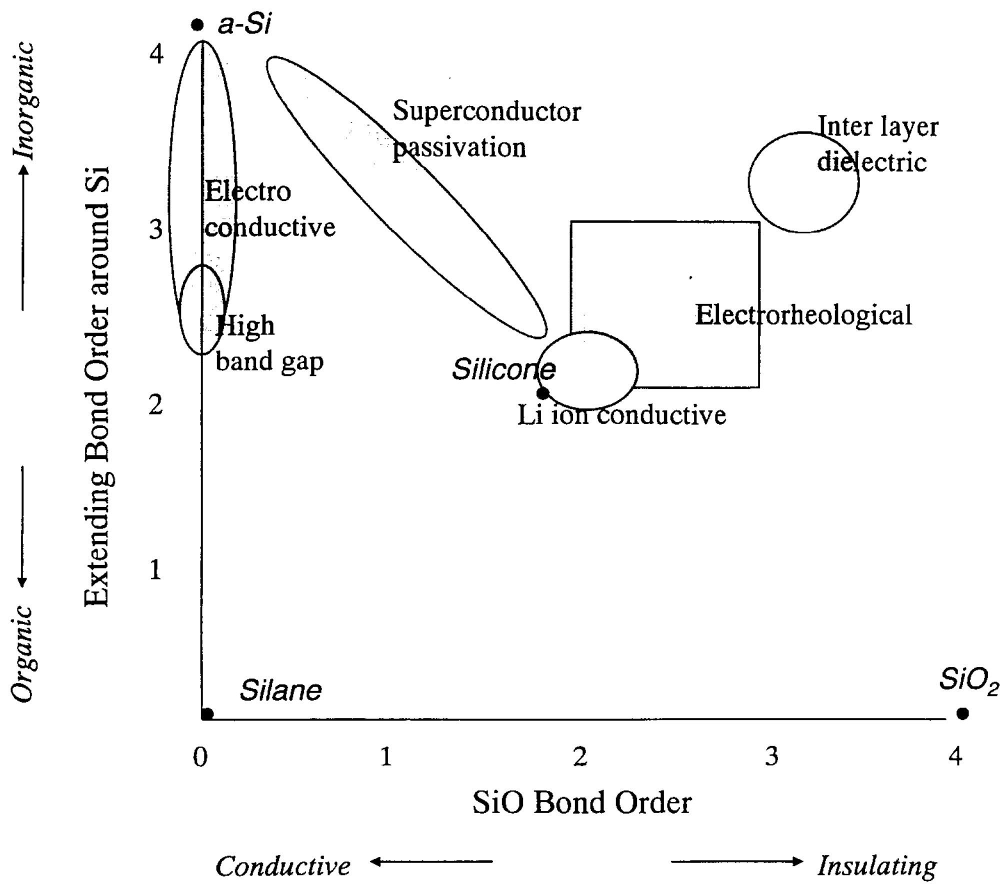


Fig. 1. Relationship between extending bond order around silicon and SiO bond order, and areas in which the best functions of the materials in this study are obtained.

# LIST OF PUBLICATIONS

Chapter 2

1) "Synthesis of Amorphous Films from Phenylsilanes by Plasma Chemical Vapor Deposition"
T. Nakamura, V. A. Sinigersky, T. Hirano, K. Fueki and H. Koinuma, *Makromol. Chem.*, **189**, 1315 (1988)

2) "Glow Discharge Decomposition of Phenylsilane in the Presence of Oxygen"
T. Nakamura, V. A. Sinigersky, K. Sato and H. Koinuma, *Makromol. Chem.*, **191**, 1555 (1990)

Chapter 3

3) "Passivation Effects of Plasma Polymerized Films from Organosilicon Compounds on Ceramic High Temperature Superconductors"
T. Nakamura, *Kobunshi Ronbunshu*, **52**(5), 249 (1995)

Chapter 4

4) "Novel Single and Double Ion Type Siloxane Polymeric Solid Electrolytes Prepared by Same Prepolymers"
H. Tsutsumi, M. Yamamoto, M. Morita, Y. Matsuda, T. Nakamura and H. Asai, *Electrochimica Acta*, **37**(7), 1183 (1992)

Chapter 5

5) "Synthesis of silicone ionomers and application for electrorheological fluid"
T. Nakamura, A. Kobayashi and R. Mikami, *Kobunshi Ronbunshu*, **58**(3), 105(2001)

Chapter 6

6) "Dynamic viscoelastic behaviors of hydrogen silsesquioxane resin at high temperatures"
T. Nakamura and K. Mine, *Kobunshi Ronbunshu*, **58**(3), 111(2001)

7) "Oxidative Curing of Hydrogen Silsesquioxane Resin Films by Electron Beam Irradiation without Additional Heatings and Characterization of the Cured Films"
T.Nakamura, M.Sasaki, A. Kobayashi, K. Sawa and K.Mine, *Jpn. J. Appl. Phys., in press.*

Others

1) "High Tc Superconductivity in Tm-Ba-Cu-O System"
S. Kanbe, T. Hasegawa, M. Aoki, T. Nakamura, H. Koinuma, K. Kishio, K. Kitazawa, H. Takagi, S. Uchida, S. Tanaka and K. Fueki, *Jpn. J. Appl. Phys.*, **26**(5), L613 (1987)

2) "High Tc Superconductivity in Screen Printed Yb-Ba-Cu-O Films"
H. Koinuma, T. Hashimoto, T. Nakamura, K. Kishio, K. Kitazawa and K. Fueki, *Jpn. J. Appl. Phys.*, **26**(5), L761 (1987)

3) "Glow Discharge Decomposition of Phenylsilane and Properties of Deposited Films"
T. Nakamura, M. Funabashi, T. Hirano, K. Fueki, and H. Koinuma, *Proceedings of ISPC-8 Tokyo, 1987, Paper number AVIII-02*, p.1436

4) "Glow Discharge Decomposition of Phenylsilanes and Properties of Deposited Films"
T. Nakamura, V. A. Sinigersky, K. Fueki, and H. Koinuma, Poster Session, *International Topical Workshop "Advances in Silicon-Based Polymer Science" (1987 Nov., Hawaii)*

5) "Novel Cross-linked Polysiloxane Solid Electrolyte for Lithium Battery"
H. Tsutsumi, Y. Matsuda, T. Nakamura and H. Asai, *Proceedings of 183$^{rd}$ Meeting of The Electrochem. Soc. (1993 May, Hawaii),* p.187

6) "Synthesis of silicone ionomers and application for ER fluids"
T. Nakamura, A. Kobayashi, R. Mikami, H. Asai, *The 41$^{st}$ Rheology Symposium Japan Proceedings(1993 Oct., Yonezawa),* p.77

7) "Polyhydrogensilsesquioxane based thin films with low dielectric constants"
A. Kobayashi, K. Sawa, T. Nakamura and K. Mine, *The 4$^{th}$ Symposium of Japan Society of Silicon Chemistry Proceedings (1999 Nov., Kiryu),* p.44